



**HAL**  
open science

## Ground-based measurements of spatial and temporal variability of snow accumulation in East Antarctica

Olaf Eisen, Massimo Frezzotti, Christophe Genthon, Elisabeth Isaksson, Olivier Magand, Michiel R. van den Broeke, Daniel A. Dixon, Alexey Ekaykin, Per Holmlund, Takao Kameda, et al.

### ► To cite this version:

Olaf Eisen, Massimo Frezzotti, Christophe Genthon, Elisabeth Isaksson, Olivier Magand, et al.. Ground-based measurements of spatial and temporal variability of snow accumulation in East Antarctica. *Reviews of Geophysics*, 2008, 46 (RG2001), 1 à 39 p. 10.1029/2006RG000218 . insu-00378349

**HAL Id: insu-00378349**

**<https://insu.hal.science/insu-00378349>**

Submitted on 25 Mar 2021

**HAL** is a multi-disciplinary open access archive for the deposit and dissemination of scientific research documents, whether they are published or not. The documents may come from teaching and research institutions in France or abroad, or from public or private research centers.

L'archive ouverte pluridisciplinaire **HAL**, est destinée au dépôt et à la diffusion de documents scientifiques de niveau recherche, publiés ou non, émanant des établissements d'enseignement et de recherche français ou étrangers, des laboratoires publics ou privés.

# GROUND-BASED MEASUREMENTS OF SPATIAL AND TEMPORAL VARIABILITY OF SNOW ACCUMULATION IN EAST ANTARCTICA

Olaf Eisen,<sup>1,2</sup> Massimo Frezzotti,<sup>3</sup> Christophe Genthon,<sup>4</sup> Elisabeth Isaksson,<sup>5</sup> Olivier Magand,<sup>4</sup> Michiel R. van den Broeke,<sup>6</sup> Daniel A. Dixon,<sup>7</sup> Alexey Ekaykin,<sup>8</sup> Per Holmlund,<sup>9</sup> Takao Kameda,<sup>10</sup> Lars Karlöf,<sup>11</sup> Susan Kaspari,<sup>7</sup> Vladimir Y. Lipenkov,<sup>8</sup> Hans Oerter,<sup>2</sup> Shuhei Takahashi,<sup>10</sup> and David G. Vaughan<sup>12</sup>

Received 31 October 2006; revised 2 July 2007; accepted 25 September 2007; published 11 April 2008.

[1] The East Antarctic Ice Sheet is the largest, highest, coldest, driest, and windiest ice sheet on Earth. Understanding of the surface mass balance (SMB) of Antarctica is necessary to determine the present state of the ice sheet, to make predictions of its potential contribution to sea level rise, and to determine its past history for paleoclimatic reconstructions. However, SMB values are poorly known because of logistic constraints in extreme polar environments, and they represent one of the biggest challenges of Antarctic science. Snow accumulation is the most important parameter for the SMB of ice sheets. SMB varies on a number of scales, from small-scale features (sastrugi) to ice-sheet-scale SMB patterns determined mainly by temperature, elevation, distance from the coast, and wind-driven processes. In situ measurements of SMB are performed at single points by stakes, ultrasonic

sounders, snow pits, and firn and ice cores and laterally by continuous measurements using ground-penetrating radar. SMB for large regions can only be achieved practically by using remote sensing and/or numerical climate modeling. However, these techniques rely on ground truthing to improve the resolution and accuracy. The separation of spatial and temporal variations of SMB in transient regimes is necessary for accurate interpretation of ice core records. In this review we provide an overview of the various measurement techniques, related difficulties, and limitations of data interpretation; describe spatial characteristics of East Antarctic SMB and issues related to the spatial and temporal representativity of measurements; and provide recommendations on how to perform in situ measurements.

**Citation:** Eisen, O., et al. (2008), Ground-based measurements of spatial and temporal variability of snow accumulation in East Antarctica, *Rev. Geophys.*, 46, RG2001, doi:10.1029/2006RG000218.

## 1. INTRODUCTION

[2] The development of the Earth's climate is strongly linked to the state of the polar regions. In particular, the large ice sheets influence components of the climate system, including the global water cycle by locking up or releasing large amounts of fresh water; the radiation budget through the high albedo of ice- and snow-covered surfaces; and the thermohaline circulation through the amount of fresh water

released to the ocean by melting or iceberg calving. Since the termination of the last glacial period, the only remaining large ice sheets are located in Antarctica and Greenland.

[3] The polar ice sheets are not only active participants in the global climate system (including being a major control on global sea level), but they also provide the only archive which gives direct access to the paleoatmosphere. *Ice cores* collected from polar regions and analyzed for atmospheric gases, stable isotopes, major ions, trace elements, etc.,

<sup>1</sup>Laboratory of Hydraulics, Hydrology and Glaciology, ETH Zurich, Zurich, Switzerland.

<sup>2</sup>Alfred Wegener Institute for Polar and Marine Research, Bremerhaven, Germany.

<sup>3</sup>Laboratory for Climate Observation, Italian National Agency for New Technologies, Energy and the Environment, Rome, Italy.

<sup>4</sup>Laboratoire de Glaciologie et Géophysique de l'Environnement, CNRS, University Joseph-Fourier, Grenoble, France.

<sup>5</sup>Norwegian Polar Institute, Tromsø, Norway.

<sup>6</sup>Institute for Marine and Atmospheric Research, Utrecht University, Utrecht, Netherlands.

<sup>7</sup>Climate Change Institute, University of Maine, Orono, Maine, USA.

<sup>8</sup>Arctic and Antarctic Research Institute, St. Petersburg, Russia.

<sup>9</sup>Department of Physical Geography and Quaternary Geology, Stockholm University, Stockholm, Sweden.

<sup>10</sup>Kitami Institute of Technology, Kitami, Japan.

<sup>11</sup>SWIX Sport AS, Lillehammer, Norway.

<sup>12</sup>British Antarctic Survey, Cambridge, UK.

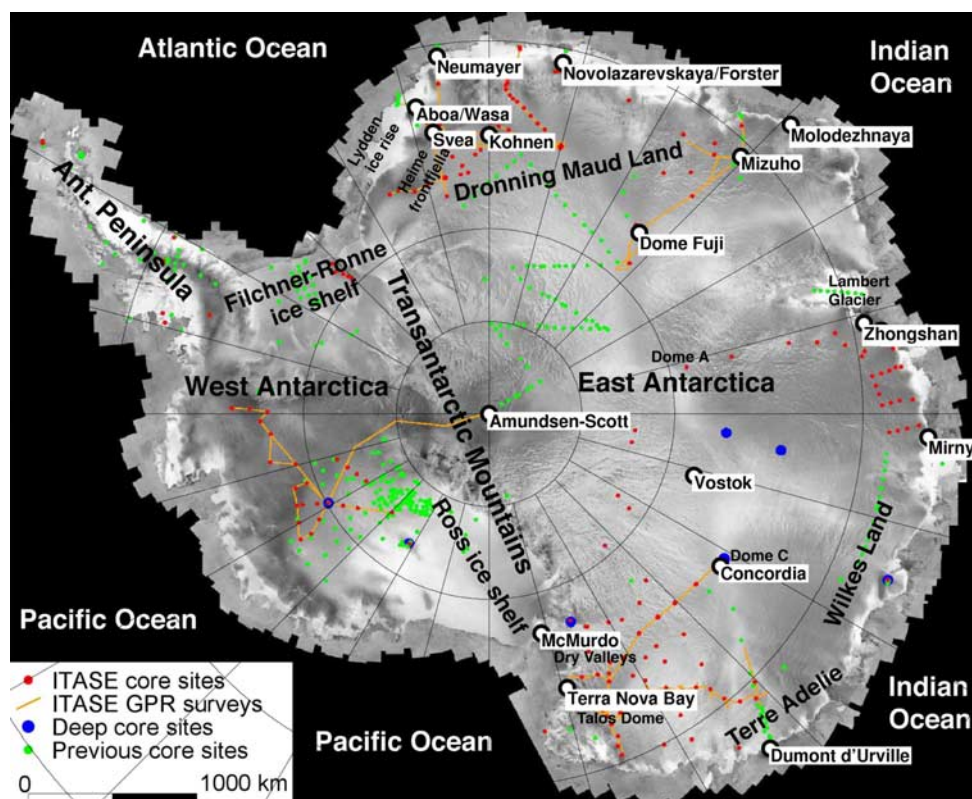


**Figure 1.** Map of Antarctica with some topographic names, drilling sites, radar profiles, and stations mentioned in the text (underlain by white rectangles), adapted from *Mayewski et al.* [2005] with permission of the International Glaciology Society. Radarsat mosaic in the background. (“Terra Nova Bay” station was renamed to “Mario Zucchelli station” in 2004.)

enable past climate conditions to be reconstructed [e.g., *Mayewski et al.*, 1993; *Dansgaard et al.*, 1993]. (Italicized terms are defined in the glossary, after the main text.) These records, currently spanning as far back in time as the past 800 ka [*Jouzel et al.*, 2007], are an important key to identification of the causes and forcing mechanisms of climate change.

[4] Understanding past conditions of the ice sheets and determining their present state are essential to predict their behavior under future climate conditions. The most important physical variable in assessing past and current ice sheet conditions is the *surface mass balance*. The current state-of-the-art ground-based techniques used to determine surface mass balance and its spatial and temporal characteristics in East Antarctica are the topic of this paper. Surface mass balance has been termed differently by many authors. Most completely, it is described as *mean net annual surface mass balance* and includes all terms that contribute to the solid, liquid, and gaseous transfer of water across the surface of the ice sheet. Hereafter, we will abbreviate this to “surface mass balance” (SMB) while maintaining the averaging implied by the full description. We also note that this term is the aggregate of many processes, such as precipitation from clouds and clear skies, the formation of hoarfrost at the surface and within the snowpack, sublimation, melting and runoff, wind scouring, and drift deposition.

### 1.1. Principal Processes

[5] Antarctica consists of West and East Antarctica, divided by the Transantarctic Mountains (Figure 1), and the Antarctic Peninsula. Whereas floating ice shelves form a considerable part of West Antarctica, the largest ones being the Filchner-Ronne and Ross ice shelves, East Antarctica is mainly formed by the inland ice sheet plateau, roughly comprising two thirds of the continent. Our main aim is to present the characteristics of SMB of the East Antarctic plateau area, which despite its apparent homogeneity shows large spatial variability. Nevertheless, we include findings based on data from West Antarctica and near-coastal sites as well for a larger context.

[6] On the *Antarctic ice sheet*, few places display a constantly negative SMB (e.g., *blue ice areas*) [e.g., *Bintanja*, 1999; *van den Broeke et al.*, 2006b]. Unlike in Greenland and the Antarctic Peninsula [*Vaughan*, 2006] where melting is an important process, wind erosion and sublimation are the key factors for negative SMB of the West and East Antarctica ice sheets. On the interior plateau of the Antarctic ice sheet, large areas have a mass balance close to zero, and negative mass balance has been reported for some areas [*Frezzotti et al.*, 2002b]. Nevertheless, annual SMB is generally positive in the long term. We will therefore use the term *accumulation* or accumulation rate synonymously to refer to a positive SMB.

[7] Solid atmospheric precipitation (snowfall or diamond dust) is deposited at the surface of the East Antarctic Ice Sheet. Atmospheric precipitation is homogeneous over tens to hundreds of kilometers. Wind erosion, wind redistribution, sublimation, and other processes during or after the precipitation event lead to a deposition at the surface which is spatially less homogeneous than the original precipitation. Variations in accumulation over tens of kilometers have been observed since the 1960s [Black and Budd, 1964; Pettré et al., 1986]. These accumulation variations and surface processes result in surface features including sastrugi, longitudinal dunes [Goodwin, 1990], dunes on the 100-m scale [Ekaykin, 2003; Karlöf et al., 2005b], and, most impressively, megadunes on a kilometer scale [Fahnestock et al., 2000; Frezzotti et al., 2002a]. Once the snow is permanently deposited, further accumulation is responsible for the submergence of surface layers. In the firn column, the snow densifies under the overburden weight, and the interplay with ice dynamics like advection begins to deform the surface layer.

[8] The spatial and temporal distribution of SMB is a primary concern for numerous issues: for determining the current state of the ice sheet and estimating mass balance changes over regional, basin-wide, and continental scales and the associated contribution to sea level change [e.g., Joughin et al., 2005, and references therein]; for ice flow modeling of the age-depth relationship and subsequent application to ice cores; for calibration of remote sensing measurements of SMB; for understanding of the SMB–surface meteorology–climate relationship; and for improving, verifying, and validating various types of models, in particular, the climate models from which predictions (future) or reconstructions (paleoclimate) of accumulation are tentatively obtained. Unfortunately, there exists a discrepancy between assumptions and needs of these applications in terms of spatiotemporal coverage and resolution of SMB and the actual data characteristics available. For instance, dating of ice cores by flow modeling usually assumes rather smooth accumulation patterns, mainly formed by larger features, accumulation time series, and ice dynamical history. Surface accumulation, on the other hand, is not smooth in time and space. Because of interaction with surface features, such as varying surface slopes, significant surface accumulation variations occur on much smaller spatial scales than precipitation, as will be demonstrated here. Analysis of *firn cores* and meteorological observations integrated with validated model reanalysis data of European Centre for Medium Range Weather Forecasts 40-Year Reanalysis (ERA 40) pointed out high variability of snow accumulation at yearly and decadal scales over the past 50 years but without a statistically significant trend [Monaghan et al., 2006].

## 1.2. General Difficulties

[9] While measurement of precipitation has been a routine part of worldwide observations for more than a hundred years, there is still no practical technique that can be used to measure SMB in East Antarctica in realtime as part of a

meteorological measurement program. This is largely due to the technical difficulties involved in making measurements without disturbing natural patterns of snow drift and measuring changes at depth in the snowpack. Thus, knowledge of SMB seasonality, trends, and spatial variability is limited. For this reason, we rely heavily on after-the-fact measurements obtained from ice cores, snow accumulation stakes, etc. Acquiring information about surface accumulation on the ice sheets with adequate sampling intervals is thus labor intensive. Only along a few selected profiles (ITASE, EPICA, JARE, RAE) (ITASE, International Transantarctic Scientific Expedition; EPICA, European Project for Ice Coring in Antarctica; JARE, Japanese Antarctic Research Expedition; RAE, Russian Antarctic Expedition) and in certain areas has area-wide information on accumulation been obtained (Figure 1).

[10] SMB observations cannot be easily extrapolated in time and space because spatial variations in SMB amount to considerable percentages of the absolute values, and often exceed these; the magnitude of the temporal variations is small compared to spatial variability, depending on the considered timescale; and the structure of the SMB covariance is unknown. To overcome these limitations, two other important techniques are therefore used to achieve area-wide information: satellite remote sensing and numerical climate modeling.

## 1.3. Remote Sensing and Numerical Modeling

[11] Currently, there is no definitive way to determine SMB from remote sensing data. There are signals in some remote sensing fields that are related to SMB as has been discussed widely by Zwally and Giovinetto [1995], Winebrenner et al. [2001], Bindshadler et al. [2005], Rotschky et al. [2006], and Arthern et al. [2006], but these are not solely dependent on accumulation rate and are thus to some extent “contaminated” by other factors. For this reason, most authors have attempted to use remote sensing fields to guide interpolation of field measurements. The most recent attempt at this by Arthern et al. [2006], who used a formal scheme to incorporate estimates of uncertainty and models of covariance, probably provides the most defensible estimate of the remotely sensed broadscale pattern of SMB across East Antarctica (Figure 2a). The typical footprint of these compilations is 20 km horizontally.

[12] In contrast to measuring area-wide precipitation in situ, as attempted by Bindshadler et al. [2005], numerical models are used to simulate atmospheric processes and related accumulation features [e.g., Gallée et al., 2005]. The first step for successful modeling is detailed understanding of the physical processes involved. The second step involves model validation. Because of computing resource limitations, there is currently no way to explicitly resolve processes that induce spatial variability of SMB at kilometer scales or less (e.g., sastrugi and dunes) with an atmospheric model run in climate mode, that is, over several years. Such features have to be at best statistically parameterized, or considered as noise, when comparing field data with model results [Genthon et al., 2005]. Although most

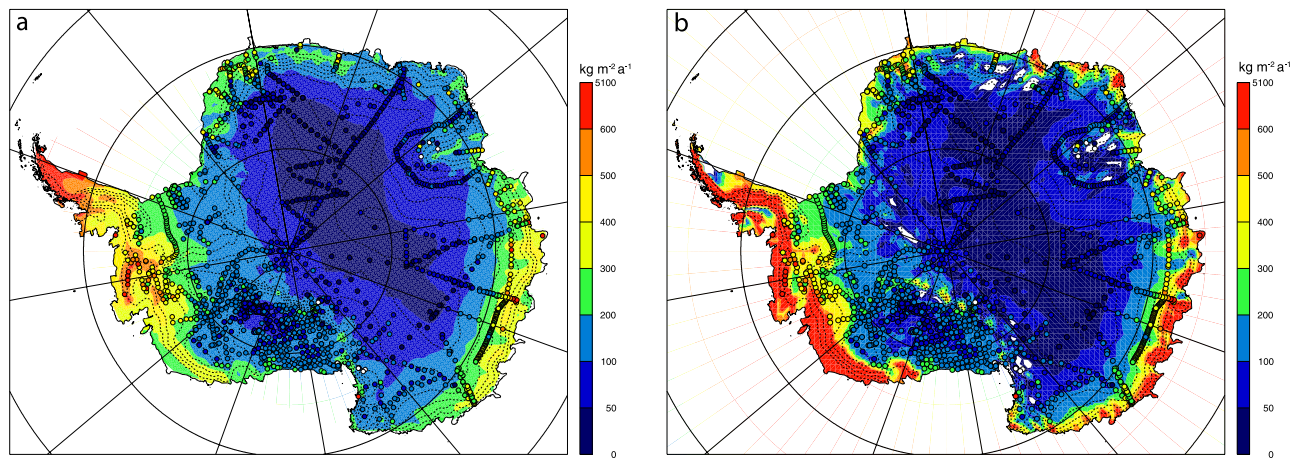


**Figure 2.** Examples for interpolated distributions of SMB (in  $\text{kg m}^{-2} \text{a}^{-1}$ ) based on point observations (circles) in Antarctica. (a) Interpolation of SMB observations guided by passive microwave remote sensing (adapted from *Arthern et al.* [2006]); (b) numerical climate modeling of SMB (solid precipitation minus sublimation and melt) [*van den Broeke et al.*, 2006a] with ground-based SMB data collection indicated by circles [*van de Berg et al.*, 2006].

global models have spatial resolutions of 100 km and greater [*Genthon and Krinner*, 2001], grid stretching in global models [*Krinner et al.*, 2007] and regional climate modeling [*van Lipzig et al.*, 2004a; *van de Berg et al.*, 2006] allow resolutions on the order of 50–60 km that can better capture the mesoscale impacts of topography on SMB distribution such as diabatic cooling of air mass along slopes, air channeling, or barrier effects. Most of the boundary conditions needed to run global (including stretchable grid) and regional atmospheric models, such as topography, sea surface temperature and sea ice, and radiatively active gases and aerosols, are the same. On the other hand, regional models also need lateral boundary conditions such as temperature, winds, and moisture. This is generally provided by meteorological analyses for recent and present-day climate simulations, but data from global climate models are necessary to run realistic climate change experiments. In this respect, stretchable grid global models are self-consistent. As an example, Figure 2b shows mass balance from RACMO2/ANT for the period 1980–2004 [*van den Broeke et al.*, 2006a], with a horizontal resolution of 55 km, as well as a selection of observed mass balance values (updated from *Vaughan et al.* [1999b]). The model is clearly capable of reproducing the large-scale features of the Antarctic SMB (direct correlation with 1900 SMB observations yields  $R = 0.82$ ) but cannot resolve the finer-scale features [*van de Berg et al.*, 2006] that are known to exist and that are one focus of the present paper. Double or triple nesting of models up to 3-km resolution is successfully used to improve weather forecasts in topographically complex regions, and could also be used to improve the model footprint of accumulation variability, once the governing processes (wind-driven snow redistribution) are properly parameterized [*Bromwich et al.*, 2003].

[13] One major use of SMB observations is to verify and validate climate models that are used to better understand the climate and SMB of Antarctica and to predict its future

evolution. Therefore, using climate model results for driving interpolations and building maps of the Antarctic SMB from the field observations [*van de Berg et al.*, 2006] requires more care to avoid circular reasoning than for satellite data [*Vaughan et al.*, 1999b; *Arthern et al.*, 2006], as these are more independent from ground observations. However, the models do provide the means for hindcasting accumulation and may be used to identify areas where additional data or verification of existing data are most needed, such as areas where several models disagree with field reports or with interpolations [*Genthon and Krinner*, 2001; *van den Broeke et al.*, 2006a]. This approach has been used to select the sites of some of the recent Italian-French ITASE surveys, and the new data have confirmed problems with the previous estimates [*Magand et al.*, 2007].

[14] Despite significant advances in either discipline (remote sensing or numerical modeling), both techniques fail in detecting or explaining small-scale (<50 km) variability in SMB observations. The processes playing part in the ice sheet–climate–weather interaction act on a broad range of spatial and temporal scales. As mentioned in section 1.1, precipitation is homogeneous on scales of roughly  $10^4 \text{ km}^2$ , mainly on the plateau, and is subject to redistribution in the atmospheric boundary layer on scales of centimeters to kilometers. The scale of temporal variability increases from a scale related to the movement, dynamic, and lifetime of frontal systems on the order of days to seasonal variations and interannual variability. Partly related to larger-scale oscillatory atmospheric and oceanographic patterns are variations on interannual to decadal scales. Variations that occur over centuries and millennia are of relevance for climate conditions. The longest variations are on the timescale of glacial cycles with a period of  $10^4$ – $10^5$  years (Table 1). The different techniques employed to observe these changes operate in a rather limited spatiotemporal window and with limited spatiotemporal resolution (Figure 3). Satellite sensors have

TABLE 1. Relevance and Scales of Surface Mass Balance Measurements

Target	Temporal Scales	Spatial Scales
Mass balance changes	1 to 10 <sup>5</sup> years	basin to ice sheet
Climate-SMB relationship	hours to 100 years	centimeter to 100–1000 km
Climate models <sup>a</sup>	hours to 100 years 10 <sup>4</sup> –10 <sup>5</sup> years in snapshots	10–100 km to ice sheet
Remote sensing <sup>b</sup>	hours to 30 years	submeter to ice sheet
Ice flow modeling <sup>c</sup>	10 to 10 <sup>5</sup> years	100 m to ice sheet

<sup>a</sup>For (in)validation of models, the model output is compared with actual measurements. This permits judging the usability of models.

<sup>b</sup>Some remote sensing applications (altimetry, gravity, passive microwave, scatterometers, etc.) profit or even require data calibration for retrieval algorithms at specific test sites for correct interpretation and further extensions of the measurements to other areas. Validations are likewise important.

<sup>c</sup>Input of SMB to ice flow models is especially important for interpreting deep ice cores.

a comparably large range of footprint sizes and spatial coverage but are usually limited in temporal resolution and length of time series. Numerical models, in contrast, can cover temporal scales from hours to millennia, but their spatial coverage and resolution depend on each other in a reciprocal manner, thus yielding either low resolution at large spatial coverage or vice versa.

#### 1.4. Outline

[15] With this background on surface accumulation in mind, the purpose of this review paper is to provide the glaciological community and those outside with a reference to measurement techniques of SMB and characteristics thereof in East Antarctica. We present the different types of measurements in section 2, including point measurements at the surface (*stakes* and *ultrasonic sounders*), point measurements at depth (*snow pits*, *firm cores*, and *ice cores*), and continuous lateral measurements (*ground-penetrating radar*). Sections 2.1–2.5 each contain a description of the mode of operation and type of analysis for the individual measurements, the basic measurement procedure for each technique and all required input quantities to derive the accumulation estimate, and an account of error estimates for each data type. We also present selected sample data to illustrate typical results obtained from these measurements and how the SMB data can form the input to other studies. Section 3 summarizes findings derived from the different measurement techniques, addresses their pros and cons, and judges the spatial and temporal representativity and limitation of SMB data. In section 4 we discuss the application of measurement data. We provide recommendations and principles for proper usage without stressing the data beyond physically justified limits to avoid misinterpretations.

Additionally, we emphasize that observers in the field should be aware of end-users' needs.

## 2. MEASUREMENT TECHNIQUES

[16] Common for all measurements of SMB at the surface is the observation of deposited mass over a certain time period, or proxies thereof. The different methods not only cover a wide spectrum of technical modes of operation, they also yield information about mass balance for varying spatial and temporal scales and resolutions, as schematically illustrated in Figures 3, 4, and 5. SMB measurements derived from stakes, ultrasonic sounders, snow pits, and firm or ice cores provide information from a single point at the surface (Figure 4). In contrast, ground-penetrating radar (GPR) is carried out along profiles in such high resolution that it can be considered a quasi-continuous measurement. Whereas stakes and ultrasonic sounders have to be operated for a longer period to obtain a time series, snow pits, firm/ice cores, and GPR are able to provide a time series from a single deployment. One could thus classify the measurements into instantaneous and retrospective methods, with unclear boundaries. Owing to the different variables measured, the methods provide accumulation rates on very different timescales and resolution, as schematically illustrated in Figure 5. The detailed differences will be set forth in this section. Before introducing the individual methods, we first discuss the important role of snow density and how it is measured.

### 2.1. Prerequisite: Determination of Snow Density

[17] All techniques aimed at the determination of SMB perform some sort of difference-length measurement (height

**Figure 3.** Schemes to illustrate the (a) resolutions and (b) coverage of the different types of measurements in time ( $x$  axis) and space ( $y$  axis) used to derive surface mass balance. In Figure 3a, the rectangles indicate the typical resolutions of the various techniques. In addition to the characteristics of an individual measurement (e.g., a snow pit or a GPR profile), the combination of these with groups and larger entities are also displayed (e.g., stake lines or GPR grids). In this sense, “single snow pit” indicates the resolution within an individual pit, whereas “(snow pits at different sites)” refers to the distance between different snow pits. Likewise for ultrasonic sounders at different sites and GPR distance between different profiles. In Figure 3b, the rectangles indicate typical temporal and spatial coverage of measurements. For instance, stake lines may be hundreds of meters to more than 1000 km long. The time series derived from such a line could be just a year or up to several decades. In contrast, a single stake covers only an area of a few square centimeters. For implementing measurement programs, the question arises as to what can be achieved by a three- to four-person team in a single season. As logistics often impose the largest constraints in Antarctica, the resolution and coverage provided here could serve as a guideline to which combination of methods seems most effective.

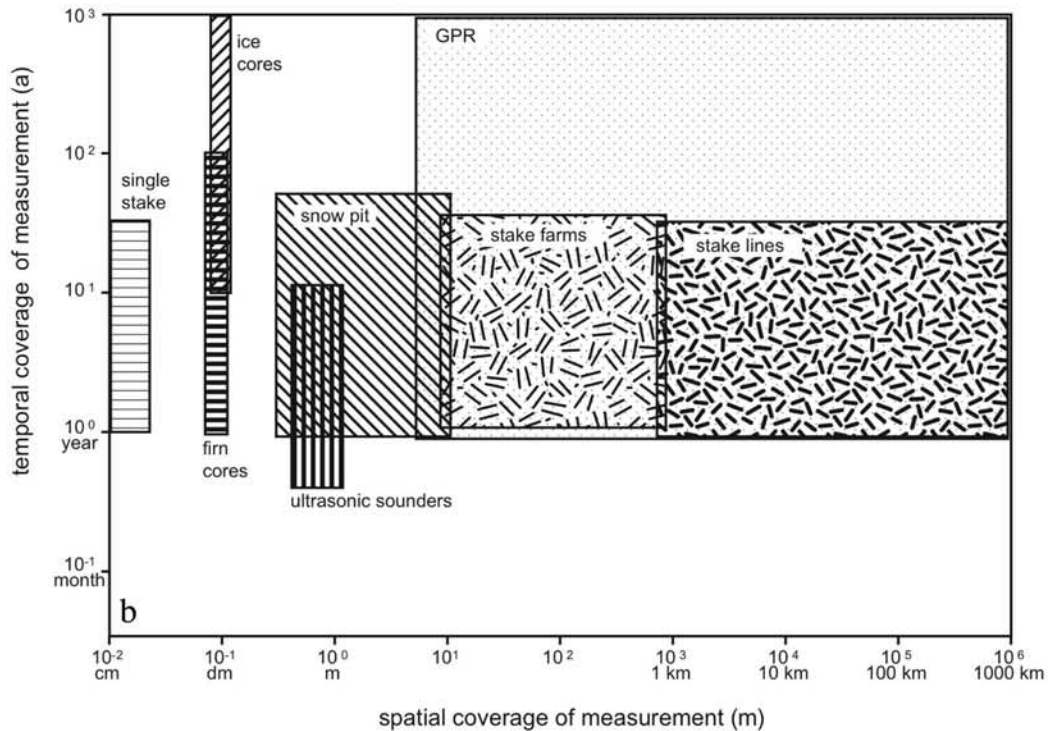
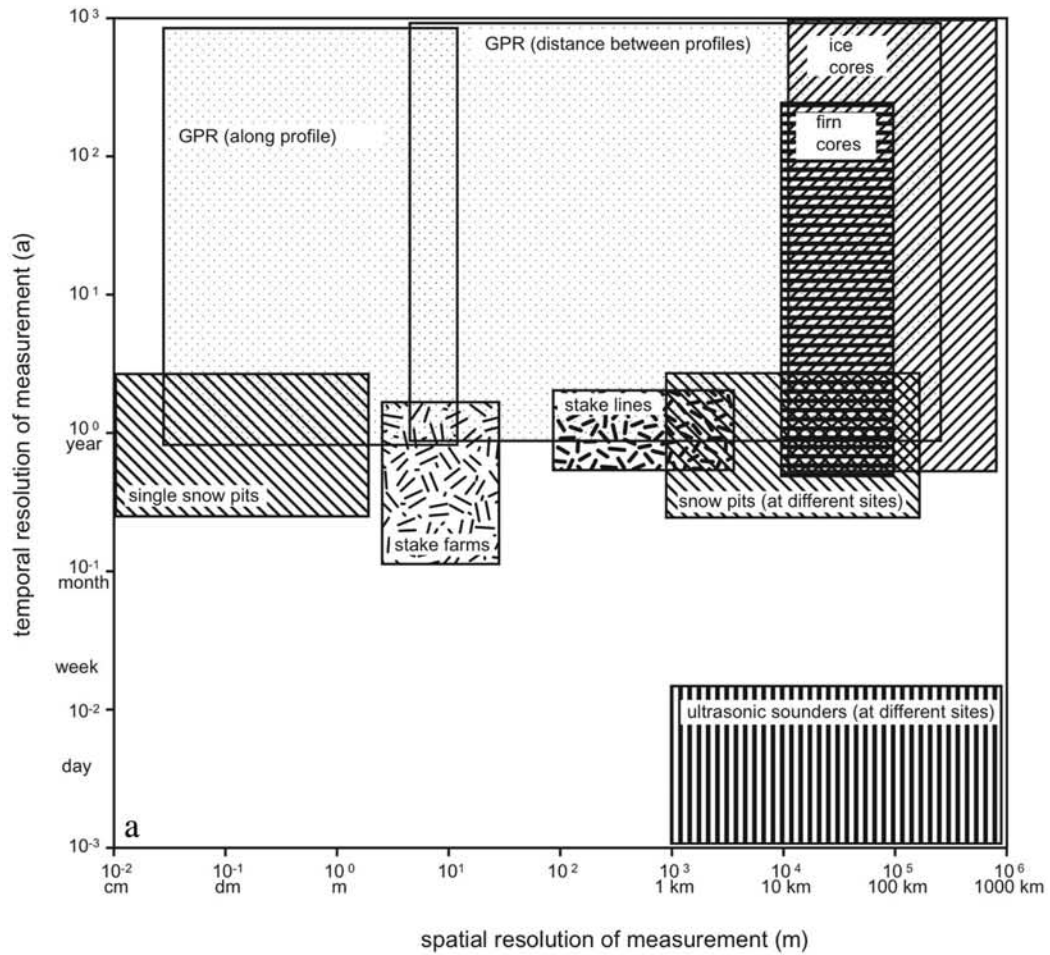
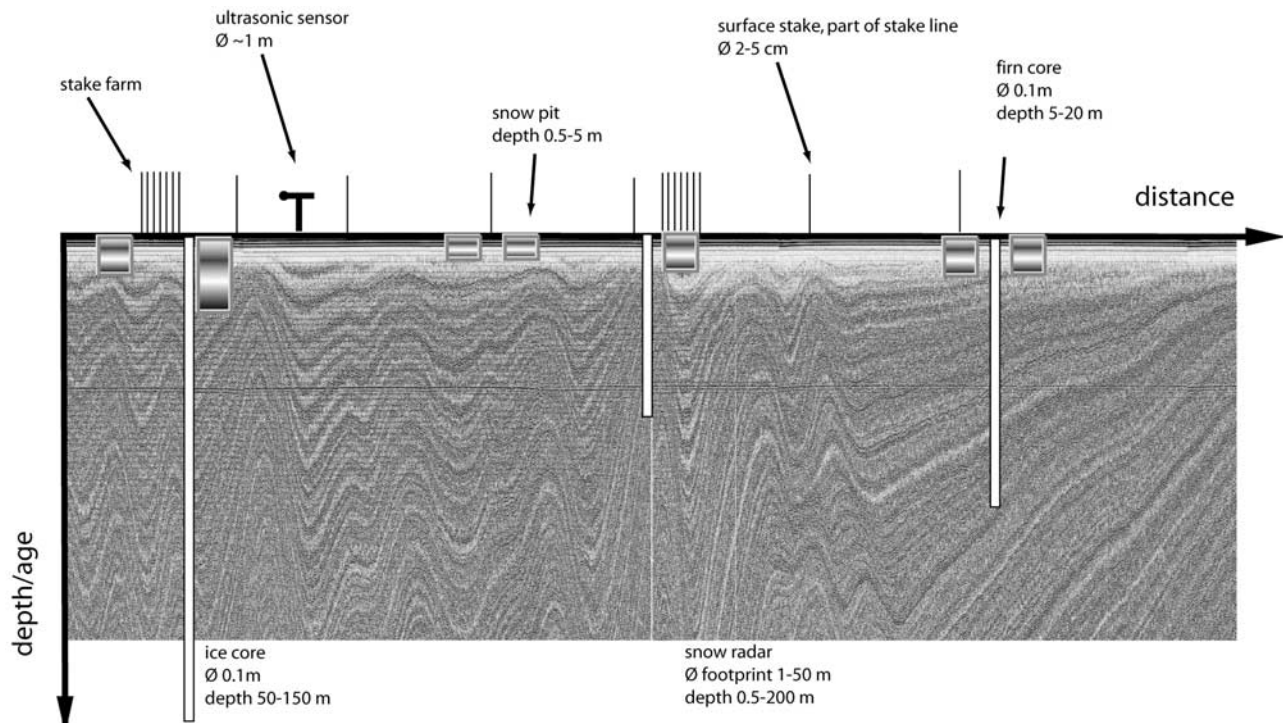


Figure 3



**Figure 4.** Scheme to illustrate spatial sampling interval and sample depths of different methods: stakes and ultrasonic sounders, at surface; snow pits, up to a few meters depth; firn cores, few tens of meters; ice cores, up to several tens to hundreds of meters, reaching below the firn-ice transition; GPR, tens to hundreds of meters. GPR data acquired along a 50-km profile [Anschütz *et al.*, 2007] are shown as background to illustrate the lateral variation. Continuous reflections present layers of equal age (isochrones). The canceled circle indicates the horizontal distance over which SMB is determined. (Note that ice core deep drilling is possible to some kilometers depths, but we are not concerned with that technique here.)

change, layer thickness, etc.) over certain time periods. To convert this length measurement to a SMB value, knowledge of the density distribution of the observed sample is fundamental. Determination of the snow density is usually more difficult and less accurate compared to the length measurements for a number of reasons. One of few exceptions for direct snow density measurements is the only recent adaptation of a neutron-scattering probe [Morris and Cooper, 2003; Hawley *et al.*, 2006].

[18] The classic method calculates density from snow sample volume and mass; however, accurately determining snow sample volume is a hard task under field conditions. The easiest method is to use a sampling probe with known volume. It is possible that each national Antarctic expedition uses different types of snow-sampling devices, which introduces additional uncertainties in the final values. A suitable field method for density measurements in snow pits is proposed in the ITASE guidelines by Mayewski and Goodwin [1997]. Because of the strong densification within the uppermost layers, density should be sampled at high vertical resolution. To avoid the risk of disturbing the underlying snow during sampling, the snow can be collected in a crossover pattern (see Figure 9c in section 2.4). Moreover, sampling snow pits from the bottom upward to the surface avoids the risk of contaminating the lower levels by snow falling down from previous sampling above. Depth

control and minimizing depth error is most easily obtained by constantly leveling the sample depth with two adjacent rulers. Depending on the equipment used, the sample volume error is around several percent, and the error in the mass determination depends on the balance used. An optimistic volume error of  $\sim 1\%$  and an accuracy of the balance of  $\pm 1$  g would yield an uncertainty of about 1.4% for the density sampled in a snow pit [Karlöf *et al.*, 2005b]. The balance error increases to about  $\pm 5$  g if spring scales are used.

[19] Density measurements are mainly made during the austral summer season (December or January), which may introduce additional errors because of seasonal changes in snow density that can result from numerous processes. For instance, surface density differs between snowfall events and precipitation-free periods, as wind can cause erosion, hardening, and redistribution of the snow. General factors causing seasonal density variations are changing wind speed and temperature, larger or smaller portions of low-density fresh snow, and vapor transfer between the surface, atmosphere, and deeper snow layers. It is not obvious which seasonal (or annual) density value best characterizes the “effective” annual density. These effects are different for snow density in the first meter in high-accumulation coastal areas (density on the order of  $400 \text{ kg m}^{-3}$ ) compared to low-accumulation inland areas (around  $300 \text{ kg m}^{-3}$ ). Sea-



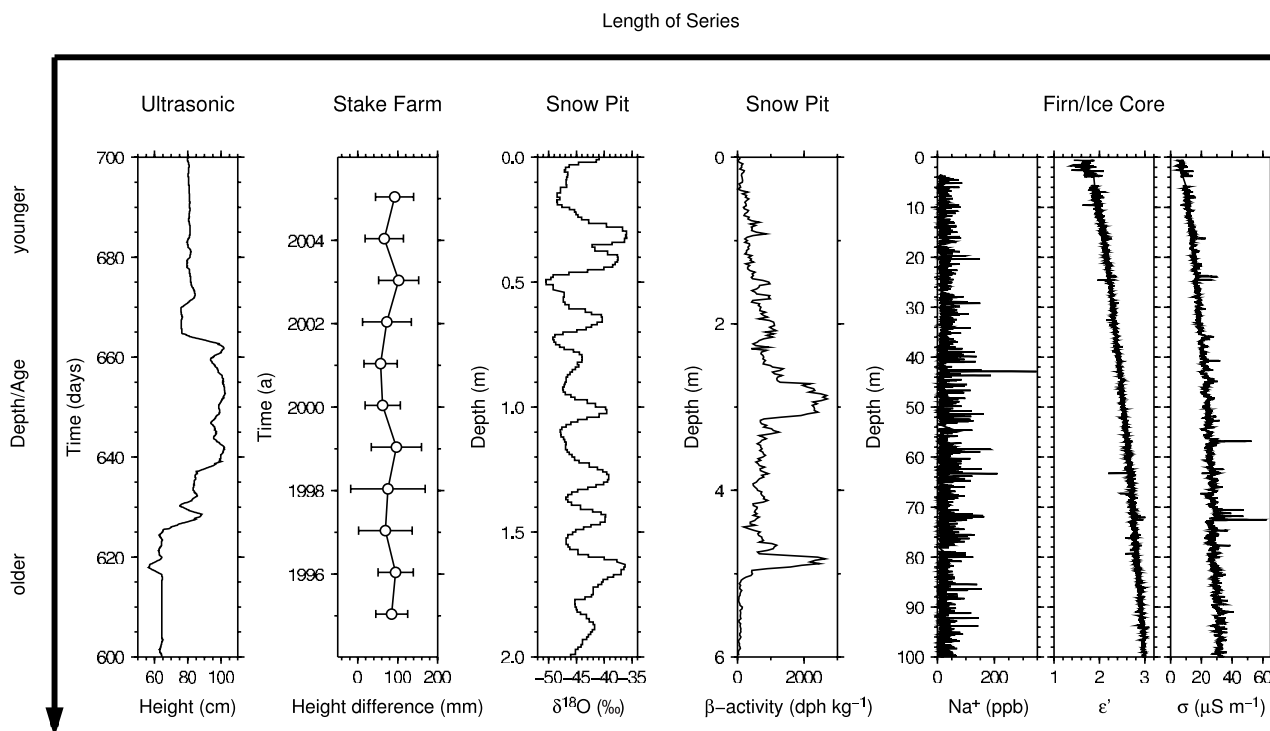


**Figure 5.** Data series obtained from various measurement techniques for single locations. The vertical axis indicates depth (for measurements made at depth) and time (for measurements made at the surface: ultrasonic sounders and stakes), respectively, increasing downward. The covered time/depth span differs between graphs. The temporal scale of the time/depth series lengths tentatively increases to the right. From left to right, 100 days of an ultrasonic sounder time series from the automatic weather station AWS9 (height above surface) [van den Broeke *et al.*, 2004b] at site DML05, near the EPICA deep drilling at Kohnen station in Dronning Maud Land (DML), illustrating the accumulation of snow and subsequent partly erosion; 11-year time series of measured height differences to previous year from a stake farm at Dome Fuji [Kameda *et al.*, 2008]. The circle indicates the average of 36 stakes, and the bar indicates the spatial standard deviation of the measurements; the oxygen stable isotope record is from a 2-m-deep snow pit (DML25 [Oerter, 2005, available at <http://doi.pangaea.de/10.1594/PANGAEA.264585>; Oerter *et al.*, 2004]), spanning roughly 10 years. Annual cycles are clearly visible;  $\beta$  activity record is from a 6-m-deep snow pit at the South Pole from 1978 [Pouchet *et al.*, 1983] spanning several decades; example of chemistry measurements ( $\text{Na}^+$  content) [Sommer *et al.*, 2000b] and dielectric profiling record (relative permittivity  $\epsilon'$  and conductivity  $\sigma$ ) is from core B32 at site DML05 [Wilhelms, 2000] near the EPICA deep drilling in DML. The shown depth section corresponds to an 1100-year period from A.D. 883 to 1997.

sonally varying density is especially a problem for SMB measurements performed at the surface (introduced in sections 2.2 (stakes) and 2.3 (ultrasonic sounders)), in which case, density variations should be tracked in the snow layer accumulated during the given period of time (month or year). Unfortunately, almost no data are available that describe the seasonal change of the near-surface snow density and thus the actual density for the measured height difference, e.g., in the case of ultrasonic sounders. Although density values can be taken from adjacent snow pit studies, the question then arises as to which depth of the surface snow best approximates the average density. For instance, Vostok mean annual snow accumulation is only 7 cm on average (varying from negative values to more than 20 cm on individual stakes). A study of density in 17 snow pits showed that snow density does not change much with depth in the uppermost 20 cm of the snow. Consequently, the

mean density from this layer is used for converting snow accumulation to SMB at Vostok. Nevertheless, at Vostok the mean density of the uppermost 20 cm changes between  $310 \text{ kg m}^{-3}$  in winter and  $330 \text{ kg m}^{-3}$  in summer, which means that the uncertainty related to this source of errors may be as much as 6%.

## 2.2. Point Measurements at the Surface: Stakes

[20] The easiest way to measure SMB is based on stakes planted in the snow by simply measuring the amount of accumulation over a certain time period. Despite its simplicity, this method is valuable as it allows a rough estimate of the local or regional distribution of SMB. Sources of error include the conversion of the accumulated snow to SMB, density measurements (see section 1.1), and the subsidence of the stake bottom. This simple technique is

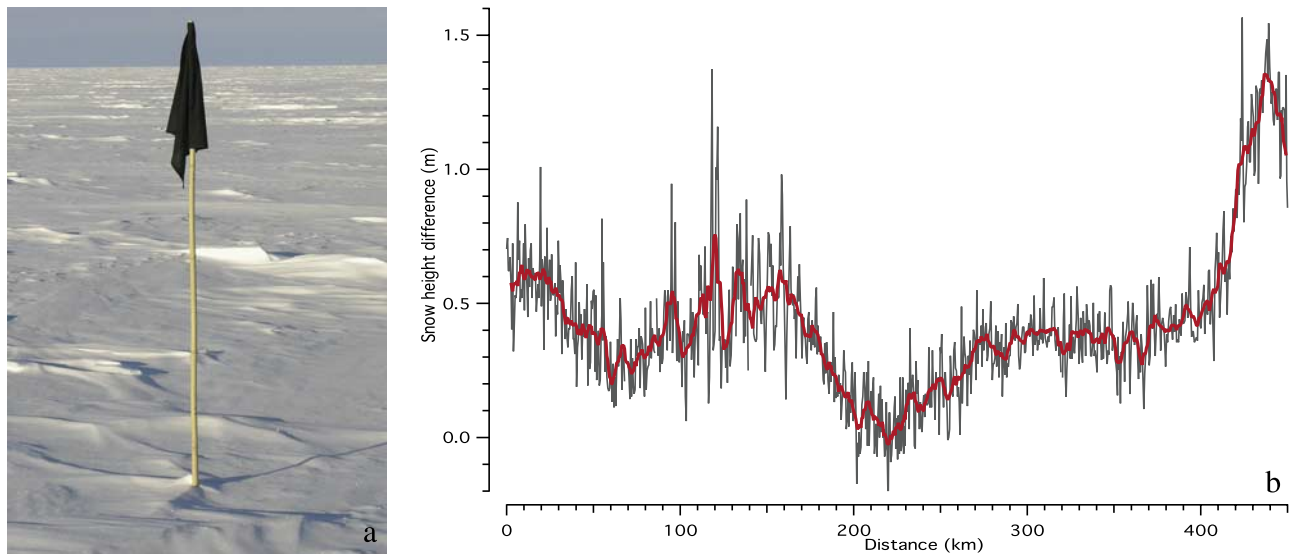


**Figure 6.** (a) Typical bamboo stake with a fabric flag at the top. Note the microrelief surrounding the stake base, which complicates height readings. (b) One year (2003) of sample data from the 450-km stake line from Neumayer station to Kottasberge, Heimefrontfjella, in DML; grey, single measurements every 500 m; bold, moving average over 5 km.

used by almost every nation in Antarctica. Examples are given in section 2.2.4.

[21] In addition to single stakes, *stake lines* and *stake farms* have also been used. Stake farms are more common at year-round stations, whereas stake lines may be established along traverse routes which are visited in more than one season. A stake farm gives single measurements for a well-defined small area, e.g., on the order of  $10^4$ – $10^6$  m<sup>2</sup> (tens of meters to kilometer side length) which are averaged to produce a single accumulation value. By using several stakes the small-scale depositional noise can be reduced. Additionally, continuous monitoring of stake farms provides a record of the buildup of the snow cover during the year and information on seasonal variations [see, e.g., *Fujii*, 1981; *Mosley-Thompson et al.*, 1999; *Schlosser et al.*, 2002], an important fact further explained in section 2.2.4. Measurements in stake farms are influenced by a slight disturbance of the natural snow deposition through the stakes themselves, the disturbance of the snow surface when people have to pass through the stake farm for measuring the stakes, and the accuracy of the height measurements itself. Stake readings are usually done on the leeward side of the prevailing wind direction to minimize the effect of footprints on the snow surface.

[22] Single stakes of a stake line are usually used primarily as markers for way points. They provide one value for each stake but over a larger distance (Figure 6). These measurements are helpful in measuring the spatial distribution of accumulation with a spacing on the order of kilometers. Single measurements are still affected by small-scale depositional noise, but because the time span for reading these lines is normally 1 year or more, the noise is a small source of error compared to the measured accumulation. The use of Global Positioning System

(GPS) receivers for positioning the stakes is an important tool to relocate the stakes. Stake locations can also be used to calculate surface velocities. In the case of traverse routes, the stakes are regularly replaced over the years and placed back in the original position. Determination of the accumulation rate from the stake observations consists of two types of observations: stake height measurements (allowing to determine the accumulation over a given time period) and density measurements.

### 2.2.1. Stake Height and Correction for Densification

[23] Stake height measurements are only possible if the stake bottom is immobile relative to the surrounding snow layer. This can be achieved by fixing the stake bottom on a horizontal slab, or by fixing it on a natural hard layer (wind slab). Usually, it is assumed that the stake bottom is firmly anchored in the snow and the stakes move down with the snow layer on which the stake bottom is fixed. Using a light weight stake, of which the bulk density is close to that of near-surface snow (e.g., commonly used bamboo stakes,  $250$ – $350$  kg m<sup>-3</sup>, 2–3 cm in diameter and 2.5 m in length), this condition is fulfilled in a first approximation. In the past, aluminum and bamboo stakes have been used, but they frequently have failed because of blizzard winds or melting due to solar radiation in coastal areas. Polycarbonate snow poles (50 mm diameter, 6 mm wall diameter), which have recently been used, are less fragile than bamboo and aluminum poles but are more expensive. However, the logistical costs of deployment and resurvey of stakes are much higher, and stake loss due to extreme environmental conditions is a critical issue. The maximum stake height for strong wind is around 4 m, being initially buried about 1.5 m in the snow (a ratio of about 35%). Additional factors that can cause uncertainty in reading the height appear if wind scouring or sastrugis with strong microrelief occur

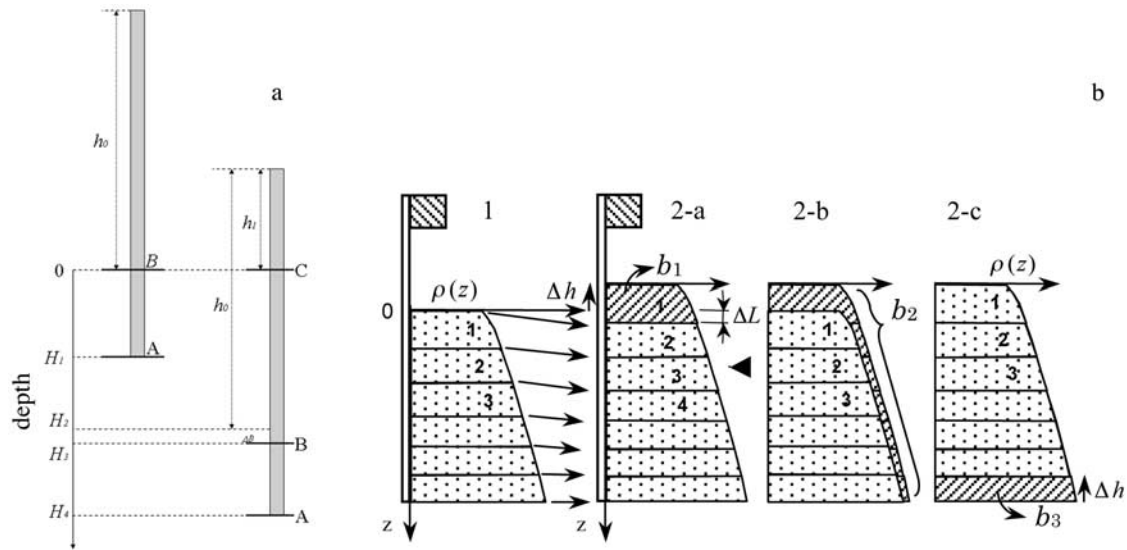


**Figure 7.** (a) Position of a stake in two moments in time. (b) Schematic diagram of the density-depth profile at Dome Fuji with flag stake for first (1, dotted area) and second year (2-a, 2-b, 2-c) to illustrate the effect of compaction and accumulation for determination of SMB from changes in stake height (redrawn from *Takahashi and Kameda* [2007] with permission of the International Glaciology Society). The mass accumulated in the second year is shown as the hatched areas  $b_1$ ,  $b_2$ , and  $b_3$  (with  $b_1 = b_2 = b_3$ ) in the second year's panels; previous layers are labeled 1–3 from the surface downward. In diagram 2-a, the first year's surface is lowered by  $\Delta L$  due to compaction.  $\Delta h$  is the change in stake height from first to second year. New snow layer is labeled 1, while the first year's layer 1 becomes layer 2, likewise for layers 2 and 3. Accumulation is thus the layer  $b_1$  of thickness  $\Delta h + \Delta L$ . In diagram 2-b, density-depth profiles for first year (dotted) in respect to first year's surface and first year's layer numbering, overlaid on profile from second year in respect to second year's surface. Assuming Sorge's law and a firmly anchored stake bottom, the density-depth profiles in both years have the same shape. Accumulation is then the (hatched) area  $b_2$  between both density profiles. 2-c: Shifting the first year's density profile upward by  $\Delta h$  to overlap with the second year's profile to the same surface level, the accumulation appears to be the hatched area at the stake base of thickness  $\Delta h$ .

around the stake (Figure 6a), and if a flexible stake is used, it can become bent.

[24] Accumulation values obtained as a difference of stake height at two moments in time must then be corrected for snow settling (densification), illustrated in Figure 7. In Figure 7 the same stake is shown at two moments in time. In the beginning, the stake bottom is fixed in the snow layer A at the depth  $H_1$ , while snow layer B is located at the surface. The stake height above the surface is  $h_0$ . Some time later, the stake has apparently sunk into the snow due to accumulation, and the new stake height is  $h_1$ . However, the actual accumulation is higher than the difference  $h_0 - h_1$  due to the snow densification (note the thinning of the AB layer). The correction  $\Delta B$  is the difference between the thickness of the AB layer in the beginning and in the end ( $H_3 - H_2$  in Figure 7a). In order to calculate the corrected snow accumulation, we have to define the snow mass in the BC layer (i.e., layer accumulated during the given period of time), which is equal to the difference of the mass in AC layer and AB layer. The latter masses can be easily determined as soon as we know the snow density profile to the depth of  $H_4$ . This approach is only valid when two conditions are met: (1) the density profile is stable in time (known as Sorge's law) and (2) the snow mass between two

fixed snow layers is constant (i.e., vapor mass transport is negligible).

[25] One can derive the equation for the correction of annual snow accumulation (the length measurement):

$$\Delta(\Delta h) = \dot{b} \left( \frac{1}{\rho_0} - \frac{1}{\rho_b} \right), \quad (1)$$

where  $\dot{b}$  is the mean annual SMB,  $\rho_b$  is the snow density at the depth of stake bottom, and  $\rho_0$  is the density of surface snow. From equation (1) it is seen that the correction value is positively related to the vertical gradient of snow density (Figure 7).

[26] Similar studies have been made by *Takahashi and Kameda* [2007]. They showed that the snow density at the stake bottom should be used for SMB calculations as

$$\dot{b} = \bar{\rho}_b \Delta h, \quad (2)$$

where  $\Delta h$  is the difference in stake height between two measurements, which is the same as the change of stake bottom depth;  $\bar{\rho}_b$  is the average snow density between the two depths of the stake bottom, assuming a stable density profile. This correction is 1 – 27% of the annual snow accumulation at inland sites like Vostok and Dome

**TABLE 2. Some Error Sources of SMB Estimates for Different Methods<sup>a</sup>**

Source	Type of Error	Affects
<i>Stakes</i>		
Length measurement	height	mass
Anchoring/submergence	height	mass
Surface roughness	height	mass
Density	mass	mass
<i>Ultrasonic Sounders</i>		
Air temperature and profile	sound velocity	mass
Sound velocity	height	mass
Density	mass	mass
Fallen rime	height	mass
Anchoring/submergence	height	mass
Surface roughness	height	mass
Drifting snow	height	mass
<i>Cores</i>		
Annual cyclicity	ambiguities in age	time
Hiatus (erosion)	ambiguities in age	time
Time markers	time of deposition	time
Density from weighing	mass, core volume	mass
Density from profiling	mass, core volume	mass
Dynamic layer thinning	layer thickness	mass
<i>GPR</i>		
IRH resolution and tracking	traveltime	time, mass
Wave speed profile	depth	time, mass
Age-depth profile	age	time
Transfer of age to IRH	age	time
Density measurements	mass, wave speed	time, mass
Extrapolating wave speed	depth error	time, mass
Interpolating/extrapolating density	mass	mass
Dynamic layer thinning	layer thickness	mass

<sup>a</sup>The source is the determined property or the assumption being made. The type of error indicates which error is physically being made. Finally, the affects indicate which of the three properties of SMB (mass per area and time) are affected by the error. For stakes and ultrasonic sounders, the date of measuring is known best, so time is not affected. For cores, the annual cyclicity is variation in signals used for counting years. For GPR, tracking is the uncertainty when following a reflection horizon along the profile, and extrapolation is estimation of density and wave speed profile between different core locations.

Fuji and cannot be neglected. Information on density is not always available (particularly for older records); thus conversion of changed snow height to mass may not be possible or will have a large uncertainty.

### 2.2.2. Accumulation Uncertainties From Stakes

[27] The uncertainty of the stake-based accumulation determination consists of two main sources: (1) measurement errors, briefly described in section 2.2.1 for accumulation and density measurements and (2) natural noise predominantly caused by the small-scale relief-related spatial variability of snow accumulation and density (Table 2). Apparent accumulation uncertainties for field data are based on all possible sources of error; however, natural noise is the largest source of error, with all other sources at least 1 order of magnitude less. It is worth noting that the uncertainty is inversely related to the number of stakes and the period of observation. As an example, the standard deviation of accumulation, as measured at an individual stake in terms  $\Delta h$ , is  $\sigma(\Delta h) = 5.3$  cm, i.e., nearly equal to the mean annual accumulation at Vostok. The corresponding standard deviation for the surface (at 20 cm depth) snow density is  $\sigma(\rho) =$

$33 \text{ kg m}^{-3}$ , i.e., about 10% of the mean. This means that the density is a comparatively less noisy parameter than the height measurement. The standard error in accumulation (calculated from the equation  $\sigma(\dot{b})/\dot{b} = \sigma(\Delta h)/h + \sigma(\rho)/\rho$ ) from a single stake is thus  $18 \text{ kg m}^{-2} \text{ a}^{-1}$ , or about 85% of the mean annual accumulation at Vostok. This means that a single-stake observation in low-precipitation areas of central Antarctica provides practically no information about the mean accumulation rate. The standard error of annual accumulation decreases as the period of observations increases. One could expect that the error would follow the known equation  $\sigma(\dot{b}) = \sigma(\dot{b}_i)/\sqrt{n}$ , where  $\sigma(\dot{b}_i)$  is the standard error of accumulation for a 1-year period and  $n$  is the number of 1-year observation periods. Thus, after 30 years of observations the error must be about  $3 \text{ kg m}^{-2} \text{ a}^{-1}$ . Instead, previous research (not published) showed that the standard accumulation rate error for a single stake in a stake farm at Vostok after a 30-year period of observations is as low as  $1.7 \text{ kg m}^{-2} \text{ a}^{-1}$ . This is related to the fact that as the observation period becomes longer, the given stake becomes representative for a wider area and thus the accumulation at the adjacent stakes becomes correlated. In this case, the uncertainty versus time function shown above becomes closer to linear:  $\sigma(\dot{b}) = \sigma(\dot{b}_i)/n$ . The uncertainty in the 1-year accumulation value from the whole stake farm is inversely proportional to the number of stakes  $k$ :  $\sigma_k(\dot{b}) = \sigma(\dot{b})/\sqrt{k}$ . For the Vostok Station stake network ( $k = 79$ ) we can expect that the error for accumulation is 0.6 cm. In fact, this value may be slightly higher because, as we showed before, the accumulation at the adjacent stakes is not completely independent. Corresponding errors for density and accumulation values are  $3 \text{ kg m}^{-3}$  and  $2.0 \text{ kg m}^{-2} \text{ a}^{-1}$ . The error of the mean annual accumulation value from the Vostok Station stake network is difficult to evaluate properly, but on the basis of the data discussed here we estimate it as  $1.7/\sqrt{79} = 0.2 \text{ kg m}^{-2} \text{ a}^{-1}$ . This value is less than the  $0.8 \text{ kg m}^{-2} \text{ a}^{-1}$  determined from the time series of annual accumulation values over the last 30 years, but the latter value also includes the natural temporal variability of accumulation. In general, only long-term observations will result in reliable accumulation values. Spectral analyses of accumulation measurements from single stakes with respect to annual average accumulation of a stake farm in the Dome C drainage area show that single stakes or cores are not representative on an annual scale. Even for a site with high accumulation ( $250 \text{ kg m}^{-2} \text{ a}^{-1}$ ), sastrugi with a height of about 20 cm cause significant noise in the individual measurements [Frezzotti et al., 2007].

### 2.2.3. Optimal Parameters for Stake Farms and Lines

[28] When planning to set up a stake network in Antarctica, the first question to be addressed after defining the accumulation scale aimed at, is “What are the optimal parameters of the network (in terms of data quality, effort needed to make the measurements) for this particular area?” Large networks containing more stakes will produce more accurate results, but more time and effort are required to make the measurements. The network size and stake number also depend on the temporal and spatial scales of

accumulation one is interested in. A trade-off has to be made between the error of the estimated accumulation mean (decreasing with the number of stakes) and the size of the area for which the estimate is representative. The distance between stakes is determined by the size of the stake farm or line and is often restricted by logistic constraints. Unfortunately, the best sampling strategy for a specific area is often made clear only after measurements of the stake farm have already been made.

[29] As an example, optimal parameters (see Appendix A) have been determined for the Vostok area from a stake farm [Barkov and Lipenkov, 1978]. For comparatively small (within first hundred meters) stake farms the accuracy of the obtained accumulation values is much more dependent on the size of the farm than on the number of stakes, which is due to the influence of microrelief of the snow surface. Keeping the same amount of stakes but increasing the size of the stake network rapidly decreases the standard error of the accumulation value. At the size of 500–1000 m a saturation value is achieved. This value depends on the dominant larger-scale glacier relief forms. For example, in the megadune areas the saturation value must be of the order of the megadune length, i.e., less than 5 km. Further increasing the stake network dimensions does not significantly change the accuracy, although it does increase the represented area.

#### 2.2.4. Examples for Long-Term Measurements and Current Approaches

[30] In Wilkes Land, the Indian-Pacific sector of Antarctica, stake measurements have been performed for half a century. An early overview of measurements and results is presented by Young *et al.* [1982]. Stake measurements of Antarctic SMB by the Russian (Soviet at that time) Antarctic Expedition (RAE) began with the opening of the first Russian base, Mirny (in 1956). Subsequently, stake networks were established at all permanent Russian stations (Vostok, Novolazarevskaya, Molodezhnaya, Bellingshausen, Leningradskaya; for a list of Antarctic stations see the Scientific Committee on Antarctic Research (SCAR) Web site <http://www.scar.org>), with varying network shapes, size, and number of stakes to obtain optimal setups. The most extensive data were obtained at Molodezhnaya (~11 stake networks and profiles operating from 1966 to 1981) and Novolazarevskaya. Stake lines were established along the RAE routes (Pionerskaya–Dome C, Komsomolskaya–Dome B, Mirny–Vostok). The best results were achieved from the permanent 1410-km-long Mirny–Vostok traverse, where about 800 stakes were set up in intervals of 0.5–3 km, as summarized by Lipenkov *et al.* [1998]. In addition, seven stake farms ( $1 \times 1 \text{ km}^2$ , 20–40 stakes each) were organized along the traverse in the 1970s and annually visited until the 1980s. The stake network at Vostok was set up in 1970 and is still in operation. Monthly observations allow for a robust characterization of SMB in this region and provide a prototype for the extremely low accumulation areas of central Antarctica. Results were obtained on the interannual and seasonal variability of SMB and responsible mechanisms [Barkov and Lipenkov, 1996; Ekaykin, 2003]. Among these results are the exclusion of temporal trends of mean accu-

mulation rate ( $22 \text{ kg m}^{-2} \text{ a}^{-1}$ ) over the observation period and the identification of different relief forms of intermediate scale, between microrelief and megadunes, called mesodunes [Ekaykin, 2003]. Migration of these mesodunes causes a relief-related (nonclimatic) temporal variability of SMB at a single point with periods of up to 20–30 years [Ekaykin *et al.*, 2002]. In eastern Wilkes Land, seasonal surface observations of stakes and relief forms were carried out by Australian expeditions [Goodwin, 1991].

[31] Since the International Geophysical Year (1957–1958), a variety of stake networks have been established at South Pole Station. These include a 42-stake pentagon and an 11-km cross consisting of six arms with a stake interval of 300 m. Details are summarized by Mosley-Thompson *et al.* [1995]. Remeasurements were carried out at irregular intervals. In November 1992, Ohio State University (OSU) set up a network of 236 stakes radiating outward from South Pole Station as six 20-km-long arms, at an interval of ~500 m. Remeasurements are performed annually in November. Results from the first 5 years of measurements indicate that earlier estimates, that one in 10 years has negative SMB [Gow, 1965; Mosley-Thompson and Thompson, 1982], are probably too high. At least in recent times at the South Pole [Mosley-Thompson *et al.*, 1999], less than 1% of all observations revealed zero or negative SMB. Moreover, the same study by Mosley-Thompson *et al.* [1999] reveals that the net accumulation of about  $85 \text{ kg m}^{-2} \text{ a}^{-1}$  during the period 1965–1994 is the highest 30-year average of the last 1000 years at the South Pole.

[32] Pettré *et al.* [1986] report SMB data along a transect from the coast near Dumont d’Urville to Dome C. Most of the data are from stakes, with the stakes from the coast to 32 km inland being surveyed over as long as 21 years (1971–1983). During the old Dome C deep ice core drilling, a stake farm was measured during 1978–1980 to study spatiotemporal variability of a single core [Palais *et al.*, 1982; Petit *et al.*, 1982]. Between 1998 and 2001, at Talos Dome and along the traverse in the Dome C drainage area [Magand *et al.*, 2004; Frezzotti *et al.*, 2005, 2007], 17 stake farms were set up by the Italian Antarctic Programme, each including from 30 to 60 stakes at 100-m intervals in the shape of a cross within an area of  $4 \text{ km}^2$ , each centered on a core site. Measurements were carried out annually at four sites where automatic weather stations (AWS) have been installed. Other stake farms have been remeasured only 2–4 times. Stake farm readings show that accumulation hiatuses (no accumulation or even ablation) can occur at sites with average accumulation rates below  $120 \text{ kg m}^{-2} \text{ a}^{-1}$ .

[33] In the Lambert Glacier Basin (LGB) area, stake measurements were performed by the Australian and Chinese National Antarctic Research Expeditions (ANARE, CHINARE). Results of early stake lines (1960s and 1970s) along the ANARE LGB traverse routes are summarized by Morgan and Jacka [1981] and Budd and Smith [1982]. Later measurements included stake networks (1983–1993) and multiannual combinations of networks and stakes (2 km interval) (about 1989–1994), comple-

mented by cores [Goodwin et al., 1994; Ren et al., 1999, 2002; Goodwin et al., 2003; Xiao et al., 2005]. Extension of earlier routes with 2-km stake intervals provides a continuous line over 1100 km from Zhongshan station to Dome A (1996–1999 [Qin et al., 2000]).

[34] Farther to the west a number of stake lines and farms have been and are still being operated along the Dronning Maud Land coast. In eastern Dronning Maud Land, the Japanese Antarctic Research Expeditions (JAREs) deployed stakes since 1968 [Takahashi and Watanabe, 1997]. Stakes spaced at 2-km intervals were set from the coastal area to inland sites at Dome Fuji over a distance of more than 1000 km. Eleven stake farms were set en route from Dome Fuji to the plateau (e.g.,  $6 \times 6$  at 20 m intervals, 50 rows of stakes over 100 m; see Kameda et al. [2007] for details). Six stake farms from the coast to Mizuho were established in 1971. Most of these stakes and stake farms have been surveyed at least once per year. Results are given by Takahashi and Watanabe [1997], Takahashi et al. [1994], Fujiwara and Endoh [1971], Endo and Fujiwara [1973], and Kameda et al. [1997, 2008].

[35] At the former Georg Forster station (GDR), three stake lines, each 85–115 km in length with stake spacings of 1–5 km, were operated from 1988 to 1993 in an area of strongly differing accumulation regimes containing blue ice areas [Korth and Dietrich, 1996]. Other examples are the stake farm operated near the German Georg-von-Neumayer station 1981–1993 and near Neumayer station since 1992 [Schlosser et al., 2002]. Measurements were extended by a 450-km stake line (500-m interval) between Neumayer station at the coast and the Heimefrontfjella (Figure 6) [see Rotschky et al., 2006] (half of the traverse route to the EPICA deep drilling at Kohnen station), which has been revisited annually since 1996. A stake line between the Swedish stations Svea and Wasa was established in January 1988 [Stroeven and Pohjola, 1991] and partly surveyed until 1998 [Isaksson and Karlén, 1994]. A new 300-km profile was established in 2002/2003 for a long-term SMB monitoring [Swedish Antarctic Research Programme, 2003]. Shorter lines, also partly in conjunction with GPR, were investigated near the Finnish Aboa station [Isaksson and Karlén, 1994; Sinisalo et al., 2005] and on Lydden ice rise (Brunt ice shelf) [Vaughan et al., 2004]. In blue ice areas occurring in mountain regions of East Antarctica, stake networks were surveyed to gain information on ablation rates and to study meteorite traps [Bintanja, 1999; Folco et al., 2002]. The data suggest that ablation rates decrease with increasing distance from the ice sheet edge, with values from 350 to 30 kg m<sup>-2</sup> a<sup>-1</sup>.

[36] An example of a contemporary integrated SMB approach is the Les Glaciers, un Observatoire du Climat (GLACIOCLIM) Surface Mass Balance of Antarctica (SAMBA, see <http://www-lgge.obs.ujf-grenoble.fr/~christo/glacioclim/samba>) observation system, a French-Italian cooperation. The French GLACIOCLIM glacier observation system consists of a  $\sim 1$ -km<sup>2</sup> stakes network (50-m interval) located on the coast of Adélie Land, with year-round surveys performed monthly. Additionally, vari-

ous meteorological instruments in the area are used to study the warm/ablating region to develop an understanding of SMB genesis and to verify local modeling capabilities in such a region. An  $\sim 100$ -km stake line (interval 0.5–2.5 km with annual observations), recently extended to 150 km from the coast toward Dome C, is used for sampling the coast to plateau transition and sampling spatial scales consistent with climate models and with satellite data. Along the stake lines, two AWS are deployed, one of which is accompanied by a 1-km<sup>2</sup> stake network (250-m interval). Aiming at the sampling of both small and large scales of accumulation (model, satellite), three 1-km<sup>2</sup> stake networks (40-m interval) were set up in the Dome C area in 2005/2006, with the stake farms located 25 km apart. This network is surveyed at least once a year and may be surveyed more frequently now that the Concordia station is permanently inhabited. Meteorological data are available from the station. The focus of future projects is the short-term variability at various sites by measuring precipitation with spectrometers and accumulation with ultrasonic sounders. The observation system and monitoring are expected to last at least 10 years. Examination of the data should allow us to address the climate–accumulation interaction as well as climate–model validation on subannual to multiannual scales, which will also enable analysis of interannual variations and processes.

### 2.3. Point Measurements at the Surface: Ultrasonic Sensors

[37] A relatively recent ( $\sim 10$ –15 years) technique for monitoring SMB in East Antarctica is tracking surface height changes by way of ultrasonic height rangefinders. These sensors determine the vertical distance to the snow surface by measuring the elapsed time between emission and return of an ultrasonic pulse. An air temperature measurement is required to correct for variations of the speed of sound in air.

[38] Until quite recently, ultrasonic height rangefinders were mainly used to study the growth and decay of the seasonal snowpack in the Northern Hemisphere. As the design evolved (for instance, by including a multiple echo processing algorithm that stores several reflected signals to improve operational efficiency and to decrease the problem of obstacles), ultrasonic height rangefinders also found their way into mass balance research of high-altitude/high-latitude ice masses, such as Alpine and Arctic valley glaciers [Oerlemans, 2003; Klok et al., 2005] and the Greenland ice sheet [Steffen and Box, 2001; Van de Wal et al., 2005; Smeets and van den Broeke, 2008]. With rugged housing and improved low-temperature specification (nowadays typically down to  $-45^\circ\text{C}$ ), application of ultrasonic height rangefinders in Antarctic mass balance studies has become widespread. They are deployed in a wide range of climate settings, such as the McMurdo Dry Valleys [Doran et al., 2002], the high accumulation coastal zone of East Antarctica [McMorrow et al., 2001] and West Antarctica [van Lipzig et al., 2004b], and the dry East Antarctic interior [Reijmer and Broeke, 2003; van den Broeke et al., 2004b] as well as in the intermediate

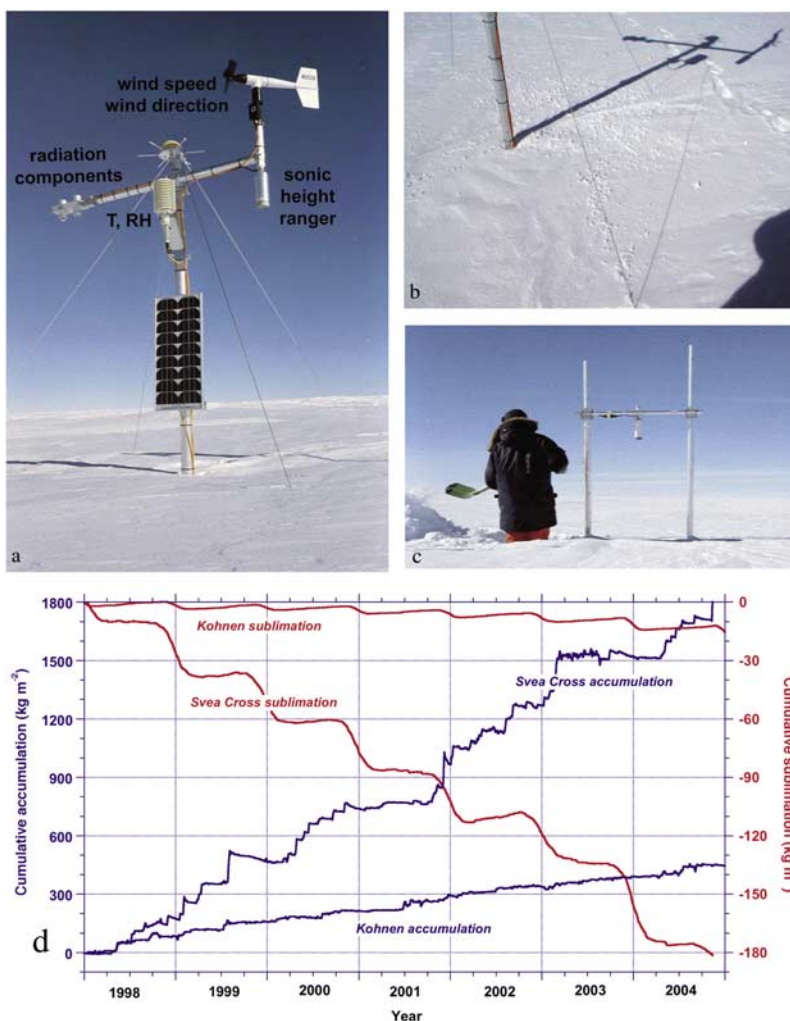


**Figure 8.** (a) Picture of AWS9 (near EPICA deep drilling in DML at Kohnen station), taken 4 years after installation, i.e., after about 1 m of snow has accumulated. The data logger and pressure sensor are buried in the snow. (b) Rime from the mast fallen on the ground might cause artificial accumulation. (c) Picture of stand-alone ultrasonic height meter, near AWS9. The data logger and pressure sensor are buried in the snow [van den Broeke et al., 2004b]. (d) Sample data from ultrasonic sounders: scale on left side is cumulative accumulation at AWS6 (Svea Cross) and AWS9 (Kohnen station) for the period 1998–2004; scale on right side is cumulative sublimation as calculated from AWS data. Note different y axis scales.

katabatic wind zone [Helsen et al., 2005] and on the ice shelves [Braaten, 1994].

[39] In East Antarctica and elsewhere, it is advantageous to mount the ultrasonic height ranger on or next to an automatic weather station (AWS, Figure 8). The AWS usually observes a range of atmospheric variables such as air pressure, air and snow temperature, air relative humidity, air velocity, and occasionally also radiation components [van den Broeke et al., 2004a]. This means that surface height changes can be interpreted in a mass balance framework, including sublimation from the surface and from drifting snow particles [Fujii and Kusunoki, 1982; Kaser, 1982; Clow et al., 1988; Stearns and Weidner, 1993; King et al., 1996, 2001; Bintanja, 2003]. Moreover, ultrasonic height data can be accepted/rejected on the basis of prevailing meteorological conditions (see section 2.3.4). Finally, the ultrasonic height ranger can be coupled to the AWS's power and data logging system. If more information is required on the spatial variability of

accumulation, several ultrasonic height rangers can be deployed in stand-alone mode, using a dedicated energy/data logger system (Figure 8c).

### 2.3.1. Typical Sensor Specifications

[40] As a typical example, here we list the specifications of a widely used ultrasonic height ranger, the SR50 produced by Campbell in Canada. Its limited dimensions (length 31 cm, diameter 7.5 cm, and weight 1.3 kg) make it convenient for use in AWS. With an operating temperature range down to  $-45^{\circ}\text{C}$  and proven working capacity down to  $-70^{\circ}\text{C}$  [van den Broeke et al., 2004b] it is suitable for operation in most parts of East Antarctica. The power requirement is 9–16 Vdc (volts direct current), so that it can be powered by the data logger's 12-Vdc power supply that is standard equipment on most AWS. The low power consumption (250 mA during measurement peaks) is favorable for operation on unmanned remote platforms. The measurement range (0.5–10 m) is suitable for operation in

accumulation as well as in ablation areas. The beam acceptance (maximum deviation from the vertical) of  $\sim 22^\circ$  poses no problem, as ablation-induced tilt of the mast normally does not occur in East Antarctica. The measurement accuracy is  $\pm 1$  cm or 0.4% of the distance to the surface, whichever is greatest, and data can be stored at a maximum resolution of 0.1 mm. To account for the temperature-dependent speed of sound, a correction for the deviation of the mean layer air temperature from a fixed calibration temperature (273 K) must be applied.

### 2.3.2. Advantages of Ultrasonic Height Ranglers for Mass Balance Studies

[41] The obvious advantage of ultrasonic height ranglers in comparison to stakes, snow pits, and cores is that individual accumulation/ablation events are unambiguously dated. This means that the temporal variability (e.g., the seasonal cycle or the summer and winter balance) of accumulation/ablation can be quantified. This has important applications in ice core paleoclimatology: if, for instance, a significant seasonal cycle in accumulation is present that changes in time, this introduces a bias in the climate signal extracted from cores. Case studies of chemical and physical anomalies in the firn can be based on individual accumulation events identified in the ultrasonic time series. In combination with AWS data, the accumulation/ablation time series of ultrasonic height ranglers can also be used to force snowpack models at their upper boundary or serve as a starting point for atmospheric trajectory calculations [Noone et al., 1999; Reijmer et al., 2002; Helsen et al., 2004]. Moreover, the temporal distribution of accumulation/ablation events is essential for validation of meteorological and/or mass balance models [Gallée et al., 2001; van Lipzig et al., 2004a]. Finally, for accurate energy balance calculations from single or multilevel AWS data it is desirable to know the exact height of the wind speed, temperature, and humidity sensors above the surface, as well as the depth of snow temperature sensors [van den Broeke et al., 2004b].

### 2.3.3. Technical Problems

[42] The ultrasonic height ranger needs to be mounted on a rack or mast so that its beam is perpendicular to the surface and is not obstructed. In accumulation areas, such as in East Antarctica, the sensor needs to be kept at least 0.5 m from the surface. This requires regular, expensive, servicing visits, the frequency of which depends on the rate of accumulation, the battery, and data storage capacity. In practice, the servicing interval will typically be once per year for coastal East Antarctica and once every 2–3 years for the interior plateau.

[43] Ultrasonic height ranglers are susceptible to failure from ageing, corrosion, or freeze-thaw delaminating of the acoustic membrane. Membrane failure rate has been observed to increase with age. Therefore, regular replacement of the acoustic membrane as a preventive measure should be considered for each visit. The proximity of open sea and/or an effective transport of sea salt to the observation site significantly reduce the lifetime of the acoustic membrane. In East Antarctica, this is usually not a big problem, and lifetimes of the membranes are typically 5 years or more.

[44] A common problem that prevents correct operation of the ultrasonic height sensor is that the acoustic membrane becomes obstructed by snow/rime. Sometimes mounting a cone around the sensor can prevent this, but this carries with it the risk of spurious ice accretion on the cone and subsequent structural failure of the mast. Riming problems are considerably reduced on the ice sheet slopes, away from the flat domes in the interior and the flat ice shelves near the coast. The reason is that along these slopes, semipermanent katabatic winds heat and dry the lower atmosphere resulting in a continuous flow of subsaturated air past the sensor, keeping it free of rime.

### 2.3.4. Data Interpretation Problems and Uncertainties

[45] Measurements from an ultrasonic height ranger performed at a single site suffer from the same problems of poor spatial representativity as single core or stake measurements (see section 2.1). These problems can be partly solved by using the same solutions as for the other techniques, i.e., operating a farm of stakes (or drilling several shallow cores) in the surroundings of the ultrasonic height sensor or deploying several sensors.

[46] Naturally, the measuring site should be far enough upwind from obstacles to avoid spurious lee accumulation or snow erosion on a flat surface. In East Antarctica, it is usually easy to find an upwind measurement site with a large fetch because surface conditions are usually very homogeneous and (katabatic) wind direction is exceptionally constant [van den Broeke and van Lipzig, 2003]. Dominant sastrugi orientation from surface or aerial surveys or a modeled wind field [van Lipzig et al., 2004a] can help in determining the prevailing wind direction if no local meteorological data are available.

[47] Once a suitable spot is found, raw distance data should be collected and the temperature-dependent speed of sound correction applied after data collection. In-sensor temperature measurements on older sensor types should preferably not be used because the sensor can overheat significantly under low wind speed/strong insolation conditions, fouling the surface height data. It is best to measure the air temperature independently with a ventilated dedicated sensor placed approximately halfway between the ultrasonic height ranger and the surface. A more elaborate alternative is to measure temperature at sensor height and at the surface (e.g., using a longwave radiation sensor), to calculate the temperature profile (using similarity theory and appropriate stability functions [e.g., Andreas, 2002; Holtslag and Brujin, 1988]) and to take the mean temperature of the air layer. In East Antarctica, it is worthwhile to spend some effort to correctly perform the temperature correction because the radiation balance at the surface is often negative so that the temperature difference between the ultrasonic height ranger and the surface in the stably stratified surface layer can be considerable, up to 5–10 K in the first couple of meters during calm, clear conditions.

[48] At sites where riming occurs frequently, rime collected on the mast structure can fall off and collect at the surface, leading to artificially enhanced accumulation



(Figure 8b). This will only affect low-accumulation sites on the interior plateau.

[49] Once the wind speed exceeds a certain threshold, snowdrift occurs in the near surface air layer [Li and Pomeroy, 1997; Mann et al., 2000]. This can lead to an erroneous height reading from a reflection from a dense drifting snow layer. Usually, AWS data can be used to detect snowdrift events so that these readings can be discarded.

[50] The technical and operational difficulties described in this section and section 2.3.3 (see also Table 2) reduce the 1-cm accuracy under laboratory conditions to an operational accuracy of typically 2–3 cm. This accuracy is sufficient for high-accumulation sites, but it is not good enough to detect the often much smaller precipitation events that are common on the interior plateau of East Antarctica. Here, small events ( $<1 \text{ kg m}^{-2}$ ) make up most of the total accumulation [Reijmer et al., 2002].

[51] A large uncertainty is introduced when converting instantaneous height changes from the ultrasonic ranger to mass changes. In practice, continuously measured height changes are converted to mass changes through multiplication by the average density of the accumulated snowpack since the last visit, as measured in a snow pit or firn core (see section 2.1). Although this yields a correct value of the total accumulation integrated over the time interval between the pit studies, the sometimes considerable density variations in the upper firn layers result in an uncertainty of up to 20% or worse for mass changes on the event timescale.

[52] Another problem affecting ultrasonic height measurements in East Antarctica is the depth and temperature dependence of the firn densification rate. Under idealized steady state conditions, assuming continuous accumulation and a constant temperature, the vertical speed in the firn depends only on the local density (Sorge's law). Under these assumptions, knowing the anchor depth of the structure holding the ultrasonic height ranger and the density profile suffices to correct for this. Unfortunately, accumulation is not a continuous, steady state process: after a stepwise increase in surface height due to an accumulation event, the densification rate of a freshly fallen snow layer decreases with time. In addition, the densification process depends on temperature, causing accelerated summertime densification of the upper snowpack [Dibb and Fahnestock, 2004; Li and Zwally, 2002] and on the microstructure [Freitag et al., 2004]. The summer heat wave slowly penetrates the firn, locally enhancing firn densification rates when it passes. This implies that only time-dependent firn densification modeling along the lines of Li and Zwally [2004], at least taking into account temperature, can account for the differential densification effect in a physically realistic way.

### 2.3.5. A Data Example From East Antarctica

[53] The following data example demonstrates both the great value and the problems of using ultrasonic height ranger data in East Antarctic mass balance research. Figure 8d shows 7 years (1998–2004) of accumulation derived from ultrasonic height ranger data from two AWS sites in western Dronning Maud Land (DML; left scale). The first AWS is

located at Svea Cross ( $74^{\circ}28.9'S$ ,  $11^{\circ}31.0'W$ , 1160 m above sea level (asl)), at the foot of the Heimefrontfjella in the katabatic wind zone. The second is located adjacent to Kohnen station ( $75^{\circ}00.2'S$ ,  $0^{\circ}00.4'E$ , 2892 m asl, see Figure 8) on the Amundsenisen of the flat East Antarctic plateau. In addition to surface height changes, the AWSs measure wind speed and direction, temperature, relative humidity, shortwave and longwave radiation fluxes, air pressure, and snow temperatures. The sampling frequency typically is 6 min from which 1-h averages are calculated and stored in a Campbell CR10 data logger with separate memory module.

[54] The ultrasonic data (Figure 8d) have been corrected for temperature but not for differential firn densification. To convert height changes to mass changes, we applied a mean density of  $396 \text{ kg m}^{-3}$  at Svea Cross and  $307 \text{ kg m}^{-3}$  at Kohnen. Missing data, mainly due to riming (20% at Kohnen,  $<1\%$  at Svea Cross), have been linearly interpolated. To remove some residual noise, a cubic spline fit was applied to the data. Applying linear fits to the cumulative mass balance curve yields values for the specific SMB of  $243 \text{ kg m}^{-2} \text{ a}^{-1}$  at Svea Cross and  $64 \text{ kg m}^{-2} \text{ a}^{-1}$  at Kohnen. These values agree with accumulation derived from shallow firn cores drilled at these sites.

[55] The data show that the measurement accuracy of the ultrasonic height ranger is insufficient to unambiguously resolve individual precipitation events at the low-accumulation site Kohnen. The record rather shows a continuous, slow accumulation interspersed with occasional larger events. No significant surface lowering is observed between accumulation events. At Kohnen, even during summer, temperatures are apparently too low to force strong sublimation and a seasonal cycle in the densification.

[56] This is very different at Svea Cross, where the accumulation occurs in large, well-defined events, some of which can also be found in the record of Kohnen. In between these accumulation events, dry periods lasting up to 8 months occur at Svea Cross. During these dry episodes, significant surface lowering occurs in the summer period (November–February). To determine which part of the surface lowering is caused by sublimation, AWS data were used to calculate the turbulent flux of latent heat [van den Broeke et al., 2004b]. The scale on the right in Figure 8d indicates the resulting cumulative sublimation/deposition. As can be seen, sublimation dominates during summer, averaging typically 25 mm water equivalent (about 6.5 cm of snow) at Svea Cross and about 10 times less at Kohnen. At Svea Cross, this accounts for part but not all of the surface lowering that is observed during summer; enhanced summer densification of the firn layer enclosed by the AWS anchor depth and the surface accounts for the residual surface lowering.

### 2.4. Point Measurements at Depth: Snow Pits, Firn, and Ice Cores

[57] Snow pits and core drilling (Figure 9) are used to access older snow and ice below the surface. Their deployment retrieves sequences of buried snow and ice from only a single operation, as layers of different age are accessed at

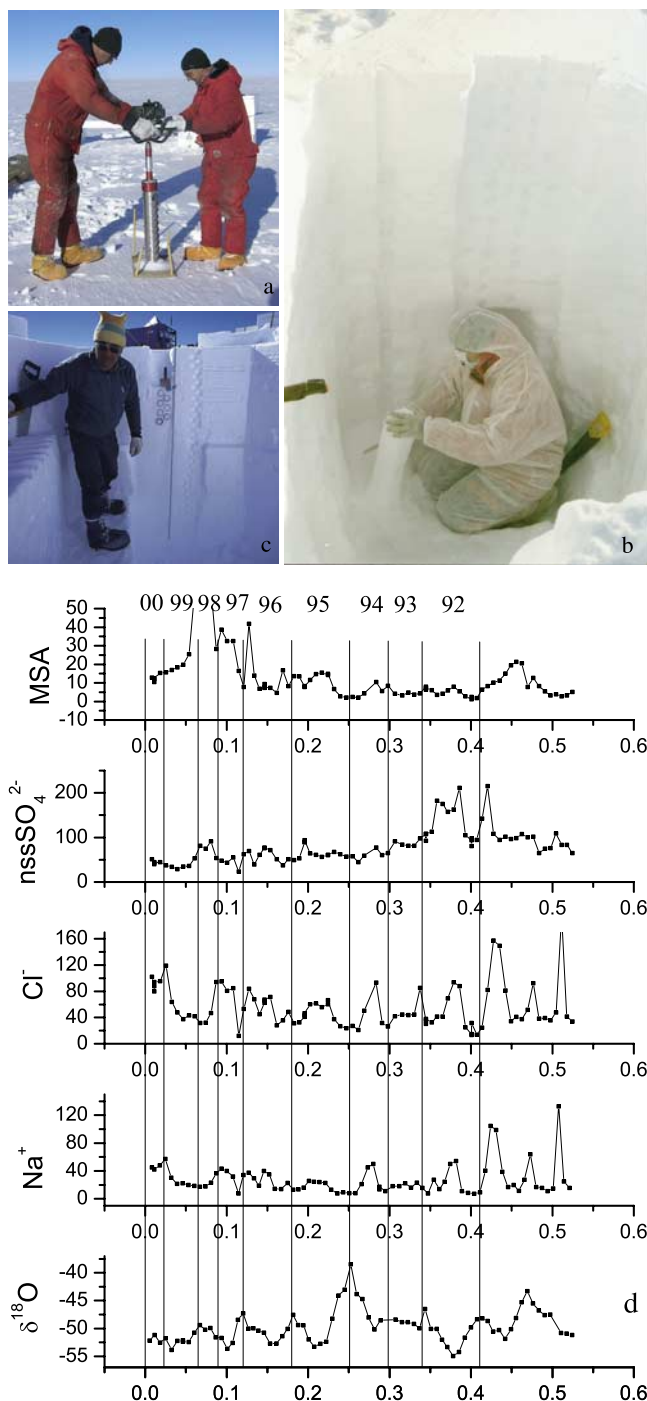


**Figure 9.** (a) Firm core drilling. Typical drill diameters are 3 inches (7.6 cm) and 4 inches (10.2 cm). The wooden board marks the reference level of the snow surface. (b) Taking samples in a 3-m-deep snow pit. To avoid sample contamination, the person wears a clean room suite. (c) Taking density measurements with tubes in a snow pit with a crossover pattern (visible to the left of the ruler in the center). (d) Example from pit MC in DML on how several different species have been used in dating the pits [Karlöf *et al.*, 2005b] (with permission of the International Glaciology Society). They mainly used the oxygen isotope data with support of ions to date the pits. Years (1992–2000) are indicated at the top; year transitions are marked with vertical lines.

once. Apart from accumulation, time series for a number of other parameters are established as well.

[58] The SMB corresponding to a sample in a certain depth interval (and thus age interval) is most generally derived from the ratio of mass (or water equivalent depth) of the considered sample to the time span that the sample range covers. As for stake and ultrasonic measurements, determination of density is thus one important key. In contrast to those methods, which monitor the surface and obtain time series of surface accumulation only by repeated observations of surface height at an accurately known point in time, the determination of the age as a function of depth is the other key parameter. One derives this function for instance by interpolating discrete *time markers* (e.g., *volcanic horizons*) or counting of layers of known origin, like annual signals [Whitlow *et al.*, 1992].

#### 2.4.1. Density Measurements

[59] The techniques presented in sections 2.4.1.1–2.4.1.3, used to determine density as a function of depth along cores, complement the classic surface snow density measurement methods described in section 2.1.

##### 2.4.1.1. Classic Technique

[60] Firm core density is most often determined by measuring core length and diameter and weighing each core section on an electronic scale directly after core retrieval in the field [Isaksson *et al.*, 1996; Oerter *et al.*, 1999; Magand *et al.*, 2004; Frezzotti *et al.*, 2005]. However, problems with this simple method are that the snow in the uppermost meter is usually poorly consolidated and loss of material is therefore unavoidable, reducing the accuracy of volume calculations. It is therefore common practice for firm core retrieval that density is measured in a pit (about 2 m depth) in direct connection to the drill site where stratigraphic studies and snow sampling can also be performed. Another problem is that the diameter of the core pieces changes depending on the snow type. For instance, less dense snow can be compacted or lost, resulting in an overestimation of density [Karlöf *et al.*, 2005b]. Cores with a wider diameter (e.g., 4 inch, 10.2 cm) reduce the uncertainty in density measurements. Core imperfections that can occur during drilling alter the volume of the core segment and can thus affect density measurements.

##### 2.4.1.2. Radiation Attenuation Profiling

[61] Radiation attenuation profiling is based on the absorption and scattering of hard radiation to determine ice density. The ratio between transmitted and received ray intensity is a measure for absorption and scattering, which can be related to snow, firm, and ice density. Currently, three types of radiation are utilized:  $\gamma$  rays, X rays, and neutrons. In the case of  $\gamma$  attenuation profiling (GAP) [Gerland *et al.*, 1999; Wilhelms, 1996, 2000] the  $\gamma$  ray originates from a radioactive source (e.g.,  $^{137}\text{Cs}$ ) and passes through the core in transverse direction to a detector. For monochromatic radiation the mass absorption coefficient is known with 0.1% relative error. The statistical intensity measurement error is determined by free-air reference. To reduce statistical errors, multiple (usually more than 10) measurements are averaged. The calibrated detector signal has to be

corrected for variations in core diameter. For high-quality cores, the diameter is accurate to  $\leq 1$  mm. The possible influence at maximum misalignment of the core within the measurement bench has to be accounted for, as well as cracks from core breaks at the end of an ice core. The precision of the GAP density measurements is typically around  $10 \text{ kg m}^{-3}$  for a 100-mm-diameter core. The depth resolution of GAP depends on the characteristics of the radioactive source, like ray diameter and dispersion characteristics. Typical resolution is on the order of 1 cm, with measurements carried for redundancy to the subcentimeter level.

[62] For X-ray attenuation profiling [Hori *et al.*, 1999], the accuracy is about 1%, the same as for the  $\gamma$  attenuation method. However, field measurements by the X-ray method are difficult since a large experimental system is required. It is therefore mostly applied in the laboratory.

[63] In contrast to these two methods, neutron probes (Walingford probe) [Morris and Cooper, 2003] are operated in the borehole instead of along the core. The neutron probe method thus has the advantage that only a (reasonably smooth) hole instead of a core is necessary for determining density profiles. The depth resolution, however, is physically limited to 10 cm. The uncertainty of the derived density is on the order of  $10 \text{ kg m}^{-3}$ .

#### 2.4.1.3. Dielectric Profiling

[64] The complex dielectric constant is expressed as  $\epsilon^* = \epsilon' - i\epsilon''$ . In the case of ice, the real part  $\epsilon'$ , the ordinary complex permittivity of the medium, mainly depends on density. The imaginary part  $\epsilon''$ , the dielectric loss factor, is related to conductivity  $\sigma$  and radian frequency  $\omega$  by  $\epsilon'' = \sigma(\epsilon_0\omega)^{-1}$ , where  $\epsilon_0$  is the permittivity of free space. Both parts of  $\epsilon^*$  can be determined with dielectric profiling (DEP) [Moore and Paren, 1987]. A DEP device is essentially a calibrated and guarded scanning capacitor. The core is put between two semispheres. Its conductance and admittance are determined by applying alternating current potentials, typically at a single frequency of 10 kHz to a few hundred kilohertz, which are then converted to  $\epsilon^*$ . For accurate devices, the real and imaginary components can each be determined to within 1% [Wilhelms, 2000]. A widely used formula relating the ordinary relative permittivity  $\epsilon'$  and density  $\rho$  is based on the approximation derived by Looyenga [1965] from theoretical consideration of air distributed in a dielectric medium, with spherical approximations of bubbles,  $\epsilon' = ((\rho/\rho_{\text{ice}})[\sqrt{3}\epsilon'_{\text{ice}} - 1] + 1)^3$ . Other approximations were derived from comparison of density and permittivity measurements, e.g., by Robin *et al.* [1969], Tiuri *et al.* [1984], or Kovacs *et al.* [1995]. The latter refined an empirical approximation,  $\epsilon' = (1 + 0.845\rho)^2$ , which is now widely used for permittivity-density conversions [Kovacs *et al.*, 1995]. They obtained a standard error of  $\pm 0.031$  for  $\epsilon'$ . Both of the above formulae take only the real part of  $\epsilon^*$  into account, causing a mixing of the complex components [e.g., Barnes *et al.*, 2002]. Recently, Wilhelms [2005] demonstrated that neglect of complex mixing for the density-permittivity relation could result in errors in  $\epsilon^*$  and suggested extension of Looyenga's formula into complex

space. In general, integration of the density-depth profile to obtain cumulative mass results in a higher accuracy, as statistical uncertainties of abnormally high or low values are averaged out.

#### 2.4.2. Age Estimates

[65] Two main methods are used to date firm and ice cores (from seasonal to century scales): counting of seasonal variations of various parameters (physical, chemical, isotopic) that show cyclic variations during the year (Figure 9d) and identifying prominent horizons of known age, such as acid layers from dated volcanic eruptions or radioactive fallout from atmospheric thermonuclear bomb tests. A third method exploits the natural decay of radioactive materials. The method used depends on the purpose of the study and the accumulation rate at the site; however, many studies utilize all three methods.

##### 2.4.2.1. Seasonal and Annual Layer Counting

[66] 1. The stable isotope ( $\delta^{18}\text{O}$  and  $\delta\text{D}$ ) stratigraphy [Dansgaard *et al.*, 1973] is a method commonly used to determine annual layers [e.g., Morgan *et al.*, 1991] in areas with higher accumulation (above about  $80\text{--}100 \text{ kg m}^{-2}\text{a}^{-1}$ ). The oxygen and hydrogen isotopic composition of polar snow is mainly related to the condensation temperature [Dansgaard, 1964]. One advantage of the stable isotope stratigraphy is that no special precautions during the sampling procedure are necessary to prevent sample contamination [Legrand and Mayewski, 1997]. However, at least seven to eight samples per year are needed to correctly resolve seasonal and thus annual signals. The seasonal cycle of  $\delta^{18}\text{O}$  (or  $\delta\text{D}$ ) is usually well developed only in the upper part (5–10 m) of the snowpack because of diffusion during densification [Johnsen, 1977; Legrand and Mayewski, 1997] in the postdepositional process. As few studies have been dedicated to the analysis of postdepositional effects on Antarctic snow composition, the possibility that wind-driven ablation [Ekaykin *et al.*, 2002; Frezzotti *et al.*, 2004] as well as sublimation [Neumann and Waddington, 2004; Neumann *et al.*, 2005; Satake and Kawada, 1997] may induce systematic effects on isotope levels has to be kept in mind. These could affect seasonal and annual signals [Masson-Delmotte *et al.*, 2008] and thus SMB measurements. As suggested by Masson-Delmotte *et al.*, systematic measurements of water vapor and snow isotopic composition should provide a means of disentangling the effect of depositional and postdepositional processes and, as a consequence, allow a better understanding of their effect on SMB estimates.

[67] 2. Chemistry of discrete firm/ice core samples has been routinely analyzed for major ion content (e.g., via ion chromatography). Over the last decade, continuous flow analysis (CFA), high-resolution fast ion chromatography (FIC), and continuous melting discrete sampling (CMDS) methods have been improved such that a quasi-continuous record of a number of different species is measured simultaneously along a single core [Fuhrer *et al.*, 1993; Sigg *et al.*, 1994; Fuhrer *et al.*, 1996; Röthlisberger *et al.*, 2000; Sommer *et al.*, 2000b, 2000a; Udisti *et al.*, 2000; Traversi *et al.*, 2002; Rasmussen *et al.*, 2005; Osterberg *et al.*, 2006].

Typical markers for seasonal layer counting are methane-sulphonic acid (MSA) and nonsea-salt (nss) sulphate ( $\text{nss SO}_4^{2-}$ ), the main oxidation products of dimethylsulphide (DMS), which are mainly produced by marine biogenic activity [Saigne and Legrand, 1987]. Study of seasonal cycles of sulfur aerosol carried out in coastal Antarctica have shown that MSA and  $\text{nss SO}_4^{2-}$  exhibit a strong seasonal cycle characterized by summer maxima [Jourdain and Legrand, 2001; Curran et al., 1998]. Another seasonal indicator is  $\text{Na}^+$ , a tracer of sea salt.  $\text{Na}^+$  concentrations peak during the winter as a consequence of more frequent advection of marine air masses over the Antarctic ice sheet [Legrand and Delmas, 1984], with the strongest seasonal signal near the coast. Among the commonly used ions, sodium, nss sulphate, and nitrate often show well-developed seasonal variations on the polar plateau [Isaksson et al., 1996; Stenni et al., 2000, 2002; Traufetter et al., 2004; Kaspari et al., 2005; Dixon et al., 2004; Karlöf et al., 2005b]. Also for these species it is important to sample with high enough frequency to capture their variations, i.e., at least seven to eight samples per year [Mayewski and Goodwin, 1997]. However, it is worth keeping in mind that nitrate diffuses and is probably reemitted from the upper layers of the ice sheet [Wolff et al., 1995; Weller et al., 2004]. Nitrate reemission is inversely related to accumulation rate and usually obliterates its seasonal signature at low accumulation sites. Therefore,  $\text{SO}_4^{2-}$  and  $\text{Na}^+$  provide the most robust annual peaks within cores. In order to avoid using occasional double peaks as dividing lines for years, multiple ions with different seasonal timings can be used to define the annual horizons [e.g., Legrand and Mayewski, 1997].

[68] 3. Some gases also display a seasonal cycle, in addition to isotopes and ions. One example is hydrogen peroxide ( $\text{H}_2\text{O}_2$ , e.g., measured via spectrofluorimeter methods), which is principally produced in the atmosphere by photochemistry in summer. Its maximum concentration occurs in the period of maximum solar radiation, from late spring to late summer [Nefstel, 1991].  $\text{H}_2\text{O}_2$  is subject to postdepositional change, caused by reemission to the atmosphere, the same as some other species. Utilization of  $\text{H}_2\text{O}_2$  for annual layer counting is thus restricted to high-accumulation areas ( $>200 \text{ kg m}^{-2} \text{ a}^{-1}$ ).

[69] 4. For electrical methods, the varying concentrations of ions are a major cause of variations in alternating current (AC) and direct current (DC) electric conductivity. Two techniques are used to determine quasi-continuously the variation of conductivity along a core. The electric conductivity method (ECM) [Hammer, 1980] is a measure of the electrical current from which acidity concentration levels may be inferred in cores. ECM is performed in a cold room with stable temperature conditions as well as in the field. In contemporary systems, two to seven electrodes with an applied high voltage of several hundred volts (AC or DC) are moved along a freshly cut ice surface, and measurements are typically taken at millimeter resolution. The original method has been modified in various ways and is used by different groups [Isaksson et al., 1996; Kaczmarzka et al., 2004; Wolff et al., 1999; Taylor and Alley, 2004]. A

direct current flowing between the electrodes is dominated by the acid content and the temperature of the ice [Schwander et al., 1983; Moore and Mulvaney, 1989] but is only slightly dependent on the salt concentration under normal conditions [Schwander et al., 1983; Wolff et al., 1997]. For alternating currents, salts have an increasing effect on conductivity [Barnes et al., 2002]. The imaginary part of the dielectric constant determined from DEP,  $\epsilon''$ , already introduced in section 2.4.1.3 in the context of density measurements, likewise reveals variations in AC conductivity [Moore and Mulvaney, 1989]. As an alternating current technique, which is nondestructive as it does not require direct contact between the ice and the electrodes [Wilhelms et al., 1998], it also responds to both the acidity and the total salt content in the ice [Barnes et al., 2002]. Measurements are performed in millimeter to centimeter increments. There is evidence that the DEP and ECM electrical methods respond to different chemical compositions. Minikin et al. [1994] suggested that DEP peaks represent winter maxima of sea salts, while peaks in ECM respond mostly to summer maxima of nss sulphate and partly to high values of  $\text{NO}_3^-$ , MSA, and  $\text{HCl}^-$ . Hammer et al. [1994] and Mulvaney et al. [2002] confirm that ECM is a sufficient method for detecting both volcanic peaks and seasonal changes in acidity. Apart from identifying volcanic signals in conductivity, ECM is also used to analyze annual peaks if conditions are favorable enough.

[70] 5. Dating firn and ice cores via visual stratigraphy is based on visual differences in summer and winter snow due to changes in atmospheric conditions and radiative fluxes [Alley et al., 1997]. To aid the identification of annual layers, the surface of the core is prepared with a microtome knife. The core is placed on a light table to identify seasonal variations in transparency and scattering associated with annual layering. Summer layers are characterized by coarse-grained, low-density hoar layers, whereas winter layers have higher density and finer grain size. Below the firn-ice transition, summer layers have fewer and larger bubbles compared to winter layers and can also be identified by the presence of summer melt layers in coastal regions. Because of annual layer thinning, annual layers become more difficult to identify with depth. In regions with low accumulation, postdepositional processes such as drifting and melting (e.g., near coastal blue ice areas or very low accumulation areas on the plateau) can preclude the presence of visible annual layers [Taylor et al., 2004]. An advantage of visible stratigraphy is that it can also be applied in the field if stratigraphic changes are strong enough to be identified without preparation of the core. At least for higher accumulation sites, and thus favorable conditions, visual stratigraphy provides an initial approximation of annual accumulation rates [Morgan et al., 1991], useful for later decisions on core processing (e.g., sampling resolution). Although the visual stratigraphy is commonly applied to derive on-site information in snow pits, accumulation rates derived from pit stratigraphy alone involve personal and subjective interpretation, which can lead to unreliable results, as pointed out by Picciotto et al. [1971].

[71] 6. New techniques build on the greater availability of more advanced chemical analysis instrumentation, such as inductively coupled plasma–mass spectrometry (ICP-MS), allows the accurate determination of many tens of chemical elements at the parts per billion, parts per trillion, and parts per quadrillion levels. Improved instrumentation coupled with advances in sample generation, e.g., by laser ablation [Reinhardt et al., 2001], ultraclean sample analysis, and continuous sampling [Knüsel et al., 2003; Osterberg et al., 2006], will likely yield new firn and ice core dating methods. This would be particularly advantageous for dating ice cores from low-accumulation sites (such as the East Antarctic plateau).

#### 2.4.2.2. Reference Horizons

[72] There are several valuable reference horizons that have been used in Antarctic accumulation studies for validating the depth-age scale developed from annual layer counting or for use as a time horizon, which can then be used for calculating the accumulation rate between horizons. Below we discuss the two most commonly used reference horizons (volcanic peaks and artificial radionuclides) and suggest additional horizons that could be worthwhile to explore further.

[73] 1. For volcanic peaks, sulphate (in the form of atmospheric  $\text{H}_2\text{SO}_4$ ) is generally the dominant ion in high-altitude Antarctic snow, with the dominant source from marine biogenic emissions and sporadic input from volcanic activity. For the Antarctic polar plateau, historical volcanic eruptions such as Pinatubo 1991, Mount Hudson 1991, Mount Agung 1963, Krakatau 1883, and Tambora 1815 (plus an unknown eruption 1809) have been shown to be easily distinguishable peaks that can be used as unambiguous time markers, either from chemical analysis or conductivity measurements [e.g., Cole-Dai et al., 1997; Oerter et al., 1999; Nishio et al., 2002; Stenni et al., 2002; Traufetter et al., 2004; Dixon et al., 2004]. Because of oxidation of  $\text{SO}_2$ ,  $\text{H}_2\text{SO}_4$  forms within about 1 month following the eruption [Coffey, 1996]. Once in the stratosphere, the atmospheric residence time of  $\text{SO}_4^{2-}$  is a few years, during which it can be transported to the polar regions and subsequently scavenged by snowfall. An increase of nss  $\text{SO}_4^{2-}$  concentrations in polar snow is observed in a period up to 3 years after a major volcanic eruption [Cole-Dai and Mosley-Thompson, 1999]. For example, the eruption of Tambora (located in Indonesia) occurred in April 1815. The rise of  $\text{SO}_4^{2-}$  above background noise is observed in late austral winter 1816, with maximum concentrations during the austral summer of 1816/1817 [Cole-Dai et al., 1997; Palmer et al., 2001] due to the lag between the eruption and nss  $\text{SO}_4^{2-}$  deposition in Antarctica. In several papers from the EPICA presite and ITASE surveys, attempts have been made to develop a useful volcanic chronology spanning the last millennium to aid in the correlation between cores [Karlöf et al., 2000; Traufetter et al., 2004; Hofstede et al., 2004]. The Tambora double peak has served as the main time horizon for the dating of many firn cores in the ITASE program [Isaksson et al., 1996, 1999; Oerter et al., 1999, 2000; Stenni et al., 1999,

2001; Karlöf et al., 2000; Ekaykin et al., 2004; Dixon et al., 2004; Karlöf et al., 2005b; Frezzotti et al., 2005; Steig et al., 2005]. The most prominent eruptions during the last millennium in addition to Tambora are the A.D. 1259 eruption suggested to be El Chichon [Palais et al., 1992] and the A.D. 1452 eruption suggested to be Kuwae [Delmas et al., 1992]. These eruptions have been identified in many Antarctic ice cores [i.e., Moore et al., 1991; Cole-Dai et al., 1997, 2000; Watanabe et al., 1997]. However, the volcanic signal at high-accumulation, low-elevation sites located near the Ross Sea coast in West Antarctica has been overwritten by large amounts of biogenic  $\text{SO}_4$  that is released by marine organisms [Dixon et al., 2004]. This may be a problem at other low-elevation coastal sites that are situated close to polynyas, too. Currently, on the polar plateau ( $\text{SMB} < 70 \text{ kg m}^{-2} \text{ a}^{-1}$ ),  $\sim 2.5\text{-m}$ -deep snow pits are deep enough to reach the 1991–1992 layer from the Mount Pinatubo and Mount Hudson eruptions. Attempts have been made to determine if dating horizons as shown in time series of DEP, ECM, and sulfate are significant with respect to natural and measurement-induced noise [Cole-Dai et al., 1997; Fischer et al., 1998; Karlöf et al., 2005a, 2006; Steig et al., 2005].

[74] 2. Time markers from artificial radionuclides are based on radioisotopes from atmospheric nuclear weapon tests (United States, United Kingdom, Soviet Union, France, China, and India) carried out between 1953 and 1980. They were deposited in Antarctica after transport in the upper atmosphere and stratosphere [Picciotto and Wilgain, 1963; Wilgain et al., 1965; Feely et al., 1966; Picciotto et al., 1971; Lambert et al., 1977; Carter and Moghissi, 1977; Jouzel et al., 1979; Kamiyama et al., 1989]. Since the signing of the Limited Nuclear Weapon Test Ban Treaty in 1963, the number of atmospheric nuclear weapon tests greatly decreased with tests being carried out mainly underground. Other sources of anthropogenic fallout post-1963 may be linked to the nuclear disaster in Chernobyl in 1986 [Dibb et al., 1990]. Very sensitive analytical techniques and procedures have been developed and improved over the last 40 years to detect and measure both artificial and natural radionuclides present in the ice sheets [Picciotto and Wilgain, 1963; Delmas and Pourchet, 1977; Pinglot and Pourchet, 1979, 1994]. The high solubility of most fission products induces the formation of distinct and stable radioactive reference horizons in areas of dry snow facies or with moderate percolation of meltwater. Among the radioactive fallout,  $^{90}\text{Sr}$  and  $^{137}\text{Cs}$  radionuclides (referred to gross  $\beta$  activity), plutonium isotopes, and  $^{241}\text{Am}$  [Pourchet et al., 2003] are best suited for the formation of distinct radioactive horizons owing to their high production yield and their low volatility, which prevents vertical migration in the firn layers as long as they remain dry [Picciotto et al., 1971]. Another artificial product, tritium ( $^3\text{H}$ ), behaves differently during its injection into the global system (by thermonuclear explosions) and its deposition than the fission products previously cited [Picciotto et al., 1971]. Nevertheless, very distinct radioactive peaks in continuous tritium profiles are also observed [Jouzel et

al., 1979; Oerter et al., 1999; Stenni et al., 2002; Frezzotti et al., 2005]. The timing of radioactive deposition from the nuclear tests is well known in Antarctica [Wilgain et al., 1965; Feely et al., 1966; Jouzel et al., 1979; Oerter et al., 1999; Pourchet et al., 1983, 1997, 2003; Magand et al., 2004], with the maximum radioactivity peaks in 1954–1955 and 1965–1966 used as convenient horizons for dating snow and ice layers and measuring SMB. Jouzel et al. [1979] observed the largest tritium peak at the South Pole during 1966. On the basis of comparison between the tritium profile in snow layers at Dronning Maud Land and the tritium distribution at the Kaitoke (New Zealand) International Atomic Energy Agency (IAEA) station, Oerter et al. [1999] attributed the highest values to the 1964–1969 years. Best fit depth–time scales were used to transform the measured depth profiles to time series similar to the tritium content of precipitation at Kaitoke. In Antarctica, total  $\beta$  counting remains the most frequent radioactivity measurement [Picciotto and Wilgain, 1963; Lambert et al., 1977; Pourchet et al., 2003]. As a consequence, there is a great deal of data on the history of artificial radioactive fallout over Antarctica since the 1950s; thus total  $\beta$  activity is a well-constrained method used to identify radioactive reference horizons for estimating SMB in accumulation areas. In situ  $\gamma$  ray spectrometers for ice boreholes [Pinglot and Pourchet, 1981] enable a rapid determination of the mean annual accumulation from 1965 to present by measuring the radioactive fallout layers. This provides valuable information in the field to estimate the depth range necessary to reach dating horizons (like volcanic signals) as previously cited.

#### 2.4.2.3. Radiochronology

[75] As in many geoscientific disciplines, the natural decay of radioactive isotopes can be used to determine the age of an investigated sample, commonly referred to as *radiochronology*. A common example for ice is  $^{210}\text{Pb}$ , a natural  $\beta$  emitter. It is a long-lived daughter nuclide (half-life 22.3 years) belonging to the  $^{238}\text{U}$  family [Picciotto et al., 1971]. Its presence in the atmosphere is a result of the  $\alpha$  radioactive decay of radon gas ( $^{222}\text{Rn}$ ). The atmosphere is the major source of  $^{210}\text{Pb}$  deposited on the Antarctic ice sheet. Many factors contribute to the low radon (and its daughter nuclide) concentrations in Antarctica [Pourchet et al., 1997, 2003]. These include ice that prevents the escape of radon from the Antarctic geological basement, the surrounding ocean without radon emission, and the time required for air masses to move from continental areas (the main source of radon emission) to the south polar region. Very little  $^{210}\text{Pb}$  was produced by the nuclear explosions during the 1960s.

[76] Studies carried out during this period show that the quantity of  $^{210}\text{Pb}$  deposited at a given place, averaged over a year or more, appears to be constant and not to have changed significantly since the advent of H-bombs [Bull, 1971]. As a result, the natural  $^{210}\text{Pb}$  continuous flux deposition over the Antarctic ice sheet could be used for dating purposes over periods of the past 100 years. Because of radioactive decay, the natural  $^{210}\text{Pb}$  activity decreases

with depth of the firn and ice layers. The age of a firn layer at  $z$  meters depth is thus given by

$$t = \frac{1}{\lambda} \ln \frac{A_0}{A_z}, \quad (3)$$

and the average rate of accumulation of snow above this depth is given by

$$\dot{b} = \frac{z\lambda}{\ln \frac{A_0}{A_z}}, \quad (4)$$

where  $A_0$  and  $A_z$  are the  $^{210}\text{Pb}$  activities per unit weight of snow at the surface and at a depth of  $z$  meters, respectively, and  $\lambda$  is the  $^{210}\text{Pb}$  decay constant. The first attempts at dating firn or ice layers in the polar regions with the  $^{210}\text{Pb}$  method were successfully validated by other direct measurements [Goldberg, 1963; Picciotto et al., 1964; Crozaz et al., 1964; Nemazi et al., 1964; Crozaz and Langway, 1966]. We have to stress that accurate dating of snow by  $^{210}\text{Pb}$  is only possible with the following assumptions: (1) The mean  $^{210}\text{Pb}$  activity in precipitation has remained constant during the last two centuries, (2) the  $^{226}\text{Ra}$  concentrations within the firn/ice samples are negligible, (3) no diffusion of air into the ice sheet occurs (bearing additional  $^{222}\text{Rn}$ ), and (4)  $^{210}\text{Pb}$  remains at its initial place of deposition (no vertical transportation by water from melting snow). Even if none of these assumptions are perfectly fulfilled, we argue that a generally reliable determination of SMB over the past few decades is achievable by this method in areas exempt from melting, i.e., in accumulation zones [Pourchet et al., 1997, 2003].

#### 2.4.2.4. Optimal Strategies for Age Estimates

[77] Counting seasonal cyclicity of chemical/isotopic parameters ( $\delta^{18}\text{O}$ ,  $\delta\text{D}$ ,  $\text{H}_2\text{O}_2$ , MSA,  $\text{Na}^+$ ,  $\text{NO}_3^-$ , nss  $\text{SO}_4^{2-}$ , etc.) is the most precise dating method, but it is also the most time- and equipment-intensive method. A multiparameter approach using several high-resolution chemical records (as shown in Figure 9d) is therefore the most reliable way to derive annual dating. Because several atmospherically derived chemical species peak during different times of the year, it may thus be possible to ensure that no year is missing [e.g., Udisti, 1996; Steig et al., 2005]. In general, however, seasonal cycles are difficult to observe at sites with low accumulation (below about 80–100  $\text{kg m}^{-2} \text{ a}^{-1}$ ), such as the polar plateau, because the seasonally deposited chemical or physical signals often have been strongly erased or reworked by the action of wind at the surface. Applying these methods to discrete samples (as from snow pits) is ineffective in the inner part of East Antarctica, e.g., in the Dome C area, unless a high (subcentimeter) sampling resolution is used. At most low accumulation areas, high-resolution continuous electric (DEP and ECM) and chemical measurements (CFA, FIC, CMDS) and the simultaneous analysis of multiple-parameter records have to be performed in order to detect seasonal signals in the physical and chemical properties of cores and thus achieve annual dating. During the past decade, high-

resolution continuous methods have been used in many studies, such as for the EPICA presite surveying in Dronning Maud Land [Sommer *et al.*, 2000b]. Thus, it was possible to perform annual layer counting back several hundred years at several places on the East Antarctic plateau with SMB below  $80 \text{ kg m}^{-2} \text{ a}^{-1}$ , e.g., at the South Pole [Meyerson *et al.*, 2002] or Dronning Maud Land [Sommer *et al.*, 2000a], and even below  $50 \text{ kg m}^{-2} \text{ a}^{-1}$  from an ice core site located approximately 600 km south of Dome A (D. A. Dixon, personal communication). Such results imply that wind scouring does not suffice to erode annual signals at these sites. However, the identification of annual layers does not unequivocally imply the possibility of resolving accumulation history with representative values ( $\pm 10\%$ ) of annual resolution [Frezzotti *et al.*, 2007]. When continuous sampling is not available, reference horizon dating may be the only available method at low accumulation sites. In such cases, only a mean accumulation rate between two reference horizons can be calculated. This precludes these records from studies interested in the interannual variability in accumulation, for instance, to assess changes in climate, to account for flux of chemical compounds, etc.

#### 2.4.3. Accumulation Errors From Pit and Core Measurements

[78] Annual layer counting using seasonal cyclicity of multiparameters can be fine tuned using atmospheric thermonuclear bomb test layers and volcanic peaks as fixed time markers to achieve the best accuracy for the evaluation of snow accumulation in cores. Dating errors may arise from incorrect or nonidentification of seasonal signals (e.g., hiatus in accumulation or erosion) and from incorrect identification or errors in identification of historical volcanic or nuclear bomb layer markers. Dating errors could be  $\pm 1$  year for the depth coincident with the marker, but they could be higher at points that are far from dated reference horizons [e.g., Steig *et al.*, 2005].

[79] The associated relative errors in accumulation  $\dot{b}$  derived from snow pits, firm, and ice cores (Table 2) can be expressed as

$$\frac{\delta \dot{b}}{\dot{b}} \leq \sqrt{2 \left( \frac{< 0.5l}{\Delta z} \right)^2 + \left( \frac{\delta(\Delta t)}{\Delta t} \right)^2 + \left( \frac{\delta(\Delta m)}{\Delta m} \right)^2}, \quad (5)$$

where  $l$  is sample length,  $\Delta z$  and  $\Delta t$  are the depth and age difference between the dating horizons used, and  $\Delta m$  is the mass difference of the two columns above the two dating horizons, sometimes expressed in meter water equivalent depth;  $\delta(\ )$  is the uncertainty of the parenthesized variable, e.g., the error in the date of volcanic deposition. When the sample length is relatively large compared to the depth between dating horizons, the first term on the right-hand side is important. On the other hand, if the age–depth profile is derived from high-resolution measurements like electrical methods, the first term can be neglected. The error estimate only applies at the identified dating horizons. Any physical variation, i.e., change in accumulation, between the dating horizons is not captured by this error estimate. The typical error  $\delta \dot{b}$  in  $\dot{b}$  is less than 10% for both snow pits and cores.

[80] The extraction of snow accumulation values from cores requires estimating the effects of thinning due to ice dynamics (densification, compression, flow, etc.). Vertical thinning of surface layers is predictable from the sum of horizontal strain rates. As firm cores are relatively shallow (less than 50–100 m) in comparison to the total thickness of ice sheets (more than 1000 m), thinning could be assumed to be less than 5%, implying negligibility. In cold, large ice sheets like the one in East Antarctica, the strain rates are expected to be around  $10^{-4} \text{ a}^{-1}$ . On fast moving glaciers, ice streams, and ice shelves, they can sometimes get close to  $10^{-2} \text{ a}^{-1}$ , and as a result, cores that represent several hundred years can be significantly affected by thinning. As an example, consider a 100-year-old layer. If both horizontal strain rates are  $10^{-4} \text{ a}^{-1}$ , the 100-year-old layer should have thinned by only 2%, but if strain rates are  $10^{-2} \text{ a}^{-1}$ , the layer is thinned to 13% of its original thickness. For a 100-m core with around  $200 \text{ kg m}^{-2} \text{ a}^{-1}$  accumulation, corresponding to 300 years of accumulation history, and at a strain rate of  $10^{-3} \text{ a}^{-1}$ , a 55% thinning of the original layer thickness should result. Whether layer thinning takes place or not has thus to be evaluated for each site individually.

#### 2.5. Laterally Continuous Measurements: Ground-Penetrating Radar

[81] GPR maps the internal structure of the firm column along a profile from the surface. Variation in depth of continuous internal layers of equal age along the profile yields information about the accumulation pattern. Combining GPR with highly resolved ice core data is required to date the internal layers.

[82] Over the last few decades, a number of methodological studies have been carried out to investigate the suitability of high-resolution GPR for mapping accumulation rates along surface profiles. The results demonstrate that GPR profiling of firm stratigraphy, coupled with precise GPS measurements is capable of complementing traditional methods like stakes, snow pits, and cores to map accumulation rates and to improve the understanding of spatial accumulation patterns. In the literature, terms like GPR (traditionally used in engineering geophysics), ice-penetrating radar, snow radar, and sometimes radio echo sounding are used synonymously. Here, we stick to the first term and imply investigations with a phase-sensitive radar. Commercial and easily transportable GPR systems have become available and are widely used to survey the near-surface firm (<100–200 m). Over recent years this had the consequence that GPR was routinely employed during operational surveys to map the internal structure of the firm column and to determine regional surface accumulation, e.g., during most campaigns related to ITASE and EPICA [Isaksson and Karlén, 1994; Richardson *et al.*, 1997; Richardson and Holmlund, 1999; Nereson *et al.*, 2000; Richardson-Näslund, 2001; Urbini *et al.*, 2001; Frezzotti *et al.*, 2002b; Frezzotti and Flora, 2002; Sinisalo *et al.*, 2005; Richardson-Näslund, 2004; Rotschky *et al.*, 2004; Karlöf, 2004; Spikes *et al.*, 2004; Eisen *et al.*, 2005; Frezzotti *et al.*, 2005; Arcone *et al.*, 2005a, 2005b; Jacobel *et al.*, 2005; Anschütz *et al.*,

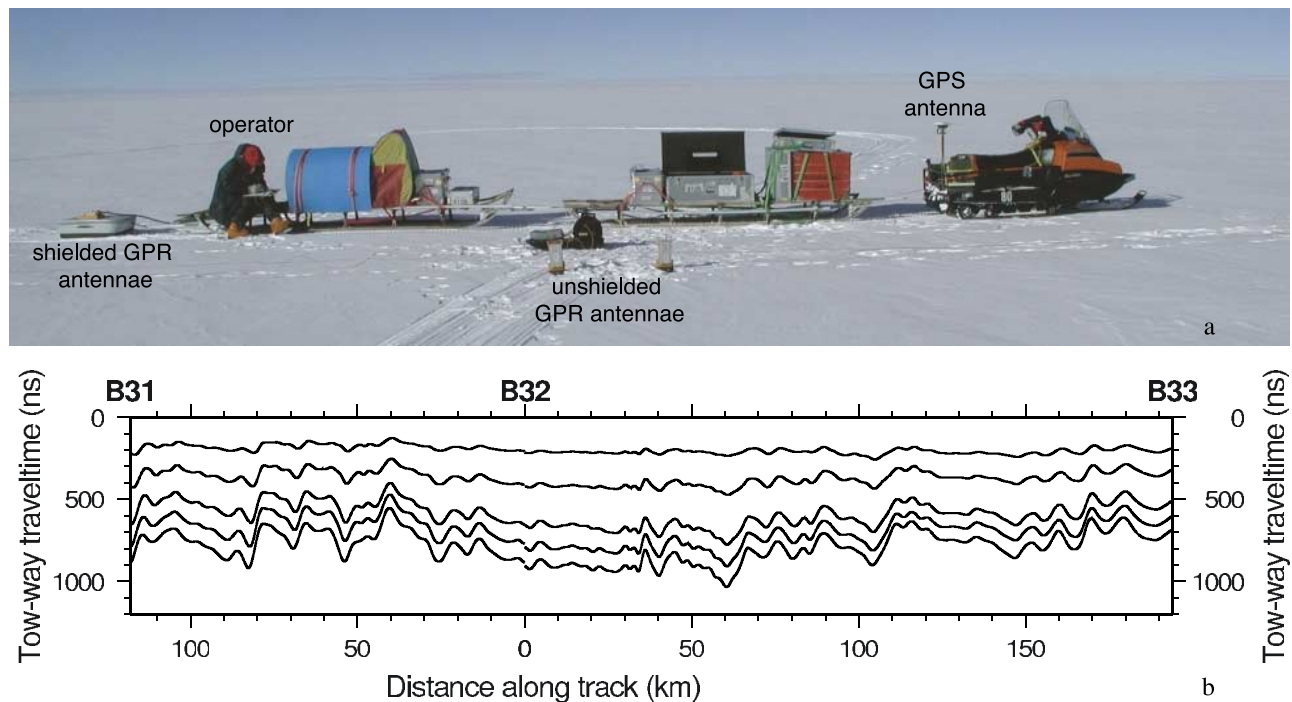


**Figure 10.** (a) Setup of GPR measurements: For common offset surveys, a shielded antenna (left) is pulled by a snowmobile. The GPS antenna is mounted at the rear of the vehicle (right). Common midpoint surveys utilize separate transmitter and receiver (front). (b) Sample profile of five internal horizons tracked in common offset GPR data over 300 km in Dronning Maud Land [Eisen et al., 2004].

2007, 2008]. High-frequency GPR in the range of 100 MHz to 1 GHz is capable of imaging the structure of the upper tens to hundreds of meters of the ice column in high resolution. On the Antarctic inland plateau, this provides a means to derive information about the local SMB over the last tens of years to about 1000 years. It has thus become possible to map accumulation rates and their spatial variations along continuous profiles within the upper parts of the snowpack.

### 2.5.1. Technical Background and Functional Principle

[83] Application of GPR for imaging the snow and firn column at shallow depths usually utilizes a transmitter and receiver moved at a fixed distance from each other across the surface along the survey profile. This setup is called common offset (CO), referring to the constant distance between transmitter and receiver. The device is either towed by hand, snowmobile, or tractor, and the geographical position is usually obtained from kinematic GPS measurements (Figure 10a). At defined intervals, either at equal temporal or spatial increments, the transmitter emits an electromagnetic pulse into the snow column. Distances between consecutive measurements vary, depending on the system performance, between about 0.1 and 10 m. The pulse penetrates into the snow column and is partly reflected where the complex dielectric  $\epsilon^*$  constant changes. The reflected signals travel back to the receiving antenna at the surface. The complete signal is recorded as a function of traveltime of the transmitted radar pulse.

[84] Three factors are known to change the dielectric constant in firn and ice: gradients in the real part, the permittivity, are mostly related to density; they dominate

reflections in the upper hundreds of meters. Variations in the imaginary part are proportional to conductivity, are related to acidity, and depend on frequency. They are the governing reflection cause in deeper ice. A third mechanism, proposed by Harrison [1973], involves dielectric anisotropy of the crystal fabric, but it becomes significant only at the deeper levels (>500–1000 m) of the ice sheet where changes in anisotropic crystal fabrics could develop [Fujita et al., 1999; Matsuoka et al., 2003, 2004; Eisen et al., 2007]. Other radar techniques are based on frequency-modulated continuous wave (FMCW) transmissions or stepped-frequency radars [Kanagaratnam et al., 2001; Corr et al., 2002]. Although the technical details on data acquisition and processing are different, the results are the same, an image of subsurface reflections along a profile (Figure 4).

[85] Studies of dielectric properties of ice and internal radar reflection horizons (IRHs, outlined in Figure 10b) show that most processes forming electromagnetic reflectors take place at the glacier surface at approximately the same time [Gudmandsen, 1975]. (Details on physical structure and processes related to the origin of reflections in firn are given by Kohler et al. [2003], Eisen et al. [2003a, 2003b], and Arcone et al. [2005a].) While some significant progress in understanding this process has been made in recent years [Eisen et al., 2003b; Arcone et al., 2005a], it is still not entirely clear how the GPR produces a continuous reflecting horizon in the ice, visible over hundreds to even thousands of kilometers. At present, there remains some uncertainty about how the material properties in firn combine to form the continuous reflecting horizons. It does



seem apparent that both density and chemical properties in the ice contribute, but since layers are visible even where the wavelength of the radar exceeds the annual layer thickness, it is clear that at least in the shallow regions some complex interference pattern is generally being observed. However, the isochrony of observed reflections has been proven heuristically by connecting firm and ice core drill sites [Jacobel and Hodge, 1995; Spikes et al., 2004; Eisen et al., 2004; Frezzotti et al., 2005] and by comparing accumulation rates deduced from GPR with those measured along surface stake lines [Vaughan et al., 2004]. The submergence rate of an isochrone surface is determined by interaction of the surface accumulation with the flow field [Robin et al., 1969; Gudmandsen, 1975; Clough, 1977; Millar, 1981; Bogorodsky et al., 1985; Moore, 1988]. Continuously moving the radar system along a surface profile and recording individual traces at high enough spatial repetition rates (on the order of decimeters to meters) makes it possible to continuously image the internal reflections along the profile (Figure 10b). As the continuous internal reflection horizon corresponds to an isochronous layer, the spatial variation of layer depth provides information on variations in the accumulation rate and changes due to ice sheet dynamics. The latter can mostly be neglected in the upper meters of the ice column in regions of slow flow (see previous discussion on accumulation errors from cores in section 2.4.2.3).

### 2.5.2. Accumulation Estimates From GPR

[86] On the Antarctic plateau, the isochronous reflections can be followed over hundreds of kilometers. The variation in depth of an individual reflector already provides a qualitative picture about the variation of surface accumulation along the profile. To determine quantitative accumulation estimates, several processing steps are necessary [Arcone et al., 2005a; Rotschky et al., 2004]: (1) track one or more internal reflections along the profile; (2) convert the radargram from time to depth domain along the whole profile; (3) date the isochrones at one or more points (the isochrony assures that the age can be distributed along the profile); (4) determine the cumulative mass as a function of depth from the surface to the reflector depth along the profile; and (5) calculate the average SMB by dividing the cumulative mass by the respective age of the reflector.

[87] These processing steps involve several other input properties. We now discuss details and peculiarities of each step.

#### 2.5.2.1. Tracking Internal Reflections

[88] After digital data processing of the raw radar data (horizontal stacking, filtering, gain control), continuous reflections can be followed in the radargrams. Depending on data processing and display, it is possible to identify a single phase, for instance, the first break, and track that along the whole profile, or track the maximum amplitude when the signal envelope is used. Tracking can be performed manually, trace by trace, or semiautomatically. Semiautomatic tracking is implemented in a number of programs, mainly based on experiences in the seismic exploration industry. The tracking algorithm exploits the

coherency of signal features (e.g., minimum, maximum, or zero amplitude) above noise level to automatically detect the same feature within a prescribed time window in adjacent traces and follows it as long as a similarity criterion is fulfilled. The tracking process is observed by the user and requires manual interaction in case of a low signal-to-noise ratio.

#### 2.5.2.2. Time-to-Depth Conversion

[89] Knowledge of the variation of the electromagnetic wave speed with depth is necessary in order to be able to convert the observed reflections from time to depth domain. Some authors directly calculate water equivalent depth of a horizon to derive accumulation [Vaughan et al., 1999b; Spikes et al., 2004]. The wave speed is mainly a function of density; contributions from conductivity can be neglected at radio frequencies. Different methods were developed to determine the wave speed–depth function. The most direct method involves the measurement of the dielectrical properties along cores by means of DEP (see section 2.4.1) [Moore and Paren, 1987; Wilhelms et al., 1998; Karlöf, 2004; Wilhelms, 2005], from which the interval velocities can be directly calculated. Instead of the dielectrical properties, density profiles from snow pits, firm, or ice cores are also often used to determine the electromagnetic wave speed from mixture models [Robin et al., 1969; Clough and Bentley, 1970; Kovacs et al., 1995; Richardson et al., 1997; Urbini et al., 2001; Eisen et al., 2002; Spikes et al., 2004; Anshütz et al., 2006]. The downhole radar technique makes use of a drilled hole to record traveltimes as a function of depth of a reflecting target lowered in the hole [e.g., Jezek and Roeloffs, 1983; Clarke and Bentley, 1994]. Interval velocities can then be derived from the transmitter–target–receiver traveltime as a function of depth. An indirect method known from reflection seismic exploration is the common midpoint (CMP) survey technique [Yilmaz, 1987]. It is a special case of the radar wide-angle reflection and refraction measurement [Annan and Davis, 1976; Jezek and Roeloffs, 1983; Morey and Kovacs, 1985; Bogorodsky et al., 1985] and has been widely applied for radar measurements in glaciology [e.g., Blindow, 1994; Hempel et al., 2000; Murray et al., 2000; Eisen et al., 2002]. It makes use of a special setup of linear geometry, such that the points of reflection at a certain depth remain constant with increasing offset between transmitter and receiver. The velocity–depth function can be inferred from the increase of traveltime with offset, assuming near-horizontal reflectors.

#### 2.5.2.3. Age Estimates of Reflection Horizons

[90] Dating IRHs is achieved by transferring age–depth distribution, as obtained from snow pit and cores as described in section 2.4.2, to the respective depth of the IRH at the location where the age–depth distribution was measured. This is usually achieved by mere comparison or correlation techniques in the depth domain. A new approach utilizes numerical forward modeling of radargrams, based on dielectric profiling of ice cores, to relate depth (and thus age) to the time domain of the radar data [Eisen et al., 2004]. A problem related to the dating of snow layers by core analysis comes along with the spatial separation of GPR

profiles and coring sites. In several cases, the GPR soundings were not always made directly over the exact coring point or in the same year; in some cases, the distance between the coring site and the radar survey exceeded 10 m [Richardson-Näslund, 2001]. In other cases, it is not possible to follow isochrones all the way to a coring site, and thus it is not always possible to determine the age of a snow layer by direct comparison with core or pit data. Such a layer can still be dated indirectly using overlapping sections of other internal layers that could be dated directly against cores and pits. This method allows one to obtain approximate estimates of spatial variability in accumulation rate that would otherwise be unobtainable [Richardson-Näslund, 2001]. Even if absolute dating is not possible, a qualitative interpretation of spatial accumulation variability can still be achieved [Vaughan et al., 2004].

#### 2.5.2.4. Cumulative Mass

[91] Integration of measured density profiles yields the distribution of cumulative mass with depth. (For more details on density measurements, see section 2.1.) Generally, snow/firn density increases with increasing depth. Thus, the density-depth profile influences the wave speed–depth profile and cumulative mass value. Cumulative mass is usually calculated from the surface down to the depth of the radar reference layer. However, depending on the time interval of interest, it is also possible to calculate the mass difference between two internal reflectors to determine spatial variability of past accumulation rates, similar to firn and ice core studies.

[92] One question coming along with the spatial extent of radar profiles is the lateral homogeneity of density-depth distributions. Snow and firn densities in the dry zone are predominantly determined by overburden pressure, which is governed by local meteorological parameters: temperature, wind, and accumulation rate [Craven and Allison, 1998; Kameda et al., 1994]. Depending on the study area, the distributions can be homogeneous over hundreds of kilometers on the polar plateau and in particular at ice divides and domes [Frezzotti et al., 2004; Richardson-Näslund, 2004; Rotschky et al., 2004; Arcone et al., 2005b] or could vary considerably at places with high spatial accumulation variability due to strong wind erosion [Richardson et al., 1997; Spikes et al., 2004; Frezzotti et al., 2005]. At Dome C and Talos Dome, dedicated density profile analyses from a number of cores and pits reveal no detectable geographical variation in density or compaction within a 50-km diameter of the dome areas [Frezzotti et al., 2005, 2007; Urbini et al., 2008]. In contrast, especially in coastal regions, variations on short distance scales can be significant [Richardson-Näslund, 2004; Vaughan et al., 2004; Frezzotti et al., 2005; Anshütz et al., 2006]. In the latter case, density profiles need to be laterally interpolated to provide information along the GPR profiles. The largest variability in density is usually in the uppermost 3–20 m.

[93] Density data surveyed by core and pit are fitted with polynomial or logarithmic functions, usually yielding a correlation coefficient ( $R^2$ ) of more than 0.9 for measured and computed densities [e.g., Richardson et al., 1997;

Frezzotti et al., 2005]. Because of a change of density function with depth, the density profiles should cover the snow radar investigation depth. The uncertainties associated with each cumulative mass measurement vary with depth.

#### 2.5.3. Errors of GPR-Based Accumulation Estimates

[94] A number of factors determine the final uncertainty of an accumulation estimate based on GPR (Table 2). They can be separated by errors related to determining the depth of the reflector, the age of the reflector, and the cumulative mass above the reflector. Other errors arise by spatially interpolating or extrapolating the density information along a radar profile. Depending on the region of investigation, the density–depth and thus the mass–depth and wave speed–depth distributions can be very homogeneous, e.g., in undisturbed regions on the Antarctic plateau, or very inhomogeneous, as near coastal sites and slope areas.

[95] The operation frequency of the radar system and the characteristic of the source signal determines the possible vertical resolution of a reflector. Theoretically, a quarter of the wavelength is the highest resolution that can be achieved. Another consideration is the ability to separate two neighboring reflectors. According to the Ricker criterion, they can be separated when the traveltime difference in the reflected signals is larger than half the cycle duration of the signal. However, most radars transmit a source signal which contains more than a single cycle, thus reducing the resolution. Two signals can then be separated when the traveltime difference exceeds half the pulse width. GPR is usually operated in a bistatic mode, which means separate antennae at a certain distance (dm to m, depending on frequency) for transmission and reception of the radar signal. This causes an error in estimated depth, especially for reflectors close to the surface (see Pälli et al. [2002] for a discussion).

[96] Accuracy of the traveltime–depth conversion depends on the source of information for the velocity profile (e.g., density measurement along a core or from common midpoint radar). Uncertainties in the age estimate of a reflector are caused by the initial uncertainty of the underlying age–depth scale (snow pit, firn, or ice core) and the transfer of the age information for, e.g., a core to the reflector. (For more details on age estimates, see section 2.4.2.) The error in accumulation depends finally on the accuracy of the depth-integrated density profile. Small-scale variations in density, like ice lenses or wind crusts, are averaged out by the integration, and neither cause large errors in cumulative depth or wave speed.

[97] Spikes et al. [2004] pointed out that uncertainties are based mainly on the three components: layer thinning due to ice advection, the procedure for depth calibration, and the isochronal accuracy of each horizon. Their results indicate that uncertainties at a firn depth of 10 m are about 4% of the calculated snow accumulation and decrease to 0.5% at a firn depth of 60 m. In general, conservative uncertainty estimates of SMB derived from GPR are some 5% on the polar plateau, most of which stems from the uncertainty in dating. A summary of factors contributing to errors is provided in Table 2.

#### 2.5.4. Spatial Variability of SMB From GPR

[98] Along the Terra Nova Bay–Dome C traverse, standard deviation of variability decreases generally from the coast (47%) to the ice divide (3%) [Frezzotti et al., 2004]. However, sites characterized by relatively complex surface morphology with abrupt changes in slope along wind direction show higher standard deviation (34–47%) than sites that have a low slope along wind direction (5–10%). High standard deviation in spatial variability is also observed inland in the areas of megadune fields (24% [Frezzotti et al., 2002b, 2005]). The lowest values are observed at domes and ice divides (3–9%). Changes in spatial distributions have been observed over the last few centuries using GPR, with a decrease in SMB gradient along the wind direction at Talos Dome and a counterclockwise rotation of SMB distribution in the northern part of Dome C. Observations at Dome C reveal a significant increase in accumulation since the 1950s, which could correlate to altered snow accumulation patterns due to changes in snowfall trajectory. Snow accumulation mechanisms are different at the two domes: a wind-driven snow accumulation process operates at Talos Dome, whereas snowfall trajectory direction is the main factor at Dome C [Urbini et al., 2008].

[99] Along the transect that crosses Talos Dome, analysis of spatial variability shows that in the coastal area, spatial variability reaches  $200 \text{ kg m}^{-2} \text{ a}^{-1}$  over 1 km and wind-driven sublimation values may be as high as  $260 \text{ kg m}^{-2} \text{ a}^{-1}$ . In the plateau area, spatial variability reaches  $40 \text{ kg m}^{-2} \text{ a}^{-1}$  over 1 km, and wind-driven ablation is as high as  $50 \text{ kg m}^{-2} \text{ a}^{-1}$  [Frezzotti et al., 2007]. Redistribution processes are only present on a local scale; wind-driven sublimation values represent 20–75% of solid precipitation. Depositional features are very rare, related to the formation of transverse dunes and negligible in the SMB. The spatial variability of SMB at the kilometer scale is 1 order of magnitude higher than its temporal variability (20–30%) at the centennial timescale [Frezzotti et al., 2004].

[100] The spatial variability at sites very close to the coast in Adélie Land is less than 10%. Along coastal and inland slopes the spatial standard deviation, also based on stake line data, increases from 20% to more than 50%. On the plateau the spatial variability varies up to about 20%, but in the undisturbed part of the plateau it was below 10%. Variations of the same order in the three regimes, coastal, transition, and plateau, are evident from stake line data [Pétré et al., 1986], although measurements are less sound than GPR results.

[101] On the plateau in DML, the small-scale variation in accumulation is on the order of 5–15% of the mean accumulation [Richardson-Näslund, 2001; Rotschky et al., 2004; Eisen et al., 2005]. Small-scale means over distances of 10 km compare to mean values over 100 km. In the perimeter of the EPICA deep drilling site, accumulation variability is less than 15% on average, but accumulation gradients can be up to  $2.5 \text{ kg m}^{-2} \text{ a}^{-1}$  over 1 km [Eisen et al., 2005]. Averaged SMB values for the last 150 years decorrelated over a distance of about 10 km [Rotschky et al.,

2004]. In contrast, increased variability of up to 45% [Richardson and Holmlund, 1999] occurs on slopes and near the coast. At Camp Victoria, Amundsenisen (2400 m above sea level), and Camp Maudheimvidda (362 m asl), both in DML, Holmlund et al. [2000] performed  $10\text{--}20 \times 20 \text{ km}^2$  grid net studies to determine the spatial variability in an area with rather low ice flow velocities. They mapped the top 30–40 m and related the observed layers to the layer depth at a drilling spot at the center of the grid. At Maudheimvidda, the variation in layer depths amounted to 40 to 240% of the layer depth at the center of the grid. According to radar data, the pattern seen at the surface could be seen some tens of meters down into the snowpack. At altitudes around 2200–2500 m, at Camp Victoria, the variability was somewhat less pronounced but still on the order of 10%.

#### 2.5.5. Point Measurements Versus GPR-Based SMB Estimates

[102] One could expect that point measurement and GPR yield principally different results because they sample different areas: the cores, stakes, and ultrasonic sensors sample centimeter-scale areas (2–10 cm), while GPR works at the meter scale. Accumulation rates derived by point measurements and GPR methods [Richardson-Näslund, 2001, 2004; Rotschky et al., 2004; Vaughan et al., 2004; Frezzotti et al., 2005; Anschütz et al., 2007; Frezzotti et al., 2007] agree fairly well, the discrepancy ranged from a few percent to 20%, and the results do not indicate any systematic errors. Frezzotti et al. [2005] found major differences between point measurements and GPR (20%) along the Terra Nova Bay–Dome C traverse in regions of large spatial variability in SMB (47% over 15 km at maximum). At this site, two cores were drilled a few tens of meters apart and show a 13% difference in accumulation for the tritium/ $\beta$  marker horizons [Frezzotti et al., 2005]. Detailed chemical studies in  $16 \times 6 \text{ m}$  snow pits combined with GPR measurements on the polar plateau in DML found that the variability of snow layer thickness at the microscale was on average 9% [Stenberg et al., 1999]. A qualitatively good comparison between stake line measurements and GPR layer architecture enabled Vaughan et al. [2004] to deduce that the observed IRH are isochrones. For layers several tens of meters deep, covering more than a century, a problem exists when comparing core and GPR measurements when GPR traverses pass several kilometers away from the core. Although values are still comparable, a detailed match is difficult [Rotschky et al., 2004].

### 3. REPRESENTATIVITY AND LIMITATIONS

[103] Section 2 presented the different techniques carried out on the ground to determine accumulation, discussed difficulties associated with the measurements, and provided error estimates. Once values for the SMB are available, one asks what these values actually mean? Are they just valid for a short period of time, or just in the very vicinity of the measurement locations, or both? This brings us to the issue of the representativity, which is fundamental, as the inter-

pretation of SMB requires consideration of the climatic context, also on larger temporal and spatial scales. In this section we summarize important accumulation characteristics derived from the different measurement techniques and discuss the spatial and temporal representativity of the data.

[104] For the application of SMB data for the different purposes described in section 1, the three key questions are (1) What is the temporal representativity? (2) What is the spatial representativity? (3) Are spatial and temporal signals linked? Related issues are the stability of accumulation patterns in time. Do values at different locations with different mean SMB fluctuate synchronously, i.e., do they covary? Or do temporal changes, for instance, induced by short- and long-term local climate changes, also change the accumulation pattern, resulting in independent fluctuations? Likewise, the effect of ice flow has to be taken into account for core and GPR interpretations on longer timescales, as advection causes mixing of temporal signals with spatial information. For a reliable interpretation of SMB data, these factors have to be separated.

### 3.1. Temporal Representativity

[105] Time series obtained from stakes and ultrasonic measurements indicate a large interannual variability in accumulation, with variations of up to nearly 50% with respect to the 50-year average accumulation from firn cores [Frezzotti et al., 2007]. Monaghan et al. [2006] combine model simulations and observations primarily from cores. They point out that yearly and decadal snowfall variability at local and continental scales is very large. Comparison between stake and core values makes it possible to measure the frequency distribution and thus to infer the probability of identifying missing layers and also the lowest and highest SMB values in cores. Significant differences between core and stake measurements have been observed at sites with  $\text{SMB} < 200 \text{ kg m}^{-2} \text{ a}^{-1}$  [Frezzotti et al., 2007]. Reasons could be the misidentification of annual layers from seasonal signals and the consequent error in the definition of high and low values (values with differences  $>40\%$  with respect to average value) or/and the slight variations in input timing of the chemical or isotopic composition (e.g., interannual variability in peak-input timing of sulphate could vary by weeks). The misidentification could be due to large annual peaks that could be interpreted as a double year or to two adjacent peaks that will not be stratigraphically detectable because they are sufficiently narrow and could therefore be interpreted as a single year. Signal noise is produced principally by postdepositional processes such as wind erosion, drift, and redeposition. Postdepositional noise primarily influences the high frequencies [Fisher et al., 1985], and misidentification of an annual layer results in overestimation of accumulation in 1 year and to an underestimation in the preceding or following year. Both noise and error reduce the temporal representativeness of the time series.

[106] At the South Pole, the frequency distribution of stratigraphic layer thicknesses in cores and in a snow pit is

not compatible with a significant number (between 1% and 5% probability) of missing layers associated with zero accumulation years inferred from measurements of stake heights. The original implication that a large percentage of years (about 10%) is missing from the ice core stratigraphy [Van der Veen and Bolzan, 1999; Mosley-Thompson et al., 1995] has been found to be an overestimate [Mosley-Thompson et al., 1999] (see also section 2.2.4). In general, stake or ultrasonic measurements are the only way to detect zero accumulation or erosion values on an annual or seasonal scale.

[107] Analysis of Gaussian distributions of accumulation versus SMB from stake farms shows that only sites with  $\text{SMB} > 750 \text{ kg m}^{-2} \text{ a}^{-1}$  have present values that are representative to within  $\pm 10\%$  at an annual scale [Frezzotti et al., 2007]. The SMB distribution shows that more than 80% of stakes at sites with low SMB around  $80 \text{ kg m}^{-2} \text{ a}^{-1}$  and more than 40% of stakes at high SMB sites ( $\sim 250 \text{ kg m}^{-2} \text{ a}^{-1}$ ) present SMB differences of more than  $\pm 10\%$  with respect to the mean. The temporal representativity increases with multiyear averages: for high SMB, values are representative at  $\pm 10\%$  using three cumulative years; for a SMB of  $80\text{--}150 \text{ kg m}^{-2} \text{ a}^{-1}$ , using 5–7 cumulative years is necessary [Frezzotti et al., 2007]. Goodwin et al. [2003] propose that the 3-year running mean accumulation data from eastern Wilkes Land cores ( $235\text{--}570 \text{ kg m}^{-2} \text{ a}^{-1}$ ) are representative for the precipitation minus evaporation signal rather than the local microrelief noise. The same timescale is found to be significant by wavelet analyses of electrical records by Karlöf et al. [2006]; that is, the correlation between different records is highest in the 1- to 3-year period. This is attributed to the fact that most material emitted by volcanic eruptions is removed from the atmosphere within 3 years of eruptions, including deposition on the ice sheets. Their study implies that the temporal and spatial representativity of SMB and the records from which it is derived are not necessarily the same. At the South Pole, McConnell et al. [1997] computed the average time (310 years) required to statistically ensure that each monthly SMB record within the year is adequately represented in the time average. They also pointed out that the averaging of adjacent cores would decrease the time window proportionally. Van der Veen and Bolzan [1999] pointed out that noise could be removed using a Gaussian weighting function with a standard deviation of about 5 years. At the coastal region of Adélie Land, reevaluation of older stake line data from Pettré et al. [1986] indicates interannual standard variations on the order of 45%.

[108] Genthon [2004] calculates the variability and the radius of decorrelation of precipitation and precipitation minus evaporation over Antarctica from climate models and meteorological analyses. Interannual variability ranges from 5 to 40% of the mean. On the century scale, however, a number of GPR studies (aiming at the spatial characteristics presented next) reveal that the accumulation patterns are stable in time.

### 3.2. Spatial Homogeneity and Variations

[109] Stake farms and lines have given an indication of the spatial variability in SMB on various scales, e.g., the quasi-uncorrelated annual accumulation caused by micro-relief at low-accumulation sites on the plateau. Given the amount of resources required to deploy and maintain stake networks, however, the volume of data that they have produced is generally low. The emergence of GPR techniques has dramatically increased our ability to measure, and therefore understand, the spatial variability in SMB. A number of GPR surveys (see section 2.5.4) reveal that spatial variability of SMB at the kilometer scale can be up to 1 order of magnitude higher than its temporal variability (maximum 20–30%) at the multidecadal/secular and centennial timescale. Generally, the patterns of spatial variability are stable in time at least over a couple of decades to centuries. Stationary features are of comparable length scales (kilometers to tens of kilometers) [Richardson-Näslund, 2004; Vaughan et al., 2004; Frezzotti et al., 2004; Eisen et al., 2005]. In rare cases, like the East Antarctic megadune fields, migrating accumulation patterns occur [Frezzotti et al., 2002b]. Recently, migrating features on the 5-km scale were observed close to the coast [Anschütz et al., 2006], although their variations are less pronounced and laterally extensive than megadunes.

[110] Several authors demonstrate the dependence of SMB on temperature, elevation, saturation vapor pressure, and distance from the open ocean [e.g., Muszynski and Birchfield, 1985; Giovinetto et al., 1990; Fortuin and Oerlemans, 1990]. Although common, large-scale patterns are not always simple [e.g., Smith et al., 2002]. The high spatial variability of SMB on the 1- to 10-km scale is mostly explained by wind-driven processes, being a function of surface slope [King et al., 2004; Frezzotti et al., 2004]. Likewise, the SMB of annual stake measurements is also related to morphology via the surface slope [McConnell et al., 1997; Frezzotti et al., 2005]. However, Frezzotti et al. [2004] point out that along some transects (Talos Dome, Dome C) the maximum value of snow accumulation is highly correlated with firn temperatures and represents the snow precipitation minus surface sublimation (ablation not induced by wind). The difference between the maximum and minimum SMB values at these sites represents mainly ablation processes driven by katabatic winds. These wind-driven sublimation phenomena, controlled by the slope along the prevalent wind direction, have considerable impact on the spatial distribution of SMB. They sublimate and export huge quantities of snow into the atmosphere and then into the ocean, leading to a nonnegligible term in continental SMB studies [Frezzotti et al., 2004, 2007]. The direct snow redistribution process is local (e.g., sastrugi formation) and has a strong impact on the annual variability of accumulation at the annual/meter scale (i.e., noise in ice cores).

[111] Whereas SMB based on GPR and stake lines shows that decadal averaged spot measurements are only representative within a small area of a few square kilometers around the site (i.e., indicate relatively short correlation

lengths), precipitation is much more homogeneous. On the basis of the analysis of climate models and meteorological data, the decorrelation length of precipitation and precipitation minus evaporation of about 500 km is comparatively large [Genthon, 2004]. Nevertheless, as for SMB features, large differences occur between the coast and the interior, with particularly low values on the ridges and domes. The correlation length for real SMB is much shorter than that of precipitation or precipitation minus evaporation due to depositional and postdepositional processes. However, by spatially smoothing the small-scale noise (e.g., as defined by Genthon et al. [2005]), one may expect a correlation with precipitation at the 100-km scale.

### 3.3. Associations Between Spatial and Temporal Variability

[112] The spatial scale of significance for a single firn or ice core record is a critical issue for the interpretation of the accumulation time series. Microrelief (sastrugis) introduces a high-frequency, quasi-stochastic variability into core records of annual layer thickness [Fisher et al., 1985; Van der Veen and Bolzan, 1999]. Medium-scale undulations (wavelengths < 20 km) in surface topography up stream from a core-drilling site can cause variations in measured accumulation rates. One of the earliest results on this topic reveals that accumulation in troughs can be 30–50% more than on exposed surface crests [Gow and Rowland, 1965]. Meanwhile, as demonstrated in section 3.2, knowledge about the spatial variability has increased significantly. The stratigraphic record of a core is affected by the flow of ice, so the material at depth is slowly moved away from the original deposition site. If topographic features capable of changing the accumulation are located up stream of a core site, they can generate decadal to centennial long periods of accumulation consistently above or below the long-term mean because layers deeper in the record will have been deposited at these topographic troughs and crests [Richardson and Holmlund, 1999; Kaspari et al., 2005; Hamilton, 2004]. The only way to really understand the significance of a core record is to know something about the spatial field of SMB surrounding the core and also to have a good idea of the rate of movement of the ice through this field. Analysis of these data would allow some separation of the spatial and temporal variability that the core represents. This is the only way to understand the true significance of accumulation rate histories in cores. Any core for which these data are not available, or that is collected on fast moving ice, or is sufficiently deep to have moved more than a fraction of the correlation length for SMB, contains an accumulation rate history that is a mixed signal and is likely not interpretable.

[113] Richardson and Holmlund [1999] demonstrate the importance of determining the spatial significance of cores and recommend radar surveys prior to drilling, as this is the easiest way to get this information. The timescale for which this influence is important depends on the specific SMB and flow velocities at the site. However, it is possible to resolve temporal signals if the effects of local topography and ice

flow are considered [Spikes et al., 2004]. The length of periodic variations due to mesoscale relief and/or megadunes depend on ice velocity and SMB and can therefore vary in space and time. Frezzotti et al. [2005] point out that in megadune areas the distortion of records is characterized by a SMB periodicity of about 1500 years. In coastal areas with relatively large flow velocities and significant topographic variations, spatial SMB variations can influence temporal records on scales as short as a few decades [Anschütz et al., 2006]. Arcone et al. [2005b] demonstrate how the same effect is present in the GPR data themselves and must be corrected for. Consequently, several techniques have been developed to deconvolve spatial from temporal effects by employing GPR data [Hamilton, 2004; Arcone et al., 2005b; Parrenin et al., 2006].

### 3.4. Spatial Interpolation

[114] There are probably several different length scales for coherence in the true field of SMB. There may be greater complexity in places, but in general, we might argue that the shortest length scale is governed by the sastrugi length (0.1–100 m), the next is governed by the topography over which the wind transport of snow occurs (10–10,000 m), and the longest is governed by the regional differences in the supply of precipitation governed by synoptic climate (100–4000 km). The efforts at interpolation on the continental scale have usually been focused on producing a map of the third correlation scale, accepting that there is variability on the other two length scales that are not represented (see treatment by Vaughan et al. [1999a]). Understood in this way, attempts to use local measurements to draw a continental-scale map make some sense, although they are fraught with pitfalls. Improved interpolation can also be achieved by subdividing data sets of local measurements in regions of comparable properties (e.g., coastal areas and plateau region) and then performing interpolation for each region separately [Rotschky et al., 2007]. The complexity and quality of the efforts have undoubtedly increased in the last few decades, culminating with the explicit and formal treatment of uncertainty given by Arthern et al. [2006]. The map presented in their study will not be definitive in any sense but is a major step forward, since it includes a formal assessment of the uncertainty involved with the gridding process.

## 4. CONCLUSION AND RECOMMENDATIONS

[115] We have presented a summary of East Antarctic SMB characteristics and techniques used to acquire these. Our goal is to improve the knowledge of potential users about the difficulties associated with interpretation of measurements but also to highlight the need to perform more measurements and to use the ones currently available. We have demonstrated that SMB varies significantly in time and space on various scales. None of available measurement techniques are able to capture all scales simultaneously, neither can they be combined to provide area-wide measurements on basin scales, mainly as a result of logistical

constraints. Nevertheless, regionally confined studies provide valuable information from which a number of recommendations for data acquisition and potential data users can be proposed:

[116] 1. Decadal SMB values decorrelate on the 1- to 10-km scale but covary over length scales of hundreds of kilometers. The recent discovery from GPR data that on this scale, there exists a static (topographically induced) pattern of SMB, which cannot be observed in or estimated from sparse point measurements of SMB, is of utmost importance. These observations clearly indicate the potential pitfalls of using isolated measurements as being representative of a larger region. These pitfalls can be avoided and point measurements (usually cores) given regional significance by the simple expedient of acquiring GPR data around the core location. Ideally, the GPR profiles should span several ice thicknesses up flow, down flow, and across flow and should be tuned to acquire layer information at least as deep as the core. A well-dated core combined with GPR data will allow independent calculation of spatial and temporal means and variations for the region, plus their errors. These are the parameters that need to be routinely acquired and used if we are to substantially advance our understanding of continent-wide patterns of SMB across the Antarctic ice sheet.

[117] 2. Spatial variability increases as topographic complexity increases, caused by wind deposition/erosion. It is important to consider aeolian processes in general but especially when selecting sites for firm and ice coring in areas with relatively complex topography. Slope variations of only a few meters per kilometer have a significant impact on wind-derived snow accumulation processes and also therefore on the accumulation records. To fully understand the dominant processes that affect SMB and to incorporate these into global climate reconstructions, high-resolution representativity of SMB from cores is needed. Statistically meaningful reconstructions at annual and/or seasonal scale can be produced using multiple cores for each “center of action.”

[118] 3. The effective use of ultrasonic height ranger data in East Antarctic mass balance research requires that meteorological data are collected simultaneously and at the same location, so that the individual components of the SMB (sublimation, melt, snowdrift sublimation) can be quantified or at least estimated. Because of the operational accuracy of 2–3 cm, ultrasonic height ranger data are less useful to the study of individual accumulation events on the dry interior plateau of Antarctica. However, they are very valuable to determination of intraannual variability and seasonal cycles, which at many places are not known, not even qualitatively.

[119] 4. A considerable problem, which presently remains unsolved, is the conversion of height to mass changes for both stakes and ultrasonic sounders. This needs urgent attention, especially if the use of ultrasonic height ranger and stake data increases in the future. Moreover, the spatial interpolation and extrapolation of density profiles require further input.

TABLE 3. Possible Usage of Ground Truth SMB Estimates<sup>a</sup>

Source	Estimated SMB Property	Ground Truth Application
Stake farm	decorrelation and covariance on (sub)annual and subkilometer scale	laser altimetry
Stake line	decorrelation and covariance on (sub)annual and kilometer scale	laser altimetry, gravimetry
Ultrasonic sounders	high temporal resolution of single events, covariance	regional climate modeling
Snow pits	high-resolution time series	regional climate modeling, microwave radiometry
Cores	high-resolution and long-term record	regional climate modeling, microwave radiometry
GPR	temporally averaged decorrelation	altimetry, gravimetry

<sup>a</sup>All methods provide estimates of SMB. Specific properties, however, can only be determined by specific methods.

[120] 5. An apparently trivial aspect is documentation. Experience with older data sets shows that documentation is essential but, unfortunately, often neglected and partly even missing. The documentation should contain an exact description of how the raw data sets (e.g., length measurements) were obtained, which auxiliary parameters (e.g., density) were determined, and how measured quantities were finally converted to SMB.

[121] 6. For subsurface measurements, it is a great advantage if one can determine in the field if a good dating horizon has been reached. This can be achieved by several nondestructive measurements, either in the hole, in the pit, or along the core. Cores should be drilled to a depth covering the period back to the eruption of Tambora in A.D. 1815 and the unknown eruption in A.D. 1809.

[122] 7. When retrieving a firn core, there is often some unrecoverable loss of core material. This occurs predominantly in the upper meters. A correction scheme similar to a procedure described by *Whillans and Bolzan* [1988] is recommended, with special attention to an accurate measurement of diameter. To facilitate the identification of overlap between the core and a snow pit, the pit should be deep enough to cover one dating horizon that can also be captured in the adjacent drilled core. This latter task, however, is difficult and not always possible.

[123] 8. Accumulation on the plateau is, in general, more “well behaved” in terms of spatial representativity (apart from megadune fields) than the transition region from the plateau to the coastal areas, where high katabatic winds occur frequently and the morphological variability is often high (e.g., nunataks, valley glaciers). We need more sampling in the coastal regions if we are to improve continental average assessments.

[124] Ground truthing is essential for methods like remote sensing and numerical modeling, which require (and provide) estimates of decorrelation lengths, covariance, and associated uncertainties. The serviceability depends on the type of field data and their usage (Table 3). As a suitable combination, stake farms and GPS surveys in 1 km<sup>2</sup> areas provide a reference for laser altimetry. Decadal measurements of stake lines provide covariance on an annual scale for gravimetry, and ultrasonic sounders provide single events for regional models. Pits, cores, and GPR provide longer-term records for regional- or continental-scale modeling as well as spatial characteristics for remote sensing.

[125] From the point of view of specific mass balance estimates, the potential that with increasing precipitation,

the East Antarctic Ice Sheet could be the single largest ameliorator of sea level rise, and could balance a few tens of centimeters of sea level rise over the coming century, means that setting and understanding the baseline (current rates and trends in accumulation) are highly important. The accounting methods reviewed in this paper to determine the mean net annual SMB provide a significant contribution to this aim. Although they may never be suitable to infer the specific mass balance of the entire ice sheet, or even regions of it, by ground-based measurements alone, the records of SMB history and its spatial characteristics are definitely required to determine if the ice sheet’s SMB is changing in a secular fashion and whether or not this pattern is related to anthropogenic climate change. Assessments of ice sheet surface elevation changes [*Davis et al.*, 2005; *Zwally et al.*, 2005] will continue to yield the most precise results for mass balance estimates of specific drainage basins or ice sheets as a whole. In the intermediate-term perspective, gravity measurements and related time series may potentially become more accurate than they are at present [e.g., *Chen et al.*, 2006; *Velicogna and Wahr*, 2006; *Ramillien et al.*, 2006], thus providing valuable contributions to other techniques.

[126] New airborne techniques for determining the internal layering near the surface of ice masses are currently being developed, mainly in the context of calibration and validation campaigns for satellite remote sensors. The Airborne Synthetic Aperture and Interferometric Radar Altimeter (ASIRAS) System [*Mavrocordatos et al.*, 2004] and the D2P (delay/Doppler phase monopulse) radar [*Stenseng et al.*, 2005], for instance, do not only operate as classical altimeters or synthetic aperture radar (SAR) but also utilize an interferometric SAR mode. They are basically a replicate of the SAR/Interferometric Radar Altimeter (SIRAL) instrument to be operated on board CryoSat-2. The systems provide vertical resolution comparable to high-frequency GPR. The larger footprints cause less horizontal resolution than GPR but allow a higher spatial coverage. The advantage lies in operating such a system from an airplane, covering a relatively large area with profiles over a short period of time. Recent ASIRAS results from the dry snow zone [*Hawley et al.*, 2006] and percolation zone [*Helm et al.*, 2007] of the Greenland ice sheet, accompanied by ground-based measurements [*Scott et al.*, 2006], indicate that annual layers can be continuously detected by this system, promising extended future measurements in Antarctica. The combination of satellite remote sensors with airborne surveys and

dedicated ground measurements will likely remain the primary line of action for the next decade to obtain mass balance estimates for large parts of the ice sheet.

## APPENDIX A: OPTIMAL ESTIMATION OF STAKE INTERVAL

[127] By studying the accumulation correlation of nearby stakes as a function of distance, *Barkov and Lipenkov* [1978] evaluated the optimal distance between stakes (putting the stakes too close to each other will not significantly increase the accuracy due to accumulation correlation at the adjacent stakes) using a “structural function”  $b_{\Delta h}(\lambda)$  as a measure of correlation:

$$b_{\Delta h}(\lambda) = 2\sigma_{\Delta h}^2(1 - r_{\Delta h}(\lambda)), \quad (\text{A1})$$

with snow buildup  $\Delta h$ , its spatial variability  $\sigma_{\Delta h}$ , distance between stakes  $\lambda$ , and the correlation coefficient between snow buildup at two stakes  $r_{\Delta h}$ . The optimal distance is reached as soon as the correlation turns insignificant (and  $b_{\Delta h}$  reaches a saturation value). They found that at Vostok Station the annual accumulation at two points is practically not correlated at the distance of 65 m. Thus, Vostok stake farm with its distance between adjacent stakes of 25 m is close to optimum and even slightly oversampled. This implies that for studies aiming at smaller scales, stake distances on the order of several tens of meters are sufficient. However, both optimal distance and the saturation values vary over Antarctica.

[128] The structural function is used to determine optimal parameters (stake farm size/profile length and amount of stakes) of the stake farm/profile [*Barkov and Lipenkov*, 1978]:

$$\sigma_{\Delta h}^2 = \sigma_{\Delta h}^2 - \frac{1}{n^2} \sum_{i=1}^{n-1} (n-i)b_{\Delta h}(i\Delta l) \quad (\text{A2})$$

where  $\sigma_{\Delta h}^2(l, n)$  is the total error of snow buildup depending on the length of the route ( $l$ ) and amount of stakes ( $n$ );  $\sigma_{\Delta h}^2$  is the spatial variability of snow buildup (standard deviation);  $i$  is the index number of a given stake;  $\Delta l$  is the interval between adjacent stakes; and  $b_{\Delta h}(i\Delta l)$  is the value of the structural function for the distance  $i\Delta l$ . The optimal parameters of the stake farm correspond to the minimum value of  $\sigma_{\Delta h}^2(l, n)$ . This method is well suited for a series, members of which are not independent, which is the case for the snow buildup spatial distribution.

## GLOSSARY

**Ablation:** Negative surface mass balance.

**Accumulation:** Positive surface mass balance.

**Antarctic ice sheet:** Grounded part of the Antarctic polar ice cap, divided in the East and West Antarctic ice sheets.

**Blue ice area:** Area of negative surface mass balance,

where ice formed up stream emerges to the surface. Because of the higher density of the ice this appears blue. Surrounding areas with positive mass balance appear white because of the lower density of firn and snow compared to ice.

**Firn core:** Core extracted from the upper tens of meters from the firn, above the pore close-off depth, where no bubbles are yet present.

**Ground-penetrating radar:** Geophysical tool that emits electromagnetic waves from the surface into the ground; measures the round-trip traveltime of the wave that is returned from reflecting horizons.

**Ice core:** Core extracted from below the pore close-off depth, where bubbles have formed and are enclosed by ice.

**Mean net annual surface mass balance:** Summary of terms contributing to the solid, liquid, and gaseous transfer of water across the surface of the ice sheet; commonly normalized to  $\text{kg m}^{-2} \text{a}^{-1}$  but often given in millimeters water equivalent.

**Radiochronology:** Determination of age from the natural decay of radioactive species.

**Snow pit:** Trench excavated in the snow, often of rectangular cross section, with a vertical wall on one side to investigate the stratigraphy and to take samples.

**Stake:** Pole put into the snow (often bamboo, sometimes aluminium or similar). The height above snow or ice surface is measured at intervals to determine mass balance.

**Stake farm:** Combination of stakes in a two-dimensional setup, often as a rectangular grid.

**Stake line:** Combination of stakes along a one-dimensional line, often hundreds of kilometers long.

**Surface mass balance:** Short for mean net annual surface mass balance.

**Time marker:** Unambiguously identifiable feature of known age in time series records.

**Ultrasonic sounder:** Device to measure the distance to the surface. Operates with sound wave at ultrasonic frequencies.

**Volcanic horizon:** Deposits from volcanic eruptions (acids, ash) identifiable in layers, which were deposited at the ice sheet surface, buried, and submerged over time.

[129] **ACKNOWLEDGMENTS.** Special thanks to Tas van Ommen for his encouragement and contributions to the initial kick-off of the paper and to Martin Sharp and Ian Goodwin for their reviews. Data contributed by Robert Arthern for Figure 2 are greatly acknowledged. The background of this work is based on decades of field measurements and generations of scientists, made possible by the different national polar research institutions. We acknowledge their long-term support for designing and organizing ground-based measurements of Antarctic surface mass balance and the efforts by logistics to making them real. This work, moreover, greatly profited from discussions with numerous colleagues at the different institutions, too many to list them all here. This research was partly funded by the Italian National Antarctic Research Program (PNRA) and the Deutsche Forschungsgemeinschaft through an “Emmy Noether” scholarship, grant EI 672/1, to O.E. The Editor responsible for this paper was Ian Fairchild. He thanks Ian Goodwin as the technical reviewer and Martin Sharp as the cross-disciplinary reviewer.



## REFERENCES

- Alley, R. B., et al. (1997), Visual-stratigraphic dating of the GISP2 ice core: Basis, reproducibility, and application, *J. Geophys. Res.*, *102*(C12), 26,367–26,381.
- Andreas, E. L. (2002), Parameterizing scalar transfer over snow and ice: A review, *J. Hydrometeorol.*, *3*, 417–432.
- Annan, A. P., and J. L. Davis (1976), Impulse radar sounding in permafrost, *Radio Sci.*, *11*(4), 383–394.
- Anschütz, H., O. Eisen, W. Rack, and M. Scheinert (2006), Periodic surface features in coastal East Antarctica, *Geophys. Res. Lett.*, *33*, L22501, doi:10.1029/2006GL027871.
- Anschütz, H., O. Eisen, H. Oerter, D. Steinhage, and M. Scheinert (2007), Investigating small-scale variations of the recent accumulation rate in Central Dronning Maud Land, East Antarctica, *Ann. Glaciol.*, *46*, 14–21.
- Anschütz, H., D. Steinhage, O. Eisen, H. Oerter, M. Horwath, and U. Ruth (2008), Small-scale spatio-temporal characteristics of accumulation rates in western Dronning Maud Land, Antarctica, *J. Glaciol.*, in press.
- Arcone, S. A., V. B. Spikes, and G. S. Hamilton (2005a), Phase structure of radar stratigraphic horizons within Antarctic firn, *Ann. Glaciol.*, *41*, 10–16.
- Arcone, S. A., V. B. Spikes, and G. S. Hamilton (2005b), Stratigraphic variation within polar firn caused by differential accumulation and ice flow: Interpretation of a 400 MHz short-pulse radar profile from West Antarctica, *J. Glaciol.*, *51*(174), 407–422.
- Athern, R. J., D. P. Winebrenner, and D. G. Vaughan (2006), Antarctic snow accumulation mapped using polarization of 4.3-cm wavelength microwave emission, *J. Geophys. Res.*, *111*, D06107, doi:10.1029/2004JD005667.
- Barkov, N. I., and V. Y. Lipenkov (1978), Nakoplenie snega v rayone stantsii Vostok v 1970–1973 (Snow accumulation in the area of Vostok Station in 1970–1973), *Inf. Bull. Sov. Antarct. Exped.*, *98*, 63–68.
- Barkov, N. I., and V. Y. Lipenkov (1996), Nakoplenie snega v rayone stantsii Vostok, Antarktida, v 1970–1992 (Snow accumulation in the area of Vostok Station, Antarctica, in 1970–1992), *Mater. Glyatsiol. Issled.*, *80*, 87–88.
- Barnes, P. R. F., E. W. Wolff, R. Mulvaney, R. Udisti, E. Castellano, R. Röthlisberger, and J.-P. Steffensen (2002), Effect of density on electrical conductivity of chemically laden polar ice, *J. Geophys. Res.*, *107*(B2), 2029, doi:10.1029/2000JB000080.
- Bindschadler, R., H. Choi, C. Shuman, and T. Markus (2005), Detecting and measuring new snow accumulation on ice sheets by satellite remote sensing, *Remote Sens. Environ.*, *98*(4), 388–402.
- Bintanja, R. (1999), On the glaciological, meteorological, and climatological significance of Antarctic blue ice areas, *Rev. Geophys.*, *37*, 337–359.
- Bintanja, R. (2003), The mass balance of a dry snow surface during a snowstorm, *Ann. Glaciol.*, *38*, 79–83.
- Black, H. P., and W. Budd (1964), Accumulation in the region of Wilkes, Wilkes Land, Antarctica, *J. Glaciol.*, *5*(37), 3–15.
- Blindow, N. (1994), The central part of the Filchner-Ronne Ice Shelf, Antarctica: Internal structures revealed by 40 MHz monopulse RES, *Ann. Glaciol.*, *20*, 365–371.
- Bogorodsky, V. V., C. R. Bentley, and P. E. Gudmandsen (1985), *Radioglaciology*, D. Reidel, Dordrecht, Netherlands.
- Braaten, D. A. (1994), Instrumentation to quantify snow accumulation and transport dynamics at two locations on the Ross Ice Shelf, *Antarct. J. U.S.*, *29*(5), 86–87.
- Bromwich, D. H., A. J. Monaghan, J. G. Powers, J. J. Cassano, H. L. Wei, Y. H. Kuo, and A. Pellegrini (2003), Antarctic mesoscale prediction system (AMPS): A case study from the 2000–01 field season, *Mon. Weather Rev.*, *131*, 412–434.
- Budd, W. F., and I. N. Smith (1982), Large-scale numerical modelling of the Antarctic ice sheet, *Ann. Glaciol.*, *3*, 42–49.
- Bull, C. (1971), Snow accumulation in Antarctica, in *Research in the Antarctic*, edited by L. Quam, pp. 367–421, Am. Assoc. for the Adv. of Sci., Washington, D. C.
- Carter, M. W., and A. A. Moghissi (1977), Three decades of nuclear testing, *Health Phys.*, *33*, 55–71.
- Chen, J. L., C. R. Wilson, D. D. Blankenship, and B. D. Tapley (2006), Antarctic mass rates from GRACE, *Geophys. Res. Lett.*, *33*, L11502, doi:10.1029/2006GL026369.
- Clarke, T. S., and C. R. Bentley (1994), High-resolution radar on Ice Stream B2, Antarctica: Measurements of electromagnetic wave speed in firn and strain history from buried crevasses, *Ann. Glaciol.*, *20*, 153–159.
- Clough, J. W. (1977), Radio echo sounding: Reflections from internal layers in ice sheets, *J. Glaciol.*, *18*(78), 3–14.
- Clough, J. W., and C. R. Bentley (1970), Measurements of electromagnetic wave velocity in the East Antarctic ice sheet, in *International Symposium on Antarctic Glaciological Exploration (ISAGE), Proceedings SCAR/IASH Symposium*, edited by A. J. Gow et al., *IAHS Publ.*, *86*, 115–128.
- Clow, G. D., C. P. McKay, G. M. Simmons Jr., and R. A. Wharton Jr. (1988), Climatological observations and predicted sublimation rates at Lake Hoare, Antarctica, *J. Clim.*, *1*, 715–728.
- Coffey, M. T. (1996), Observations of the impact of volcanic activity on stratospheric chemistry, *J. Geophys. Res.*, *101*(D3), 6767–6780.
- Cole-Dai, J., and E. Mosley-Thompson (1999), The Pinatubo eruption in South Pole snow and its potential value to ice-core paleovolcanic records, *Ann. Glaciol.*, *29*, 99–105.
- Cole-Dai, J., E. Mosley-Thompson, and L. G. Thompson (1997), Annually resolved Southern Hemisphere volcanic history from two Antarctic ice cores, *J. Geophys. Res.*, *102*(D14), 16,761–16,771.
- Cole-Dai, J. H., E. Mosley-Thompson, S. P. Wight, and L. G. Thompson (2000), A 4100-year record of explosive volcanism from an East Antarctica ice core, *J. Geophys. Res.*, *105*(D19), 24,431–24,441.
- Corr, H. F. J., A. Jenkins, K. W. Nicholls, and C. S. M. Doake (2002), Precise measurement of changes in ice-shelf thickness by phase-sensitive radar to determine basal melt rates, *Geophys. Res. Lett.*, *29*(8), 1232, doi:10.1029/2001GL014618.
- Craven, M., and I. Allison (1998), Firnification and the effects of wind-packing on Antarctic snow, *Ann. Glaciol.*, *27*, 239–245.
- Crozaz, G., and C. C. Langway Jr. (1966), Dating Greenland firn-ice cores with <sup>210</sup>Pb, *Earth Planet. Sci. Lett.*, *1*(4), 194–196.
- Crozaz, G., E. Picciotto, and W. D. Breuck (1964), Antarctic snow chronology with <sup>210</sup>Pb, *J. Geophys. Res.*, *69*(12), 2597–2604.
- Curran, M. A. J., G. B. Jones, and H. Burton (1998), Spatial distribution of dimethylsulfide and dimethylsulfoniopropionate in the Australasian sector of the Southern Ocean, *J. Geophys. Res.*, *103*(D13), 16,677–16,689.
- Dansgaard, W. (1964), Stable isotopes in precipitation, *Tellus*, *16*, 436–468.
- Dansgaard, W., S. J. Johnsen, H. B. Clausen, and N. Gundestrup (1973), Stable isotope glaciology, *Medd. Groenl.*, *197*(2), 53.
- Dansgaard, W., et al. (1993), Evidence for general instability of past climate from a 250-kyr ice-core record, *Nature*, *364*, 218–220, doi:10.1038/364218a0.
- Davis, C. H., Y. Li, J. R. McConnell, M. M. Frey, and E. Hanna (2005), Snowfall-driven growth in East Antarctic ice sheet mitigates recent sea-level rise, *Science*, *308*(5730), 1898–1901.
- Delmas, R., and M. Pourchet (1977), Utilisation de filtres échangeurs d’ions pour l’étude de l’activité Béta globale d’un carottage glaciologique, *IAHS Publ.*, *118*, 159–163.
- Delmas, R. J., S. Kirchner, J. M. Palais, and J. R. Petit (1992), 1000 years of explosive volcanism recorded at the South Pole, *Tellus, Ser. B*, *44*, 335–350.
- Dibb, J. E., and M. Fahnestock (2004), Snow accumulation, surface height change, and firn densification at Summit, Greenland: Insights from 2 years of in situ observation, *J. Geophys. Res.*, *109*, D24113, doi:10.1029/2003JD004300.

- Dibb, J. E., P. A. Mayewski, C. S. Buck, and S. M. Drummey (1990), Scientific correspondence: Beta radiation from snow, *Nature*, *345*, 25.
- Dixon, D., P. A. Mayewski, S. Kaspari, S. Sneed, and M. Handley (2004), A 200-year sub-annual record of the primary sources of sulfate in West Antarctica, *Ann. Glaciol.*, *39*, 545–556.
- Doran, P. T., C. P. McKay, G. D. Clow, G. L. Dana, A. G. Fountain, T. Nylen, and W. B. Lyons (2002), Valley floor climate observations from the McMurdo dry valleys, Antarctica, 1986–2000, *J. Geophys. Res.*, *107*(D24), 4772, doi:10.1029/2001JD002045.
- Eisen, O., U. Nixdorf, F. Wilhelms, and H. Miller (2002), Electromagnetic wave speed in polar ice: Validation of the CMP technique with high resolution DEP and  $\gamma$ -density measurements, *Ann. Glaciol.*, *34*, 150–156.
- Eisen, O., F. Wilhelms, U. Nixdorf, and H. Miller (2003a), Identifying isochrones in GPR profiles from DEP-based forward modelling, *Ann. Glaciol.*, *37*, 344–350.
- Eisen, O., F. Wilhelms, U. Nixdorf, and H. Miller (2003b), Revealing the nature of radar reflections in ice: DEP-based FDTD forward modeling, *Geophys. Res. Lett.*, *30*(5), 1218, doi:10.1029/2002GL016403.
- Eisen, O., U. Nixdorf, F. Wilhelms, and H. Miller (2004), Age estimates of isochronous reflection horizons by combining ice core, survey, and synthetic radar data, *J. Geophys. Res.*, *109*, B04106, doi:10.1029/2003JB002858.
- Eisen, O., W. Rack, U. Nixdorf, and F. Wilhelms (2005), Characteristics of accumulation rate in the vicinity of the EPICA deep-drilling site in Dronning Maud Land, Antarctica, *Ann. Glaciol.*, *41*, 41–46.
- Eisen, O., I. Hamann, S. Kipfstuhl, D. Steinhage, and F. Wilhelms (2007), Direct evidence for radar reflector originating from changes in crystal-orientation fabric, *Cryosphere Discuss.*, *1*(1), 1–16.
- Ekaykin, A. A. (2003), Meteorological regime of central Antarctica and its role in the formation of isotope composition of snow thickness, Ph.D. thesis, Univ. Joseph Fourier, Grenoble, France.
- Ekaykin, A. A., V. Y. Lipenkov, N. I. Barkov, J. R. Petit, and V. Masson-Delmotte (2002), Spatial and temporal variability in isotope composition of recent snow in the vicinity of Vostok Station: Implications for ice-core interpretation, *Ann. Glaciol.*, *35*, 181–186.
- Ekaykin, A. A., V. Y. Lipenkov, I. N. Kuzmina, J. R. Petit, V. Masson-Delmotte, and S. J. Johnsen (2004), The changes in isotope composition and accumulation of snow at Vostok Station over the past 200 years, *Ann. Glaciol.*, *39*, 569–575.
- Endo, Y., and K. Fujiwara (1973), Characteristics of the snow cover in East Antarctica along the route of the JARE South Pole Traverse and factors controlling such characteristics, *JARE Sci. Rep., Ser. C, Earth Sci.*, *7*, 38 pp.
- Fahnestock, M. A., T. A. Scambos, C. A. Shuman, R. J. Arthern, D. P. Winebrenner, and R. Kwok (2000), Snow megadune fields on the East Antarctic Plateau: Extreme atmosphere-ice interaction, *Geophys. Res. Lett.*, *27*(22), 3719–3722.
- Feely, H. W., H. Seitz, R. J. Lagomarsino, and P. E. Biscaye (1966), Transport and fallout of stratospheric radioactive debris, *Tellus*, *18*, 316–328.
- Fischer, H., D. Wagenbach, and J. Kipfstuhl (1998), Sulfate and nitrate firn concentrations on the Greenland ice sheet: 2. Temporal anthropogenic deposition changes, *J. Geophys. Res.*, *103*(D17), 21,935–21,942.
- Fisher, D. A., N. Reeh, and H. B. Clausen (1985), Stratigraphic noise in time series derived from ice cores, *Ann. Glaciol.*, *7*, 76–83.
- Folco, L., A. Capra, M. Chiappini, M. Frezzotti, M. Mellini, and I. E. Tabacco (2002), The Frontier Mountain meteorite trap (Antarctica), *Meteorit. Planet. Sci.*, *37*, 209–228.
- Fortuin, J. P. F., and J. Oerlemans (1990), The parameterization of the annual surface temperature and mass balance of Antarctica, *Ann. Glaciol.*, *14*, 78–84.
- Freitag, J., F. Wilhelms, and S. Kipfstuhl (2004), Microstructure dependent densification of polar firn derived from X-ray microtomography, *J. Glaciol.*, *50*(169), 243–250.
- Frezzotti, M., and O. Flora (2002), Ice dynamic features and climatic surface parameters in East Antarctica from Terra Nova Bay to Talos Dome and Dome C: ITASE Italian Traverse, *Terra Antarct.*, *9*(1), 47–54.
- Frezzotti, M., S. Gandolfi, F. L. Marca, and S. Urbini (2002a), Snow dunes and glazed surfaces in Antarctica: New field and remote-sensing data, *Ann. Glaciol.*, *34*, 81–88.
- Frezzotti, M., S. Gandolfi, and S. Urbini (2002b), Snow megadunes in Antarctica: Sedimentary structure and genesis, *J. Geophys. Res.*, *107*(D18), 4344, doi:10.1029/2001JD000673.
- Frezzotti, M., et al. (2004), New estimations of precipitation and surface sublimation in East Antarctica from snow accumulation measurements, *Clim. Dyn.*, *23*(7–8), 803–813, doi:10.1007/s00382-004-0462-5.
- Frezzotti, M., et al. (2005), Spatial and temporal variability of snow accumulation in East Antarctica from traverse data, *J. Glaciol.*, *51*(172), 113–124.
- Frezzotti, M., S. Urbini, M. Proposito, C. Scarchilli, and S. Gandolfi (2007), Spatial and temporal variability of surface mass balance near Talos Dome, East Antarctica, *J. Geophys. Res.*, *112*, F02032, doi:10.1029/2006JF000638.
- Fuhrer, K., A. Neftel, M. Anklin, and W. Maggi (1993), Continuous measurements of hydrogen peroxide, formaldehyde, calcium and ammonium concentrations along the new GRIP ice core from Summit, central Greenland, *Atmos. Environ., Part A*, *27*(12), 1873–1880.
- Fuhrer, K., A. Neftel, M. Anklin, M. Staffelbach, and T. Legrand (1996), High-resolution ammonium ice core record covering a complete glacial-interglacial cycle, *J. Geophys. Res.*, *101*(D2), 4147–4164.
- Fujii, Y. (1981), Formation of surface snow layer at Mizuho Station, Antarctica, *Mem. Nat. Inst. Polar Res. Spec. Issue*, *19*, 280–296.
- Fujii, Y., and K. Kusunoki (1982), The Role of sublimation and condensation in the formation of ice sheet surface at Mizuho Station, Antarctica, *J. Geophys. Res.*, *87*(C6), 4293–4300.
- Fujita, S., H. Maeno, S. Uratsuka, T. Furukawa, S. Mae, Y. Fujii, and O. Watanabe (1999), Nature of radio echo layering in the Antarctic ice sheet detected by a two-frequency experiment, *J. Geophys. Res.*, *104*(B6), 13,013–13,024.
- Fujiwara, K., and Y. Endoh (1971), Preliminary report of glaciological studies, *Jpn. Antarct. Res. Exped. Sci. Rep., Special Issue*, *2*, 68–109.
- Gallée, H., G. Guyomarch, and E. Brun (2001), Impact of snow drift on the Antarctic ice sheet surface mass balance: Possible sensitivity to snow surface properties, *Boundary Layer Meteorol.*, *99*, 1–19.
- Gallée, H., V. Peyaud, and I. Goodwin (2005), Simulation of the net snow accumulation along the Wilkes Land transect, Antarctica, with a regional climate model, *Ann. Glaciol.*, *41*, 17–22.
- Genthon, C. (2004), Space-time Antarctic surface mass balance variability from climate models, *Ann. Glaciol.*, *39*, 271–275.
- Genthon, C., and G. Krinner (2001), Antarctic surface mass balance and systematic biases in general circulation models, *J. Geophys. Res.*, *106*(D18), 20,653–20,664.
- Genthon, C., S. Kaspari, and P. A. Mayewski (2005), Interannual variability of the surface mass balance of West Antarctica from ITASE cores and ERA40 reanalyses, *Clim. Dyn.*, *24*, 759–770, doi:10.1007/s00382-005-0019-2.
- Gerland, S., H. Oerter, J. Kipfstuhl, F. Wilhelms, H. Miller, and W. Miners (1999), Density log of a 181 m long ice core from Berkner Island, Antarctica, *Ann. Glaciol.*, *29*, 215–219.
- Giovinetto, M. B., N. M. Waters, and C. R. Bentley (1990), Dependence of Antarctic surface mass balance on temperature, elevation, and distance to open ocean, *J. Geophys. Res.*, *95*(D4), 3517–3531.

- Goldberg, E. D. (1963), Geochronology with lead-210, in *Radioactive Dating*, pp. 121–131, Int. At. Energy Agency, Vienna.
- Goodwin, I. D. (1990), Snow accumulation and surface topography in the katabatic zone of eastern Wilkes Land, Antarctica, *Antarct. Sci.*, 2(3), 232–235.
- Goodwin, I. D. (1991), Snow-accumulation variability from seasonal surface observations and firn-core stratigraphy, eastern Wilkes Land, Antarctica, *J. Glaciol.*, 37(127), 383–387.
- Goodwin, I. D., M. Higham, I. Allison, and R. Jaiwen (1994), Accumulation variation in eastern Kemp Land, Antarctica, *Ann. Glaciol.*, 20, 202–206.
- Goodwin, I., M. de Angelis, M. Pook, and N. W. Young (2003), Snow accumulation variability in Wilkes Land, East Antarctica, and the relationship to atmospheric ridging in the 130°–170°E region since 1930, *J. Geophys. Res.*, 108(D21), 4673, doi:10.1029/2002JD002995.
- Gow, A. J. (1965), On the accumulation and seasonal stratification of snow at the South Pole, *J. Glaciol.*, 5(40), 467–477.
- Gow, A. J., and R. Rowland (1965), On the relationship of snow accumulation to surface topography at “Byrd Station”, Antarctica, *J. Glaciol.*, 5(42), 843–847.
- Gudmandsen, P. (1975), Layer echoes in polar ice sheets, *J. Glaciol.*, 15(73), 95–101.
- Hamilton, G. (2004), Topographic control of regional accumulation rate variability at South Pole and implications for ice core interpretation, *Ann. Glaciol.*, 39, 214–218.
- Hammer, C. (1980), Acidity of polar ice cores in relation to absolute dating, past volcanism, and radio-echoes, *J. Glaciol.*, 25(93), 359–372.
- Hammer, C. U., H. B. Clausen, and C. C. Langway Jr. (1994), Electrical conductivity method (ECM) stratigraphic dating of the Byrd Station ice core, Antarctica, *Ann. Glaciol.*, 20, 115–120.
- Harrison, C. H. (1973), Radio echo sounding of horizontal layers in ice, *J. Glaciol.*, 12(66), 383–397.
- Hawley, R. L., E. M. Morris, R. Cullen, U. Nixdorf, A. P. Shepherd, and D. J. Wingham (2006), ASIRAS airborne radar resolves internal annual layers in the dry-snow zone of Greenland, *Geophys. Res. Lett.*, 33, L04502, doi:10.1029/2005GL025147.
- Helm, V., W. Rack, R. Cullen, P. Nienow, D. Mair, V. Parry, and D. J. Wingham (2007), Winter accumulation in the percolation zone of Greenland measured by airborne radar altimeter, *Geophys. Res. Lett.*, 34, L06501, doi:10.1029/2006GL029185.
- Helsen, M. M., R. S. W. van de Wal, M. R. van den Broeke, E. R. T. Kerstel, V. Masson-Delmotte, H. A. J. Meijer, C. H. Reijmer, and M. P. Scheele (2004), Modelling the isotopic composition of snow using backward trajectories: A particular precipitation event in Dronning Maud Land, Antarctica, *Ann. Glaciol.*, 39, 293–299.
- Helsen, M. M., R. S. W. van de Wal, M. R. van den Broeke, D. van As, H. A. J. Meijer, and C. H. Reijmer (2005), Oxygen isotope variability in snow from western Dronning Maud Land, Antarctica and its relation to temperature, *Tellus, Ser. B*, 57, 423–435.
- Hempel, L., F. Thyssen, N. Gundestrup, H. B. Clausen, and H. Miller (2000), A comparison of radio-echo sounding data and electrical conductivity of the GRIP ice core, *J. Glaciol.*, 46(154), 369–374.
- Hofstede, C. M., et al. (2004), Firn accumulation records for the past 1000 years on the basis of dielectric profiling of six cores from Dronning Maud Land, Antarctica, *J. Glaciol.*, 50(169), 279–291.
- Holmlund, P., et al. (2000), Spatial gradients in snow layering and ten metre temperatures at potential EPICA-DML drill sites, *Ann. Glaciol.*, 30, 13–19.
- Holtslag, A. A. M., and E. I. F. D. Bruijn (1988), Applied modelling of the nighttime surface energy balance over land, *J. Appl. Meteorol.*, 27, 689–704.
- Hori, A., et al. (1999), A detailed density profile of the Dome Fuji (Antarctica) shallow ice core by X-ray transmission method, *Ann. Glaciol.*, 29, 211–214.
- Isaksson, E., and W. Karlén (1994), Spatial and temporal patterns in snow accumulation, western Dronning Maud Land, Antarctica, *J. Glaciol.*, 40(135), 399–409.
- Isaksson, E., W. Karlén, N. Gundestrup, P. Mayewski, S. Whitlow, and M. Twickler (1996), A century of accumulation and temperature changes in Dronning Maud Land, Antarctica, *J. Geophys. Res.*, 101(D3), 7085–7094.
- Isaksson, E., M. R. van den Broeke, J.-G. Winther, L. Karlöf, J.-F. Pinglot, and N. Gundestrup (1999), Accumulation and proxy-temperature variability in Dronning Maud Land, Antarctica, determined from shallow firn cores, *Ann. Glaciol.*, 29, 17–22.
- Jacobel, R. W., and S. M. Hodge (1995), Radar internal layers from the Greenland summit, *Geophys. Res. Lett.*, 22(5), 587–590.
- Jacobel, R. W., B. C. Welch, E. J. Steig, and D. P. Schneider (2005), Glaciological and climatic significance of Hercules Dome, Antarctica: An optimal site for deep ice core drilling, *J. Geophys. Res.*, 110, F01015, doi:10.1029/2004JF000188.
- Jezek, K. C., and E. A. Roeloffs (1983), Measurements of radar wave speeds in polar glaciers using a down-hole radar target technique, *Cold Reg. Sci. Technol.*, 8, 199–208.
- Johnsen, S. J. (1977), Stable isotope homogenization of polar firn and ice, *IAHS Publ.*, 118, 388–392.
- Joughin, I., et al. (2005), Continued deceleration of Whillans Ice Stream, West Antarctica, *Geophys. Res. Lett.*, 32, L22501, doi:10.1029/2005GL024319.
- Jourdain, B., and M. Legrand (2001), Seasonal variations of atmospheric dimethylsulfide, dimethylsulfoxide, sulphur dioxide, methanesulfonate, and non-sea-salt sulphate aerosols at Dumont d’Urville (coastal Antarctica) (December 1998 to July 1999), *J. Geophys. Res.*, 106(D13), 14,391–14,408.
- Jouzel, J., L. Merlivat, M. Pourchet, and C. Lorius (1979), A continuous record of artificial tritium fallout at the South Pole (1954–1978), *Earth Planet. Sci. Lett.*, 45(1), 188–200.
- Jouzel, J., et al. (2007), Orbital and millennial Antarctic climate variability over the past 800,000 years, *Science*, 317(5839), 793–796, doi:10.1126/science.1141038.
- Kaczmarek, M., et al. (2004), Accumulation variability derived from an ice core from coastal Dronning Maud Land, Antarctica, *Ann. Glaciol.*, 39, 339–345.
- Kameda, T., H. Shoji, K. Kawada, O. Watanabe, and H. B. Clausen (1994), An empirical relation between overburden pressure and firn density, *Ann. Glaciol.*, 20, 87–94.
- Kameda, T., N. Azuma, T. Furukawa, Y. Ageta, and S. Takahashi (1997), Surface mass balance, sublimation and snow temperatures at Dome Fuji Station, Antarctica, in 1995, *Proc. NIPR Symp. Pol. Meteorol. Glaciol.*, 11, 24–34.
- Kameda, T., K. Fujita, O. Sugita, and G. Hashida (2007), Glaciological data collected by the 44th Japanese Antarctic Research Expedition during 2003–2004, *JARE Data Rep. Glaciol.*, 32, 92 pp.
- Kameda, T., H. Motoyama, S. Fujita, and S. Takahashi (2008), Temporal and spatial variability of surface mass balance at Dome Fuji, East Antarctica, by the stake method from 1995 to 2006, *J. Glaciol.*, 54(84), 107–116.
- Kamiyama, K., Y. Ageta, and Y. Fujii (1989), Atmospheric and depositional environments traced from unique chemical compositions of the snow over an inland high plateau, Antarctica, *J. Geophys. Res.*, 94(D15), 18,515–18,519.
- Kanagaratnam, P., S. P. Gogineni, N. Gundestrup, and L. Larsen (2001), High-resolution radar mapping of internal layers at the North Greenland Ice Core Project, *J. Geophys. Res.*, 106(D24), 33,799–33,812.
- Karlöf, L. (2004), Temporal and spatial variability of snow accumulation and redistribution, and its impact on the interpretation of ice cores, Ph.D. thesis, Fac. of Math. and Nat. Sci., Univ. of Oslo, Oslo.
- Karlöf, L., et al. (2000), A 1500 years record of accumulation at Amundsenisen western Dronning Maud Land, Antarctica, derived from electrical and radioactive measurements on a 120 m ice core, *J. Geophys. Res.*, 105(D10), 12,471–12,483.

- Karlöf, L., T. A. Oigard, F. Godtliebsen, M. Kaczmarek, and H. Fischer (2005a), Statistical techniques to select detection thresholds for peak signals in ice-core data, *J. Glaciol.*, *51*(175), 655–662.
- Karlöf, L., et al. (2005b), Accumulation variability over a small area in east Dronning Maud Land, Antarctica, as determined from shallow firn cores and snow pits: Some implications for ice-core records, *J. Glaciol.*, *51*(174), 343–352.
- Karlöf, L., D. P. Winebrenner, and D. B. Percival (2006), How representative is a time series derived from a firn core? A study at a low-accumulation site on the Antarctic plateau, *J. Geophys. Res.*, *111*, F04001, doi:10.1029/2006JF000552.
- Kaser, G. (1982), Measurement of evaporation from snow, *Meteorol. Atmos. Phys.*, *30*, 333–340.
- Kaspari, S., P. A. Mayewski, D. A. Dixon, V. B. Spikes, S. B. Sneed, M. J. Handley, and G. S. Hamilton (2005), Climate variability in West Antarctica derived from annual accumulation rate records from ITASE firn/ice cores, *Ann. Glaciol.*, *39*, 585–594.
- King, J. C., P. S. Anderson, M. C. Smith, and S. D. Mobbs (1996), The surface energy and mass balance at Halley, Antarctica, during winter, *J. Geophys. Res.*, *101*(D14), 19,119–19,128.
- King, J. C., P. S. Anderson, and G. W. Mann (2001), The seasonal cycle of sublimation at Halley, Antarctica, *J. Glaciol.*, *47*(156), 1–8.
- King, J. C., P. S. Anderson, D. G. Vaughan, G. W. Mann, S. D. Mobbs, and S. B. Vosper (2004), Wind-borne redistribution of snow across an Antarctic ice rise, *J. Geophys. Res.*, *109*, D11104, doi:10.1029/2003JD004361.
- Klok, E. J., M. Noland, and M. R. van den Broeke (2005), Analysis of meteorological data and the surface energy balance of McCall Glacier, Alaska, USA, *J. Glaciol.*, *51*(174), 451–461.
- Knüsel, S., D. E. Pignatelli, M. Schwikowski, and H. W. Gäggeler (2003), First results of trace element analysis in ice cores using Continuous Ice Melting (CIM) Inductively Coupled Plasma Sector Field Mass Spectrometry (ICP-SFMS), *J. Phys. IV Fr.*, *107*, doi:10.1051/jp4:20030399.
- Kohler, J., J. C. Moore, and E. Isaksson (2003), Comparison of modelled and observed responses of a glacier snowpack to ground-penetrating radar, *Ann. Glaciol.*, *37*, 293–297.
- Korth, W., and R. Dietrich (1996), *Ergebnisse geodätischer Arbeiten im Gebiet der Schirmacheroase/Antarctica 1988–1993*, *Publ. Ser. B Angew. Geod.*, vol. 301, Dtsch. Geod. Komm., Bayer. Akad. der Wiss., Munich, Germany.
- Kovacs, A., A. J. Gow, and R. M. Morey (1995), The in-situ dielectric constant of polar firn revisited, *Cold Reg. Sci. Technol.*, *23*, 245–256.
- Krinner, G., O. Magand, I. Simmonds, C. Genthon, and J.-L. Dufresne (2007), Simulated Antarctic precipitation and surface mass balance at the end of the 20th and 21st centuries, *Clim. Dyn.*, *28*, 215–230, doi:10.1007/s00382-006-0177-x.
- Lambert, G., B. Ardouin, J. Sanak, C. Lorius, and M. Pourchet (1977), Accumulation of snow and radioactive debris in Antarctica: A possible refined radiochronology beyond reference levels, in *Symposium Isotopes et Impuretés dans les neiges et glaces, Colloque de Grenoble, IAHS Publ.*, *118*, 146–158.
- Legrand, M., and R. J. Delmas (1984), The ionic balance of Antarctic snow: A 10-year detailed record, *Atmos. Environ.*, *18*, 1867–1874.
- Legrand, M., and P. A. Mayewski (1997), Glaciochemistry of polar ice cores: A review, *Rev. Geophys.*, *35*, 219–243.
- Li, J., and H. J. Zwally (2002), Modeled seasonal variations of firn density induced by steady-state surface air-temperature cycle, *Ann. Glaciol.*, *34*, 299–302.
- Li, J., and H. J. Zwally (2004), Modeling the density variation in the shallow firn layer, *Ann. Glaciol.*, *38*, 309–313.
- Li, L., and J. W. Pomeroy (1997), Estimates of threshold wind speeds for snow transport using meteorological data, *J. Appl. Meteorol.*, *36*, 205–213.
- Lipenkov, V. Y., A. A. Ekaykin, N. I. Barkov, and M. Pourchet (1998), O svyazi plotnosti poverhnostnogo sloya snega v Antarktide so skorost'yu vetra (On the relationship of surface snow density in Antarctica and wind speed), *Mater. Glyatsiol. Issled.*, *85*, 148–158.
- Looyenga, H. (1965), Dielectric constant of heterogeneous mixtures, *Physica*, *31*(3), 401–406.
- Magand, O., M. Frezzotti, M. Pourchet, B. Stenni, L. Genoni, and M. Fily (2004), Climate variability along latitudinal and longitudinal transects in East Antarctica, *Ann. Glaciol.*, *39*, 351–358.
- Magand, O., C. Genthon, M. Fily, G. Krinner, G. Picard, M. Frezzotti, and A. A. Ekaykin (2007), An up-to-date quality-controlled surface mass balance data set for the 90°–180°E Antarctica sector and 1950–2005 period, *J. Geophys. Res.*, *112*, D12106, doi:10.1029/2006JD007691.
- Mann, G. W., P. S. Anderson, and S. D. Mobbs (2000), Profile measurements of blowing snow at Halley, Antarctica, *J. Geophys. Res.*, *105*(D19), 24,491–24,508.
- Masson-Delmotte, V., et al. (2008), A review of Antarctic surface snow isotopic composition: Observations, atmospheric circulation and isotopic modelling, *J. Clim.*, in press.
- Matsuoka, K., T. Furukawa, S. Fujita, H. Maeno, S. Uratsuka, R. Naruse, and O. Watanabe (2003), Crystal orientation fabrics within the Antarctic ice sheet revealed by a multipolarization plane and dual-frequency radar survey, *J. Geophys. Res.*, *108*(B10), 2499, doi:10.1029/2003JB002425.
- Matsuoka, K., S. Uratsuka, S. Fujita, and F. Nishio (2004), Ice-flow induced scattering zone within the Antarctic ice sheet revealed by high-frequency airborne radar, *J. Glaciol.*, *50*(170), 382–388.
- Mavrocordatos, C., E. Attema, M. Davidson, H. Lentz, and U. Nixdorf (2004), Development of ASIRAS (Airborne SAR/ Interferometric Altimeter System), in *Geoscience and Remote Sensing Symposium IGARSS '04*, vol. 4, pp. 2465–2467, IEEE Int., New York, doi:10.1109/IGARSS.2004.1369792.
- Mayewski, P. A., and I. D. Goodwin (1997), International Trans-Antarctic Scientific Expedition (ITASE), *PAGES Rep. 1997-1*, 48 pp., Past Global Changes Proj., Bern.
- Mayewski, P. A., L. D. Meeker, S. Whitlow, M. S. Twickler, M. C. Morrison, R. B. Alley, P. Bloomfield, and K. Taylor (1993), The atmosphere during the Younger Dryas, *Science*, *261*(5118), 195–197, doi:10.1126/science.261.5118.195.
- Mayewski, P. A., et al. (2005), The International Trans-Antarctic Scientific Expedition (ITASE): An overview, *Ann. Glaciol.*, *41*, 180–185.
- McConnell, J. R., R. C. Bales, and D. R. Davis (1997), Recent intra-annual snow accumulation at South Pole: Implications for ice core interpretation, *J. Geophys. Res.*, *102*(D18), 21,947–21,954.
- McMorrow, A. J., M. A. J. Curran, T. D. van Ommen, V. Morgan, I. Allison, and M. J. Pook (2001), Intercomparison of firn core and meteorological data, *Antarct. Sci.*, *13*(3), 329–337.
- Meyerson, E. A., P. A. Mayewski, K. J. Kreutz, L. D. Meeker, S. I. Whitlow, and M. S. Twickler (2002), The polar expression of ENSO and sea-ice variability as recorded in a South Pole ice core, *Ann. Glaciol.*, *35*, 430–436.
- Millar, D. H. H. (1981), Radio echo layering in polar ice sheets and past volcanic activity, *Nature*, *292*, 441–443.
- Minikin, A., D. Wagenbach, W. Graf, and J. Kipfstuhl (1994), Spatial and seasonal variations of the snow chemistry at the central Filchner–Ronne Ice Shelf, Antarctica, *Ann. Glaciol.*, *20*, 283–290.
- Monaghan, A. J., et al. (2006), Insignificant change in Antarctic snowfall since the International Geophysical Year, *Science*, *313*(5788), 827–831, doi:10.1126/science.1128243.
- Moore, J. C. (1988), Dielectric variability of a 130 m Antarctic ice core: Implications for radar sounding, *Ann. Glaciol.*, *11*, 95–99.
- Moore, J. C., and R. Mulvaney (1989), Dielectrical stratigraphy of ice: A new technique for determining total ionic concentrations in polar ice cores, *Geophys. Res. Lett.*, *16*(10), 1171–1179.

- Moore, J. C., and J. G. Paren (1987), New technique for dielectric logging of Antarctic ice cores, *J. Phys. Colloq. C1*, 48(3), 155–160.
- Moore, J. C., H. Narita, and N. Maeno (1991), A continuous 770-year record of volcanic activity from East Antarctica, *J. Geophys. Res.*, 96(D9), 17,353–17,359.
- Morey, R. M., and A. Kovacs (1985), Analysis of wide-angle reflection and refraction measurements, *CRREL Spec. Rep.*, 85-5, 53–60.
- Morgan, V. I., and T. H. Jacka (1981), Mass balance studies in East Antarctica, in *Sea Level, Ice, and Climatic Change*, edited by I. Allison, *IAHS Publ.*, 131, 253–260.
- Morgan, V. I., I. D. Goodwin, D. M. Etheridge, and C. W. Wookey (1991), Evidence from Antarctic ice cores for recent increases in snow accumulation, *Nature*, 354, 58–60.
- Morris, E. D., and J. D. Cooper (2003), Density measurements in ice boreholes using neutron scattering, *J. Glaciol.*, 49(167), 599–604.
- Mosley-Thompson, E., and L. G. Thompson (1982), Nine centuries of microparticle deposition at the South Pole, *Quat. Res.*, 17, 1–13.
- Mosley-Thompson, E., L. G. Thompson, J. F. Paskievitch, M. Pourchet, A. J. Gow, M. E. Davis, and J. Kleinman (1995), South Pole snow accumulation has increased in recent decades, *Ann. Glaciol.*, 21, 131–138.
- Mosley-Thompson, E., J. F. Paskievitch, A. J. Gow, and L. G. Thompson (1999), Late 20th century increase in South Pole snow accumulation, *J. Geophys. Res.*, 104(D4), 3877–3886.
- Mulvaney, R., H. Oerter, D. A. Peel, W. Graf, C. Arrowsmith, E. C. Pasteur, B. Knight, G. C. Littot, and W. D. Miners (2002), 1000 year ice-core records from Berkner Island, Antarctica, *Ann. Glaciol.*, 35, 45–51.
- Murray, T., G. W. Stuart, P. J. Miller, J. Woodward, A. M. Smith, P. R. Porter, and H. Jiskoot (2000), Glacier surge propagation by thermal evolution at the bed, *J. Geophys. Res.*, 105(B6), 13,491–13,507.
- Muszynski, I., and G. E. Birchfield (1985), The dependence of Antarctic accumulation rates on surface temperature and elevation, *Tellus, Ser. A*, 37, 204–208.
- Nefel, A. (1991), Use of snow and firn analysis to reconstruct past atmospheric composition, in *Seasonal Snowpacks, NATO ASI, Ser. G*, vol. 28, edited by T. D. Davies, M. Tranter, and H. Jones, pp. 385–415, Springer, Berlin.
- Nemazi, M., G. Lambert, C. Lorius, and J. Labeyrie (1964), Mesure du taux d'accumulation de la neige au bord du continent Antarctique par la méthode du Plomb-210, *C. R. Hebd. Seances Acad. Sci.*, 259(19), 3319–3322.
- Nereson, N. A., C. F. Raymond, R. W. Jacobel, and E. D. Waddington (2000), The accumulation pattern across Siple Dome, West Antarctica, inferred from radar-detected internal layers, *J. Glaciol.*, 46(156), 75–87.
- Neumann, T. A., and E. D. Waddington (2004), Effects of firn ventilation on isotopic exchange, *J. Glaciol.*, 50(169), 183–194.
- Neumann, T. A., E. D. Waddington, E. J. Steig, and P. M. Grootes (2005), Non-climate influences on stable isotopes at Taylor Mouth, Antarctica, *J. Glaciol.*, 51(173), 248–258.
- Nishio, F., et al. (2002), Annual-layer determinations and 167 year records of past climate of H72 ice core in east Dronning Maud Land, Antarctica, *Ann. Glaciol.*, 35, 471–479.
- Noone, D., J. Turner, and R. Mulvaney (1999), Atmospheric signals and characteristics of accumulation in Dronning Maud Land, Antarctica, *J. Geophys. Res.*, 104(D16), 19,191–19,211.
- Oerlemans, J. (2003), Analysis of a 3 year meteorological record from the ablation zone of Morteratschgletscher, Switzerland: Energy and mass balance, *J. Glaciol.*, 46(155), 571–579.
- Oerter, H. (2005), Stable oxygen isotopes of snow pit DML25S02\_03 (SS0203), *PANGAEA*, doi:10.1594/PANGAEA.264585.
- Oerter, H., W. Graf, F. Wilhelms, A. Minikin, and H. Miller (1999), Accumulation studies on Amundsenisen, Dronning Maud Land, Antarctica, by means of Tritium, dielectric profiling and stable-isotope measurements: First results from the 1995–96 and 1996–97 field seasons, *Ann. Glaciol.*, 29, 1–9.
- Oerter, H., F. Wilhelms, F. Jung-Rothenhäusler, F. Göktas, H. Miller, W. Graf, and S. Sommer (2000), Accumulation rates in Dronning Maud Land as revealed by dielectrical-profiling measurements at shallow firn cores, *Ann. Glaciol.*, 30, 27–34.
- Oerter, H., W. Graf, H. Meyer, and F. Wilhelms (2004), The EPI-CA ice core Dronning Maud Land: First results from stable-isotope measurements, *Ann. Glaciol.*, 39(39), 307–312.
- Osterberg, E. C., M. J. Handley, S. B. Sneed, P. A. Mayewski, and K. J. Kreutz (2006), Continuous ice core melter system with discrete sampling for major ion, trace element and stable isotope analyses, *Environ. Sci. Technol.*, 40, 3355–3361.
- Palais, J. M., I. M. Whillans, and C. Bull (1982), Snow stratigraphic studies at Dome C, East Antarctica: An investigation of depositional and diagenetic processes, *Ann. Glaciol.*, 3, 239–242.
- Palais, J. M., M. S. Germani, and G. A. Zielinski (1992), Inter-hemispheric transport of volcanic ash from a 1259 A.D. volcanic eruption to the Greenland and Antarctic ice sheets, *Geophys. Res. Lett.*, 19(8), 801–804.
- Pälli, A., J. C. Kohler, E. Isaksson, J. C. Moore, J. F. Pinglot, V. A. Pohjola, and H. Samuelsson (2002), Spatial and temporal variability of snow accumulation using ground-penetrating radar and ice cores on a Svalbard glacier, *J. Glaciol.*, 48(162), 417–424.
- Palmer, A. S., T. D. van Ommen, M. A. J. Curran, V. Morgan, J. M. Souney, and P. A. Mayewski (2001), High-precision dating of volcanic events (A.D. 1301–1995) using ice cores from Law Dome, Antarctica, *J. Geophys. Res.*, 106(D22), 28,089–28,095.
- Parrenin, F., R. Hindmarsh, and F. Remy (2006), Analytical solutions for the effect of topography, accumulation rate and flow divergence on isochrone layer geometry, *J. Glaciol.*, 52(177), 191–202.
- Petit, J.-R., J. Jouzel, M. Pourchet, and L. Merlivat (1982), A detailed study of snow accumulation and stable isotope content in Dome C (Antarctica), *J. Geophys. Res.*, 87(C6), 4301–4308.
- Pettré, P., J. F. Pinglot, M. Pourchet, and L. Reynaud (1986), Accumulation in Terre Adélie, Antarctica: Effect of meteorological parameters, *J. Glaciol.*, 32(112), 486–500.
- Picciotto, E., and S. Wilgain (1963), Fission products in Antarctic snow, a reference level for measuring accumulation, *J. Geophys. Res.*, 68(21), 5965–5972.
- Picciotto, E., G. Crozaz, and W. D. Breuck (1964), Rate of accumulation of snow at South Pole as determined by radioactive measurements, *Nature*, 203, 393–394.
- Picciotto, E., G. Crozaz, and W. de Breuck (1971), Accumulation on the South Pole–Queen Maud Land Traverse, 1964–1968, in *Antarctic Snow and Ice Studies II, Antarct. Res. Ser.*, vol. 16, edited by A. Crary, pp. 257–315, AGU, Washington, D. C.
- Pinglot, F., and M. Pourchet (1979), Low-level beta counting with an automatic sample changer, *Nucl. Instrum. Methods*, 166(3), 483–490.
- Pinglot, J. F., and M. Pourchet (1981), Gamma-ray bore-hole logging for determining radioactive fallout layers in snow, in *Methods of Low-Level Counting and Spectrometry*, pp. 161–172, Int. At. Energy Agency, Vienna.
- Pinglot, J. F., and M. Pourchet (1994), Spectrométrie Gamma à très bas niveau avec anti-compton NaI (T1) pour l'étude des glaciers et des sédiments, *J. Spectrom. Gamma X*, 93, 291–296.
- Pourchet, M., F. Pinglot, and C. Lorius (1983), Some meteorological applications of radioactive fallout measurements in Antarctic snows, *J. Geophys. Res.*, 88(C10), 6013–6020.
- Pourchet, M., et al. (1997), Distribution and fall-out of <sup>137</sup>Cs and other radionuclides over Antarctica, *J. Glaciol.*, 43(145), 435–445.
- Pourchet, M., O. Magand, M. Frezzotti, A. A. Ekaykin, and J. G. Winter (2003), Radionuclides deposition over Antarctica, *J. Environ. Radioact.*, 68, 137–158.

- Qin, D. H., J. W. Ren, J. C. Kang, C. D. Xiao, Z. Q. Li, Y. S. Li, B. Sun, W. Z. Sun, and X. X. Wang (2000), Primary results of glaciological studies along an 1100 km transect from Zhongshan station to Dome A, East Antarctic ice sheet, *Ann. Glaciol.*, *31*, 198–204.
- Ramillien, G., A. Lombard, A. Cazenave, E. R. Ivins, M. Llubes, F. Remy, and R. B. Ramilien (2006), Interannual variations of the mass balance of the Antarctica and Greenland ice sheets from GRACE, *Global Planet. Change*, *53*(3), 198–208, doi:10.1016/j.gloplacha.2006.06.003.
- Rasmussen, S. O., K. K. Andersen, S. J. Johnsen, M. Bigler, and T. McCormack (2005), Deconvolution-based resolution enhancement of chemical ice core records obtained by continuous flow analysis, *J. Geophys. Res.*, *110*, D17304, doi:10.1029/2004JD005717.
- Reijmer, C. H., and M. R. V. D. Broeke (2003), Temporal and spatial variability of the surface mass balance in Dronning Maud Land, Antarctica, as derived from automatic weather stations, *J. Glaciol.*, *49*(167), 512–520.
- Reijmer, C. H., M. R. van den Broeke, and M. P. Scheele (2002), Air parcel trajectories to five deep drilling locations on Antarctica, based on the ERA-15 data set, *J. Clim.*, *15*, 1957–1968.
- Reinhardt, H., M. Kriews, H. Miller, O. Schrems, C. Ludke, E. Hoffmann, and J. Skole (2001), Laser ablation inductively coupled plasma mass spectrometry: A new tool for trace element analysis in ice cores, *Fresenius J. Anal. Chem.*, *370*, 629–636.
- Ren, J. W., Q. Dahe, and I. Allison (1999), Variations of snow accumulation and temperature over past decades in the Lambert Glacier basin, Antarctica, *Ann. Glaciol.*, *29*, 29–32.
- Ren, J. W., I. Allison, C. D. Xiao, and D. H. Qin (2002), Mass balance of the Lambert Glacier basin, East Antarctica, *Sci. China Ser. D, Earth Sci.*, *45*(9), 842–850.
- Richardson, C., and P. Holmlund (1999), Spatial variability at shallow snow-layer depths in central Dronning Maud Land, East Antarctica, *Ann. Glaciol.*, *29*, 10–16.
- Richardson, C., E. Aarholt, S.-E. Hamram, P. Holmlund, and E. Isaksson (1997), Spatial distribution of snow in western Dronning Maud Land, East Antarctica, mapped by a ground-based snow radar, *J. Geophys. Res.*, *102*(B9), 20,343–20,353.
- Richardson-Näslund, C. (2001), Spatial distribution of snow in Antarctica and other glacier studies using ground-penetrating radar, *Thesis Geogr. Emphasis Phys. Geogr.*, vol. 18, Dep. of Phys. Geogr. and Quat. Geol., Stockholm Univ., Stockholm.
- Richardson-Näslund, C. (2004), Spatial characteristics of snow accumulation in Dronning Maud Land, Antarctica, *Global Planet. Change*, *42*, 31–43.
- Robin, G. d. Q., S. Evans, and J. T. Bailey (1969), Interpretation of radio echo sounding in polar ice sheets, *Philos. Trans. R. Soc. London, Ser. A*, *146*, 437–505.
- Röthlisberger, R., M. Bigler, M. Hutterli, S. Sommer, B. Stauffer, H. G. Junghans, and D. Wagenbach (2000), Technique for continuous high-resolution analysis of trace substances in firn and ice cores, *Environ. Sci. Technol.*, *34*, 338–342.
- Rotschky, G., O. Eisen, F. Wilhelms, U. Nixdorf, and H. Oerter (2004), Spatial characteristics of accumulation patterns derived from combined data sets in Dronning Maud Land, Antarctica, *Ann. Glaciol.*, *39*, 265–270.
- Rotschky, G., W. Rack, W. Dierking, and H. Oerter (2006), Retrieving snowpack properties and accumulation estimates from combination of SAR and scatterometer measurements, *IEEE Trans. Geos. Rem. Sens.*, *44*(4), 943–956, doi:10.1109/TGRS.2005.862524.
- Rotschky, G., P. Holmlund, E. Isaksson, R. Mulvaney, H. Oerter, M. R. van den Broeke, and J.-G. Winther (2007), A new surface accumulation map for western Dronning Maud Land, Antarctica, from interpolation of point measurements, *J. Glaciol.*, *53*(182), 385–398, doi:10.3189/002214307783258459.
- Saigne, C., and M. Legrand (1987), Measurements of methanesulphonic acid in Antarctic ice, *Nature*, *330*, 240–242, doi:10.1038/330240a0.
- Satake, H., and K. Kawada (1997), The quantitative evaluation of sublimation and the estimation of original hydrogen and oxygen of a firn core at east Queen Maud Land, Antarctica, *Bull. Glacier Res.*, *15*, 93–97.
- Schlosser, E., N. van Lipzig, and H. Oerter (2002), Temporal variability of accumulation at Neumayer station, Antarctica, from stake array measurements and a regional atmospheric model, *J. Glaciol.*, *48*(160), 87–94.
- Schwander, J., A. Neftel, H. Oeschger, and B. Stauffer (1983), Measurement of direct current conductivity on ice samples for climatological applications, *J. Phys. Chem.*, *87*, 4157–4160.
- Scott, J. B. T., D. Mair, P. Nienow, V. Parry, and E. Morris (2006), A ground-based radar backscatter investigation in the percolation zone of the Greenland ice sheet, *Remote Sens. Environ.*, *104*(4), 361–373.
- Sigg, A., K. Fuhrer, M. Anklin, T. Staffelbach, and D. Zurmühle (1994), A continuous analysis technique for trace species in ice cores, *Environ. Sci. Technol.*, *28*(2), 204–209.
- Sinisalo, A., A. Grinsted, J. C. Moore, E. Kärkäs, and R. Pettersson (2005), Snow-accumulation studies in Antarctica with ground-penetrating radar using 50, 100 and 800 MHz antenna frequencies, *Ann. Glaciol.*, *37*, 194–198.
- Smeets, C. J. P. P., and M. R. van den Broeke (2008), Temporal and spatial variation of momentum roughness length in the ablation zone of the Greenland ice sheet, *Boundary Layer Meteorol.*, in press.
- Smith, B. T., T. D. Van Ommen, and V. I. Morgan (2002), Distribution of oxygen isotope ratios and snow accumulation rates in Wilhelm II Land, East Antarctica, *Ann. Glaciol.*, *35*, 107–110.
- Sommer, S., D. Wagenbach, R. Mulvaney, and H. Fischer (2000a), Glacio-chemical study spanning the past 2 kyr on three ice cores from Dronning Maud Land, Antarctica: 2. Seasonally resolved chemical records, *J. Geophys. Res.*, *105*(D24), 29,423–29,433.
- Sommer, S., et al. (2000b), Glacio-chemical study covering the past 2 kyr on three ice cores from Dronning Maud Land, Antarctica: 1. Annually resolved accumulation rates, *J. Geophys. Res.*, *105*(D24), 29,411–29,421.
- Spikes, V. B., G. S. Hamilton, S. A. Arcone, S. Kaspari, and P. A. Mayewski (2004), Variability in accumulation rates from GPR profiling on the West Antarctic plateau, *Ann. Glaciol.*, *39*, 238–244.
- Stearns, C. R., and G. A. Weidner (1993), Sensible and latent heat flux estimates in Antarctica, in *Antarctic Meteorology and Climatology, Studies Based on Automatic Weather Stations, Antarct. Res. Ser.*, vol. 61, edited by D. H. Bromwich and C. R. Stearns, pp. 109–138, AGU, Washington, D. C.
- Steffen, K., and J. Box (2001), Surface climatology of the Greenland ice sheet: Greenland Climate Network 1995–1999, *J. Geophys. Res.*, *106*(D24), 33,951–33,964.
- Steig, E. J., et al. (2005), High-resolution ice cores from US ITASE (West Antarctica): Development and validation of chronologies and determination of precision and accuracy, *Ann. Glaciol.*, *41*, 77–84.
- Stenberg, M., M. Hansson, P. Holmlund, and L. Karlöf (1999), Variability in snow layering and snow chemistry in the vicinity of two drill sites in western Dronning Maud Land, Antarctica, *Ann. Glaciol.*, *29*, 33–37.
- Stenni, B., R. Caprioli, L. Cimino, C. Cremisini, O. Flora, R. Gragnani, A. Longinelli, V. Maggi, and S. Torcini (1999), 200 years of isotope and chemical records in a firn core from Hercules Néé, northern Victoria Land, Antarctica, *Ann. Glaciol.*, *29*, 106–112.
- Stenni, B., F. Serra, M. Frezzotti, V. Maggi, R. Traversi, S. Becagli, and R. Udisti (2000), Snow accumulation rates in Northern Victoria Land (Antarctica) by firn core analysis, *J. Glaciol.*, *46*(155), 541–552.
- Stenni, B., V. Masson-Delmotte, S. Johnsen, J. Jouzel, A. Longinelli, E. Monnin, R. Röthlisberger, and E. Selmo (2001), An oceanic cold reversal during the last deglaciation, *Science*, *293*(5537), 2074–2077, doi:10.1126/science.1059702.

- Stenni, B., M. Proposito, R. Gragnani, O. Flora, J. Jouzel, S. Falourd, and M. Frezzotti (2002), Eight centuries of volcanic signal and climate change at Talos Dome (East Antarctica), *J. Geophys. Res.*, *107*(D9), 4076, doi:10.1029/2000JD000317.
- Stenseng, L., R. Forsberg, K. Keller, S. M. Hvidegaard, and C. Leuschen (2005), Comparison of airborne laser scanning and D2P radar altimetry, *Geophys. Res. Abst.*, *7*, 06393.
- Stroeven, A. P., and V. A. Pohjola (1991), Glaciological studies in Scharffenbergbotnen, in *The Expedition ANTARKTIS-VIII of RV "POLARSTERN" 1989/90, Report of Leg ANT-VIII/5, Ber. Polarforschung*, vol. 86, edited by H. Miller and H. Oerter, pp. 126–130, Alfred-Wegener-Inst. für Polar- und Meeresforsch., Bremerhaven, Germany.
- Swedish Antarctic Research Programme (2003), Annual report, Stockholm.
- Takahashi, S., and T. Kameda (2007), Snow density for measuring the surface mass balance using the stake method, *J. Glaciol.*, *53*(183), 677–680.
- Takahashi, S., and O. Watanabe (1997), Snow accumulation in Antarctica: East Queen Maud Land, *Glaciol. Folio, sheet 3-1*, Natl. Inst. of Pol. Res., Tokyo.
- Takahashi, S., Y. Ageta, Y. Fujii, and O. Watanabe (1994), Surface mass balance in east Dronning Maud Land, Antarctica, observed by Japanese Antarctic Research Expeditions, *Ann. Glaciol.*, *20*, 242–253.
- Taylor, K. C., and R. B. Alley (2004), Two-dimensional electrical stratigraphy of the Siple Dome (Antarctica) ice core, *J. Glaciol.*, *50*(16), 231–235.
- Taylor, K. C., et al. (2004), Dating the Siple Dome (Antarctica) ice core by manual and computer interpretation of annual layering, *J. Glaciol.*, *50*(170), 453–461.
- Tiuri, M. T., A. H. Sihvola, E. G. Nyfors, and M. T. Hallikainen (1984), The complex dielectric constant of snow at microwave frequencies, *IEEE J. Oceanic Eng.*, *9*(5), 377–382.
- Trauffer, F., H. Oerter, H. Fischer, R. Weller, and H. Miller (2004), Spatio-temporal variability in volcanic sulphate deposition over the past 2 kyr in snow pits and firn cores from Amundsenisen, Antarctica, *J. Glaciol.*, *50*(168), 137–146.
- Traversi, R., S. Becagli, E. Castellano, A. Migliori, M. Severi, and R. Udisti (2002), High resolution fast ion chromatography (FIC) measurements of chloride, nitrate and sulphate along the EPICA Dome C ice core, *Ann. Glaciol.*, *35*, 291–298.
- Udisti, R. (1996), Multiparametric approach for chemical dating of snow layers from Antarctica, *Int. J. Environ. Anal. Chem.*, *63*, 225–244.
- Udisti, R., S. Becagli, E. Castellano, R. Mulvaney, J. Schwander, S. Torcini, and E. Wolff (2000), Holocene electrical and chemical measurements from the EPICA Dome C ice core, *Ann. Glaciol.*, *30*, 20–26.
- Urbini, S., L. Vittuari, and S. Gandolfi (2001), GPR and GPS data integration: Examples of application in Antarctica, *Ann. Geofis.*, *44*(4), 687–702.
- Urbini, S., M. Frezzotti, S. Gandolfi, C. Vincent, C. Scarchilli, L. Vittuari, and M. Fily (2008), Historical behaviour of Dome C and Talos Dome (East Antarctica) as investigated by snow accumulation and ice velocity measurements, *Global Planet. Change*, *60*(3–4), 576–588, doi:10.1016/j.gloplacha.2007.08.002.
- van de Berg, W. J., M. R. van den Broeke, C. H. Reijmer, and E. van Meijgaard (2006), Reassessment of the Antarctic surface mass balance using calibrated output of a regional atmospheric climate model, *J. Geophys. Res.*, *111*, D11104, doi:10.1029/2005JD006495.
- van den Broeke, M. R., and N. P. M. van Lipzig (2003), Factors controlling the near-surface wind field in Antarctica, *Mon. Weather Rev.*, *131*, 733–743.
- van den Broeke, M., C. Reijmer, and R. van de Wal (2004a), Surface radiation balance in Antarctica as measured with automatic weather stations, *J. Geophys. Res.*, *109*, D09103, doi:10.1029/2003JD004394.
- van den Broeke, M. R., W. J. van de Berg, and E. van Meijgaard (2004b), A study of the surface mass balance in Dronning Maud Land, Antarctica, using automatic weather stations, *J. Glaciol.*, *50*(171), 565–582.
- van den Broeke, M., W. J. van de Berg, and E. van Meijgaard (2006a), Snowfall in coastal West Antarctica much greater than previously assumed, *Geophys. Res. Lett.*, *33*, L02505, doi:10.1029/2005GL025239.
- van den Broeke, M., W. J. van de Berg, E. van Meijgaard, and C. Reijmer (2006b), Identification of Antarctic ablation areas using a regional atmospheric climate model, *J. Geophys. Res.*, *111*, D18110, doi:10.1029/2006JD007127.
- Van der Veen, C. J., and J. F. Bolzan (1999), Interannual variability in the net accumulation on the Greenland Ice Sheet: Observations and implications for the mass-balance measurements, *J. Glaciol.*, *34*(118), 355–357.
- Van de Wal, R. S. W., W. Greuell, M. R. van den Broeke, C. Reijmer, and J. Oerlemans (2005), Mass balance observations and automatic weather station data along a transect near Kangerlussuaq, West Greenland, *Ann. Glaciol.*, *42*, 311–316.
- van Lipzig, N. P. M., J. C. King, T. A. Lachlan-Cope, and M. R. van den Broeke (2004a), Precipitation, sublimation, and snow drift in the Antarctic Peninsula region from a regional atmospheric model, *J. Geophys. Res.*, *109*, D24106, doi:10.1029/2004JD004701.
- van Lipzig, N. P. M., J. Turner, S. R. Colwell, and M. R. van den Broeke (2004b), The near-surface wind field over the Antarctic continent, *Int. J. Climatol.*, *24*(15), 1973–1982.
- Vaughan, D. G. (2006), Recent trends in melting condition on the Antarctic Peninsula and their implications for ice-sheet mass balance and sea level, *Arctic Antarct. Alpine Res.*, *38*(1), 147–152.
- Vaughan, D. G., J. L. Bamber, M. Giovinetto, and A. P. R. Cooper (1999a), Reassessment of net surface mass balance in Antarctica, *J. Clim.*, *12*, 933–946.
- Vaughan, D. G., H. F. J. Corr, C. S. M. Doake, and E. D. Waddington (1999b), Distortion of isochronous layers in ice revealed by ground-penetrating radar, *Nature*, *398*, 323–326.
- Vaughan, D. G., P. S. Anderson, J. C. King, G. W. Mann, S. D. Mobbs, and R. S. Ladkin (2004), Imaging of firn isochrones across an Antarctic ice rise and implications for patterns of snow accumulation rate, *J. Glaciol.*, *50*(170), 413–418.
- Velicogna, I., and J. Wahr (2006), Measurements of time-variable gravity show mass loss in Antarctica, *Science*, *311*(5768), 1754, doi:10.1126/science.1120808.
- Watanabe, O., et al. (1997), A preliminary study of ice core chronology at Dome Fuji Station, Antarctica, *Proc. NIPR Symp. Polar Meteorol. Glaciol.*, *11*, 9–13.
- Weller, R., F. Trauffer, H. Fischer, H. Oerter, C. Piel, and H. Miller (2004), Postdepositional losses of methane sulfonate, nitrate, and chloride at the European Project for Ice Coring in Antarctica deep-drilling site in Dronning Maud Land, Antarctica, *J. Geophys. Res.*, *109*, D07301, doi:10.1029/2003JD004189.
- Whillans, I. M., and J. F. Bolzan (1988), A method for computing shallow ice-core depths, *J. Glaciol.*, *34*(118), 355–357.
- Whitlow, S., P. A. Mayewski, and J. E. Dibb (1992), A comparison of major chemical species input timing and accumulation at South Pole and Summit Greenland, *Atmos. Environ., Part A*, *26*(11), 2045–2054.
- Wilgain, S., E. Picciotto, and W. D. Breuck (1965), Strontium 90 fallout in Antarctica, *J. Geophys. Res.*, *70*(24), 6023–6032.
- Wilhelms, F. (1996), *Leitfähigkeits- und Dichtemessung an Eisbohrkernen* (Measuring the Conductivity and Density of Ice Cores), *Ber. Polarforsch.*, vol. 191, Alfred-Wegener-Inst. für Polar- und Meeresforsch., Bremerhaven, Germany.
- Wilhelms, F. (2000), *Messung dielektrischer Eigenschaften polarer Eiskerne* (Measuring the Dielectric Properties of Polar Ice Cores), *Ber. Polarforsch.*, vol. 367, Alfred-Wegener-Inst. für Polar- und Meeresforsch., Bremerhaven, Germany.

- Wilhelms, F. (2005), Explaining the dielectric properties of firn as a density-and-conductivity mixed permittivity (DECOMP), *Geophys. Res. Lett.*, *32*, L16501, doi:10.1029/2005GL022808.
- Wilhelms, F., J. Kipfstuhl, H. Miller, K. Heinloth, and J. Firestone (1998), Precise dielectric profiling of ice cores: A new device with improved guarding and its theory, *J. Glaciol.*, *44*(146), 171–174.
- Winebrenner, D. P., R. J. Arthern, and C. A. Shuman (2001), Mapping Greenland accumulation rates using observations of thermal emission at 4.5-cm wavelength, *J. Geophys. Res.*, *106*(D24), 33,919–33,934.
- Wolff, E. B., J. C. Moore, H. B. Clausen, C. U. Hammer, J. Kipfstuhl, and K. Fuhrer (1995), Long-term changes in the acid and salt concentrations of the Greenland Ice Core Project ice core from electrical stratigraphy, *J. Geophys. Res.*, *100*(D8), 16,249–16,263.
- Wolff, E. B., W. D. Miners, J. C. Moore, and J. G. Paren (1997), Factors controlling the electrical conductivity of ice from the polar regions—A summary, *J. Phys. Chem. B*, *101*, 6090–6094.
- Wolff, E. B., I. Basile, J.-R. Petit, and J. Schwander (1999), Comparison of Holocene electrical records from Dome C and Vostok, Antarctica, *Ann. Glaciol.*, *29*, 89–93.
- Xiao, C. D., D. H. Qin, L. G. Bian, X. J. Zhou, I. Allison, and M. Yan (2005), A precise monitoring of snow surface height in the region of Lambert Glacier basin-Amery Ice Shelf, East Antarctica, *Sci. China, Ser. D, Earth Sci.*, *48*(1), 100–111.
- Yilmaz, O. (1987), *Seismic Data Processing, Invest. Geophys.*, vol. 2, Soc. of Explor. Geophys., Tulsa, Okla.
- Young, N. W., M. Pourchet, V. M. Kotlyakov, P. A. Korolev, and M. B. Dyugeroev (1982), Accumulation distribution in the IAGP area, Antarctica: 90°E–150°E, *Ann. Glaciol.*, *3*, 333–338.
- Zwally, H. J., and M. B. Giovinetto (1995), Accumulation in Antarctica and Greenland derived from passive-microwave data: A comparison with contoured compilations, *Ann. Glaciol.*, *21*, 123–130.
- Zwally, H. J., M. B. Giovinetto, J. Li, H. G. Cornejo, M. A. Beckley, A. C. Brenner, J. L. Saba, and D. Yi (2005), Mass changes of the Greenland and Antarctic ice sheets and shelves and contributions to sea-level rise: 1992–2002, *J. Glaciol.*, *51*(175), 509–527, 19.
- 
- D. A. Dixon and S. Kaspari, Climate Change Institute, Department of Earth Sciences, University of Maine, 5790 Edward T. Bryand Global Sciences Center, Orono, ME 04469-5790, USA. (daniel\_dixon@umit.maine.edu; susan.kaspari@maine.edu)
- O. Eisen and H. Oerter, Stiftung Alfred-Wegener-Institut für Polar- und Meeresforschung, Postfach 120161, D-27515 Bremerhaven, Germany. (olaf.eisen@awi.de; hans.oerter@awi.de)
- A. Ekaykin and V. Y. Lipenkov, Arctic and Antarctic Research Institute, 38 Bering Street, 199397 St. Petersburg, Russia. (ekaykin@aari.nw.ru; lipenkov@aari.nw.ru)
- M. Frezzotti, ENEA Laboratory for climate observation, SP. Anguillarese, 301 I-00123 S.M. di Galeria (Roma), Roma, Italy. (frezzotti@casaccia.enea.it)
- C. Genthon and O. Magand, LGGE, CNRS, Université Joseph-Fourier Grenoble, 54, Rue Molière, BP 96, Domaine Universitaire, F-38402 Saint-Martin d’Hères, France. (genthon@lgge.obs.ujf-grenoble.fr; magand@lgge.obs.ujf-grenoble.fr)
- P. Holmlund, Department of Physical Geography and Quaternary Geology, Stockholm University, SE-10691 Stockholm, Sweden. (per.holmlund@natgeo.su.se)
- E. Isaksson, Norwegian Polar Institute, Polar Environmental Centre, N-9296 Tromsø, Norway. (elli@npolar.no)
- T. Kameda and S. Takahashi, Snow and Ice Research Laboratory, Kitami Institute of Technology, 165 Koencho, Kitami, Hokkaido 090-8507, Japan. (kameda@mail.kitami-it.ac.jp; shuhei@mail.kitami-it.ac.jp)
- L. Karlöf, Research and Development, SWIX SPORT AS, Servicebox, N-2626 Lillehammer, Norway. (l.karlof@swixsport.no)
- M. R. van den Broeke, Institute for Marine and Atmospheric Research, Utrecht University, PO Box 80 005, NL-3508 TA Utrecht, Netherlands. (m.r.vandenbroeke@phys.uu.nl)
- D. G. Vaughan, British Antarctic Survey, Natural Environment Research Council, High Cross, Madingley Road, Cambridge CB3 0ET, UK. (dgv@bas.ac.uk)